ELECTRICAL PROPERTIES AND PHASE TRANSITIONS IN SOME AMMONIUM CONTAINING FERROELECTRICS

U. SYAMAPRASAD

THESIS SUBMITTED IN PARTIAL FULFILMENT OF
THE REQUIREMENTS FOR THE DEGREE OF
DOCTOR OF PHILOSOPHY

TO MY PARENTS

CERTIFICATE

Certified that the work presented in this thesis is based on the original work done by Mr. U. Syamaprasad, U.G.C. Senior Research Fellow, under my guidance in the Department of Physics, University of Cochin, and has not been included in any other thesis submitted previously for the award of any degree.

Cochin - 22,)
7 December 1981. (

Dr. C.P. Girijavallabhan,
Supervising Teacher.

DECLARATION

Certified that the work presented in this thesis is based on the original work done by me under the guidance of Dr.C.P. Girijavallabhan in the Department of Physics, University of Cochin and has not been included in any other thesis submitted previously for the award of any degree.
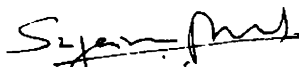
Cochin - 22,)
7 December 1981. (

U. Syamaprasad.

PREFACE

The work presented in this thesis has been carried out by the author in the Department of Physics, University of Cochin during the years 1977-81.

The thesis aims to present the results of the experimental investigations on the electrical properties like electrical conductivity, dielectric constant and ionic thermo-currents in certain ammonium containing ferroelectric crystals viz. $LiNH_4SO_4$, $(NH_4)_2SO_4$ and $(NH_4)_3H(SO_4)_2$. Special attention has been paid in revealing the mechanisms of electrical conduction in the various phases of these crystals and those associated with the different phase transitions occurring in them, by making studies on doped, quenched and deuterated crystals. The report on the observation of two new phase transitions in $(NH_4)_2SO_4$ and of a similar one in $(NH_4)_3H(SO_4)_2$ are included. The relaxation mechanisms of the impurity-vacancy complexes and the space charge phenomena in pure and doped crystals of $LiNH_4SO_4$ and $(NH_4)_2SO_4$ and the observation of a new type of ionic thermo-current viz. Protonic Thermo-Current (PTC) in these crystals are also presented here.

Many of the instruments and pieces of apparatus like the crystal growing furnace, low temperature cells and high temperature furnaces for temperature variation studies,

i

sample holders and temperature indicators and controllers had to be fabricated specially for the purpose of the investigations presented here. Most of the single crystal specimens in the pure as well as in the doped and deuterated form were grown by the author during the course of these studies. All the experimental results presented in this work were confirmed by repeating these measurements on dozens of crystal samples.

The thesis contains seven chapters which are generally self-contained with separate abstracts; however there exists many cross references among chapters. Chapter I is of an introductory nature in which some general considerations based on the scope and importance of this investigation along with brief introduction including theoretical background and experimental techniques pertinent to phase transitions in solids, ferroelectricity, ionic conductivity and to thermally stimulated discharge processes are given. The current status and some applications of these are also presented here. Chapter II deals with the experimental techniques and method of measurements used in this study.

The study of electrical conductivity on pure, doped, quenched and deuterated samples of $LiNH_4SO_4$, $(NH_4)_2SO_4$ and $(NH_4)_3H(SO_4)_2$ are presented in chapters III, IV and V. The mechanisms of the electrical

transport processes and of the different phase transitions in these crystals are discussed in these chapters. The observation of two new phase transitions in $(NH_4)_2SO_4$ and a new transition in $(NH_4)_3H(SO_4)_2$ are also presented here. Chapter VI deals with the dielectric studies of these crystals. The confirmation of many of the results obtained from electrical conductivity studies have been made by these measurements and are given here.

An extensive study of ionic thermo-currents (ITC) in pure and doped samples of $LiNH_4SO_4$ and $(NH_4)_2SO_4$ is presented in chapter VII. A detailed analysis of the ITC spectra of these crystals as a function of impurity concentration, poling temperature, poling time and polarizing field has been carried out, and these studies reveal the origin and nature of each of the peaks occurring in the ITC spectra. The phenomenon of Protonic Thermo-Current was observed in both these crystals for the first time.

The studies presented here also establish the superiority and sensitivity of the electrical conductivity measurements in detecting and characterising phase transitions in ionic crystals especially in the case of improper ferroelectrics.

Part of the investigations presented in this thesis has been published/communicated in the form of following papers:

1. D.C. Electrical Conductivity in $LiNH_4SO_4$

   U. Syamaprasad and C.P.G. Vallabhan

   Solid State Commun. 34, 899 (1980)

2. Detection of Ferroelectric Phase Transitions in Lithium Ammonium Sulphate by Electrical Conductivity Studies

   U. Syamaprasad and C.P.G. Vallabhan

   National Acad. Sci. Lett. (India) 3, 364 (1980)

3. Anomalous Behaviour of Electrical Conductivity and Thermally Stimulated Current in the Paraelectric Phase of Ammonium Sulphate Single Crystals

   U. Syamaprasad and C.P.G. Vallabhan

   Proc. Nuclear Phys. and Solid State Phys. Symp. IIT Delhi (India), Paper No.SLA10 (1980)

4. Electrical Conductivity and Thermally Stimulated Current in the Paraelectric Phase of $(NH_4)_2SO_4$

   U. Syamaprasad and C.P.G. Vallabhan

   Solid State Commun. 38, 555 (1981)

5. D.C. Electrical Conductivity and Phase Transi-
    tions in $(NH_4)_3H(SO_4)_2$

    U. Syamaprasad and C.P.G. Vallabhan

    J. Phys. C 14, L571 (1981)

6. Observation of a High Temperature Phase Transi-
    tion in $(NH_4)_2SO_4$ from Dielectric Studies

    U. Syamaprasad and C.P.G. Vallabhan

    J. Phys. C (To appear in Vol.14, 1981)

7. Low Temperature Electrical Conductivity,
    Dielectric Constant and Phase Transitions in
    $(NH_4)_2SO_4$ and $(ND_4)_2SO_4$

    U. Syamaprasad and C.P.G. Vallabhan

    Solid State Commun. (In Press)

8. Protonic Conduction in Lithium Ammonium
    Sulphate

    U. Syamaprasad and C.P.G. Vallabhan

    (Accepted for presentation in the Silver
    Jubilee Physics Symp. BARC Bombay 1981)

9. Phase Transitions in $LiND_4SO_4$

    U. Syamaprasad and C.P.G. Vallabhan

    (Accepted for presentation in the Silver
    Jubilee Physics Symp. BARC Bombay 1981)

10. Ionic Thermo-Currents in $LiNH_4SO_4$

   U. Syamaprasad and C.P.G. Vallabhan

   (Communicated to Phys. Rev.)

11. Effect of Deuteration on Electrical Condu-
   ctivity, Dielectric Constant and Phase
   Transitions in $LiNH_4SO_4$

   U. Syamaprasad and C.P.G. Vallabhan

   (Communicated to Phys. Lett.)

12. Ionic Thermo-Current Studies in $(NH_4)_2SO_4$

   U. Syamaprasad and C.P.G. Vallabhan

   (Communicated to Pramana)

ACKNOWLEDGEMENTS

The investigations presented in this thesis have been carried out under the guidance and supervision of Dr. C.P. Girijavallabhan, Reader, Department of Physics, Cochin University. It is with great pleasure I express my sincere gratitude for his able guidance and competent advice throughout the progress of this work.

I am extremely grateful to Dr. K. Sathianandan, Professor and Head of the Department of Physics, Cochin University for providing all the necessary facilities for carrying out this work. I am also indebted to him for the kind interest and encouragement he has shown during the course of this work.

I am highly indebted to Dr. K.T. Ramavarma, Retd. Professor of Physics, S.N. College, Quilon for encouraging me with necessary guidance and advice to take up research work in Physics.

I would like to thank Professor J. Ramakrishna of Indian Institute of Science for bringing our attention to the interesting case of phase transitions in lithium ammonium sulphate crystals and also for giving a few crystal samples in the early stages of this investigation. Thanks are also due to Dr.K.G. Nair, Professor and Head of the Department of Electronics and Communication Systems, Cochin University for lending an X-Y recorder for the measurements of ITC. I am also thankful to Dr. V.P.N. Nampoori, Lecturer, Department of Physics, Cochin University for providing the Atomic Absorption data of the crystals used

in these studies. Mr. C. Raghavan, Technical Staff of
the Department of Physics, Cochin University helped me
a lot in the fabrication and maintenance of certain
electronic equipments used in this work. I extend my
sincere thanks to him also.

The immense help and encouragement I have
received from all the members of the Faculty of the
Department of Physics, University of Cochin are acknow-
ledged. Thanks are also due to the technical, administra-
tive and library staff of the Department of Physics and
the staff of the Central Workshop and Instrumentation
Services Laboratories of the University of Cochin for
the help and co-operation I have received from them.

I express my sincere thanks to all the research
scholars of the Department of Physics, University of
Cochin for their kind co-operation and immense help through-
out the entire programme.

The junior research fellowship awarded by the
University of Cochin in the earlier stages and the junior
as well as the senior research fellowships awarded by the
University Grants Commission, New Delhi in the rest of the
period of this work are gratefully acknowledged.

Finally, I would like to thank Mr.K.P.Sasidharan
for neatly typing the manuscript.

U. Syamaprasad.

CONTENTS

Page

CHAPTER I

INTRODUCTION

Abstract

Some general considerations based on the scope and importance of the studies presented in this thesis are given. The chapter also provides a brief introduction to the subject of phase transitions in solids. Theoretical background including thermodynamical considerations and various experimental techniques pertinent to phase transitions in solids are given. Dielectric properties of solids, ferroelectricity, ionic conductivity and thermally stimulated discharge processes are the remaining topics on which brief discussions are presented here. The current status and some applications of these are also mentioned.

1

1.1   Some General Considerations

Phenomena like melting, solidification, condensation and evaporation are impressive examples of transformation of states of matter. But there exist some less spectacular transformations which occur within the solid itself. Such subtle transitions taking place within the solids are accompanied by notable changes in certain physical properties of the substance like specific heat, dielectric constant, electrical conductivity etc. Hence measurement of such quantities as a function of an external parameter like pressure or temperature is a direct way of investigating these phase transitions.

There exist already a large wealth of experimental data from these measurements on a variety of solids under a wide range of pressure and temperature. But the unprecedented power, precision and sensitivity of modern experimental methods, which employ very sophisticated electronic techniques, are such that a careful repetition of these experiments almost always gives new insight into the various aspects of the phenomenon. Many transitions which had not been detected in earlier measurements have come to light in some of these later experiments as can be seen from the results presented in the succeeding chapters of this thesis.

The investigations presented in this thesis are mainly concerned with the measurements of d.c. electrical conductivity; dielectric constant and ionic thermo-currents in certain ammonium containing ionic crystals of the sulphate group—viz., lithium ammonium sulphate, ammonium sulphate and triammonium hydrogen disulphate. A number of previously unreported phase transitions have been observed during the course of these investigations. Results of studies on deuterated samples have revealed the mechanism of many of these transitions. The mechanisms of electrical charge transport in these crystals have been understood by studies made on doped as well as on deuterated samples. The thesis also contains a detailed study of ionic thermo-currents and the report of the observation of an extremely interesting new phenomena viz., PTC (Protonic thermo-current).

1.2   Phase Transitions in Solids

The subject of phase transitions in solids is of vital interest to physicists, chemists, metallurgists, ceramists and others involved in the study of solids. This cross-disciplinary subject is not only of academic importance, but also of technological relevance. The literature abounds in experimental and theoretical studies of phase transitions in solids and the subject is continuously growing. Novel systems undergoing transitions and newer kinds of transitions

are being constantly reported. At the same time many uni-
fying concepts have emerged in recent years which provide
a better understanding of the nature of phase transitions.

The homogeneous parts of a given assembly of atoms
or molecules, called phases, are characterised by thermo-
dynamic properties like volume, pressure, temperature and
energy. An isolated phase is stable only when its energy—
or more generally its free energy—is a minimum for the
specified thermodynamic conditions. As the temperature,
pressure or any other variable like an electric or magnetic
field acting on the system is varied, the energy of the
system changes smoothly and continuously. Whenever variations
of free energy are associated with changes in structural
details of the phase, a phase transformation is said to
occur.

1.2.1 Thermodynamic classification

The classical Clapeyron equation satisfactorily
predicts the features of the first-order phase transitions
involving discontinuous changes in the first derivatives of
Gibbs free energy such as entropy and volume. A number of
transitions brought out by variation of temperature and
pressure are known [1-4]. Although one often classifies
second or higher-order transitions depending on the relation

between the thermodynamic property undergoing discontinuity and the Gibbs free energy function [5], these transitions are not readily explained by classical thermodynamics. Unlike the case of the first order transitions, where the free energy surfaces, $G(P,T)$, of the two phases intersect sharply at the transition temperature [5], it is difficult to visualize the nature of the free energy surfaces in second or higher-order transitions. In second-order transitions, changes in heat capacity as well as incompressibility and thermal expansivity are noticed at the transition temperature while the so-called λ -transitions (often grouped with second order transitions), the heat capacity tends towards infinity at the transition temperature. Landau [6] introduced the concept of order parameter to the understanding of structural phase transitions which provides a general way of examining phase transitions and related physical phenomena.

Although it is convenient to classify phase transitions as first or second-order, many real transformations are truly of mixed order, exhibiting features of both. Generally in thermal transformations, the high temperature form is higher symmetry as well as higher order [7].

During a phase transition, whereas the free energy of the system remains continuous, thermodynamic quantities like entropy, volume, heat capacity etc. undergo discontinuous changes. Depending on the relation between the thermodynamic quantity undergoing discontinuity and the Gibbs free energy function, Ehrenfest [5] has classified phase transitions. In this simple scheme, a transition is said to be of the same order as the derivative of the Gibbs free energy which shows a discontinuous change at the transition. Gibbs free energy is given by

$$G = H - TS = E + PV - TS \qquad (1.1)$$

Hence

$$dG = dE + PdV + VdP - TdS - SdT \qquad (1.2)$$

$$= VdP - SdT \qquad (1.3)$$

The first and second derivatives of the free energy may be written as

$$\left(\frac{\partial G}{\partial P}\right)_T = V \qquad \left(\frac{\partial G}{\partial T}\right)_P = -S \qquad (1.4)$$

$$\left(\frac{\partial^2 G}{\partial P^2}\right)_T = \left(\frac{\partial V}{\partial P}\right)_T = -V\beta \qquad \left(\frac{\partial^2 G}{\partial P \partial T}\right) = \left(\frac{\partial V}{\partial T}\right)_P = V\alpha \qquad (1.5)$$

$$\left(\frac{\partial^2 G}{\partial T^2}\right)_P = -\left(\frac{\partial S}{\partial T}\right)_P = -\frac{C_P}{T} \qquad (1.6)$$

Here C_p, α and β are the heat capacity, volume thermal exp-ansivity and compressibility respectively. We see that transformations in which a discontinuous change occurs in volume and entropy (that is, when there is a latent heat of transformation) belong to the first order, and those in which discontinuous change occurs in heat capacity, thermal expansi-vity and compressibility belong to the second order. Third and higher-order transitions involve further differential quantities.

A first-order transition involving discontinuous change in entropy is represented graphically in Fig. 1.1(a). In Fig. 1.1(b) a similar first-order pressure transition involving discontinuous change in volume at constant tempera-ture is shown.

Transformations belonging to the second-order are almost always associated with some kind of ordering process. In Fig. 1.2 variations of enthalpy, heat capacity and the "order parameter" with temperature during a second-order transformation are depicted.

There are a large number of examples of both thermal and pressure transformations in inorganic solids belonging to the first order [8-11]. Transitions which have finite discontinuities in specific heat etc. are very uncommon. The superconducting transition in tin at zero
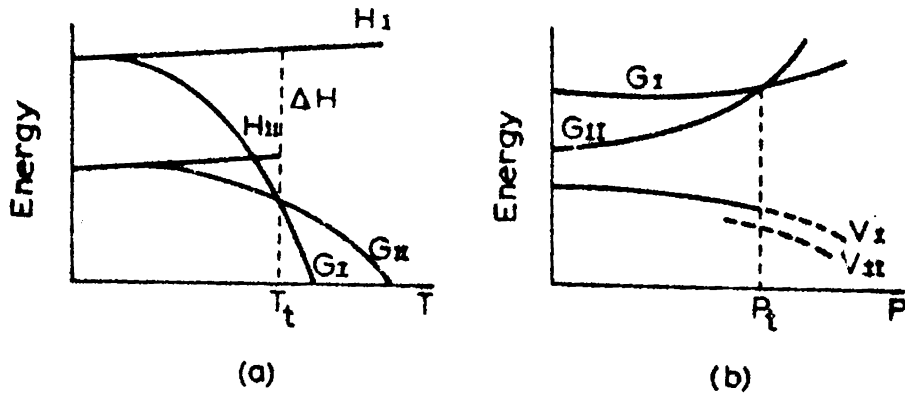
Fig. 1.1 Variation of enthalpy and free energy with
(a) temperature and
(b) pressure in a first-order phase transition.
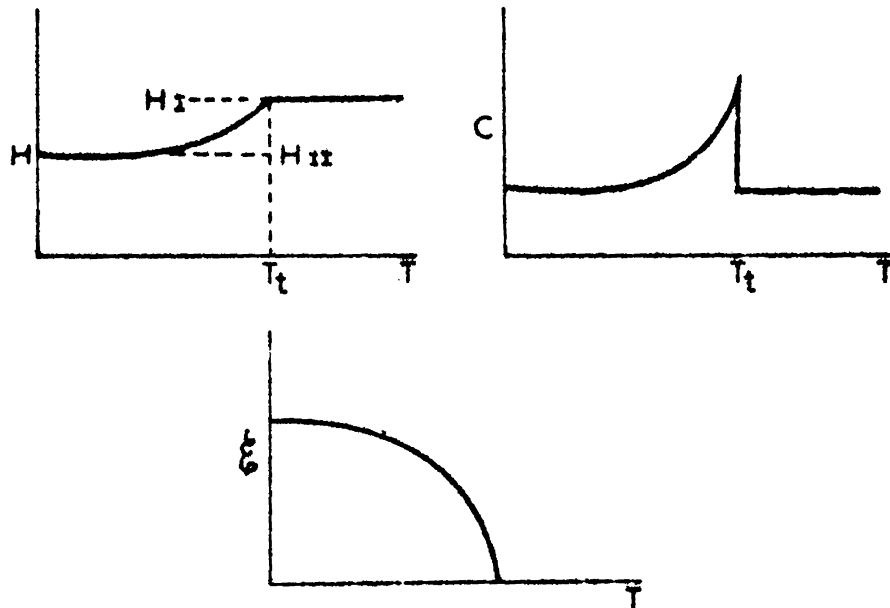
Fig. 1.2 Variation of enthalpy, specific heat and order
parameter in a second - order phase transition.

field is an example for such a transition [12]. The Curie

points in many ferromagnetics could be considered as

examples of third order transitions.

A large number of transitions which are often

incorrectly referred to as second-order transitions are

actually lambda (λ) transitions. In these transitions, the

heat capacity often plotted as a function of temperature

tends to infinity at T_c. There are transitions in which

the plots are symmetrical around T_c and are known as

symmetrical λ-transitions.

1.3   Techniques Employed in the Study
of Phase Transitions

Several techniques are employed to investigate

phase transitions depending on the nature of the solid and

the properties of interest. Such studies are not only of

academic value in understanding the structural and mechani-

cal aspects of phase transitions, but also be of technologi-

cal importance. The literature covers a wide range of

techniques like diffraction, thermal, optical, spectro-

scopic, electrical, dielectric and some other methods.

Reviews of such techniques are already available in the

literature [8-14].

1.3.1 Diffraction technique

The two important thermodynamic variables in the study of phase transitions are temperature and pressure. Any study of a phase transition therefore involve measurements of properties as a function of temperature or pressure. X-ray diffraction forms an essential part of any investigation quite apart from others in the study of phase transition in solids. Electron diffraction has certain special advantages, because of the shorter wavelength possible for electrons in studying super-structures and small domains. Neutron diffraction studies are most useful in studying position of light atoms like hydrogen,and in magnetic structures. The analysis of powder neutron diffraction profiles [15] yields valuable structural information.

1.3.2 Thermal measurements

Thermal measurements have been widely used to identify and characterise transitions. Heat capacity measurements provide precise data on enthalpy changes and indicate the thermodynamic order of transitions. Differential thermal analysis (DTA) has been routinely employed to obtain the same information [16,17]. Information on the activation energies of transformations has also been obtained by fitting the DTA peak to first order kinetic equations [16,17]. Thermal hysterisis has also conveniently

studied by DTA. Being a dynamic technique DTA suffers
from certain disadvantages. The ΔH values obtained by
DTA are not reliable. Differential scanning calorimetry
(DSC) has become popular in recent years for obtaining heat
capacity data and ΔH values of transitions, the ΔH
values of DSC being much more reliable than those of DTA.

1.3.4 Optical methods

The optical microscope is a very valuable tool
for studying phase transitions, particularly with respect
to the movement of boundaries, growth of nuclei and changes
in grain size. Pressure transitions can also be studied
by using an optical microscope and a diamond anvil press.
Electron microscope examination would give useful informat-
ion on dislocations and structural aspects if the solids
can be studied in the transition region [7].

1.3.5 Spectroscopic and related techniques

Optical spectroscopy in the infrared, visible and
ultraviolet regions has been used extensively to study
solids undergoing transitions. Laser Raman spectroscopy
has been particularly exploited in recent years to investi-
gate these transitions. In addition to neutron scattering,
Raman spectroscopy also yield direct information on soft
modes in solids. X-ray and ultraviolet photoelectron

spectra of solids through their phase transitions can provide valuable information on the changes in electronic structure (if any). Positron annihilation is a technique in which the phenomenon of e^+, e^- recombination with consequent emission of γ-rays is used to study phase transitions in solids.

Preparation, purification and characterisation of materials undoubtedly form an important part of phase transition studies. The purity of the material is particularly crucial, since it has been known that impurities affect characteristics of transitions significantly. It is therefore important to get the purest material possible while studying phase transitions. In this context, all the well-known techniques for the analysis and characterisation of materials like mass spectrometry, spectrography, atomic absorption spectrometry and electron microprobe analysis have to be employed.

1.3.6 Magnetic properties and resonance techniques

Magnetic properties of materials can be studied by a variety of techniques such as susceptibility measurements, neutron diffraction, Mossbauer spectroscopy and magnetic resonance spectroscopy (including NMR, ESR and double resonance).

NMR spectroscopy has been employed to study phase transitions of solids containing the appropriate nuclei (eg. V in VO_2 and V_2O_3; Mn in $MnCr_2O_4$). Phase transitions in NaCN and NaHS has been studied by NMR spectroscopy. Studies of hindered rotations of NH_4^+ or CH_3 groups and phase transitions in hydrogen bonded ferroelectrics like KH_2PO_4 are other applications of NMR spectroscopy. ESR spectra of solids undergoing phase transitions have been reported in the literature; a useful application of ESR spectroscopy is to study a diamagnetic crystal with a paramagnetic ion (Mn^{2+} in KNO_3) in the region of the phase transition. Nuclear quadrupole resonance spectroscopy has been employed to study phase transitions of halides (eg. $CsPbCl_3$), nitrites and nitrates ($NaNO_2$ and $NaNO_3$) containing nuclei like halogen, nitrogen and others with quadrupole moments. Ferromagnetic and antiferromagnetic resonance experiments also provide useful information on magnetically ordered solids. Excellent treatments on magnetism and chemical bond [18] and detailed studies of several magnetic transitions [19-48] on a variety of solids are available in the literature.

1.3.7 Electrical methods

Electrical properties like electrical conductivity, thermoelectric effect and Hall effect have been exploited in

the study of phase transitions, but these have mostly
been confined to some electronic materials such as oxides
and sulphides of vanadium, titanium etc. [54-76]. Only few
exceptions [49-53] exist where these techniques have been
employed in the study of other materials showing transitions.
No serious attempt has so far been made in studying the
phase transitions of ionic materials employing electrical
properties. A detailed description of electrical conductivity
in ionic materials is given in Sec.1.5 of this chapter.

1.3.8 Dielectric methods

The dielectric properties of a material are governed
by the response of the material to an applied electric field
at the electronic, atomic, molecular and macroscopic levels.
Polarization and dielectric loss in materials are phenomena
of interest and these are generally studied as a function of
frequency. According to Maxwell's equations,

$$D = \varepsilon E \tag{1.7}$$

where D is the dielectric displacement, E the electric field
strength and ε is the dielectric constant of the medium;
ε is equal to the product $\varepsilon_v \varepsilon_r$, where ε_r is the dielectric
constant relative to vacuum and ε_v is the dielectric constant
of vacuum. Application of an electric field to a material
causes a displacement of electric charges, creating or

reorienting dipoles in the material. This property specified by a quantity called polarization, P is given by

$$P = \varepsilon_v(\varepsilon_r - 1)E = \varepsilon_v \, \chi_e E \qquad (1.8)$$

where χ_e is the electric susceptibility. P can be expressed in terms of the elementary dipole moments, p , as $P = Np$ where N is the number of dipoles per unit volume and $p = \alpha E$, where α is the polarizability.

The total polarization of a multiphase material containing permanent dipoles will have electronic, ionic, orientational and interfacial (space charge) contributions:

$$P = P_e + P_i + P_o + P_s \qquad (1.9)$$

In a single phase material, the last term due to interfacial polarization, P_s will be absent and P will be given by

$$P = P_e + P_i + P_o = P_e + P_i + Np^2 E/3kT \qquad (1.10)$$

A dipole in a crystal experiences not only the external field E but also the field due to the polarization of the medium around it. The effective field (local field), E' is given by

$$E' = E + \frac{P}{3\varepsilon_v} = (\frac{\varepsilon_r + 2}{3})E \qquad (1.11)$$

so that polarizability per unit volume is related to the
relative dielectric constant of the material, ϵ_r, by the
expression,

$$\frac{N\alpha}{3\epsilon_v} = \frac{\epsilon_r - 1}{\epsilon_r + 2} \qquad (1.12)$$

In terms of molecular polarization π, the above equation
becomes

$$\pi = \frac{N_o\alpha}{3\epsilon_v} = \frac{\epsilon_r - 1}{\epsilon_r + 2} \left(\frac{M}{\rho} \right)(m^3) \qquad (1.13)$$

where $N_o = NM/\rho$ = Avagadro number per Kg mole and ρ is
the density in Kg/m^3. This equation is the well known
Clausius-Mosotti equation.

When a time dependent electric field is applied
to a dielectric material,

$$D = \epsilon^* E \quad \text{where} \quad \epsilon^* = \epsilon' - i\epsilon''; \qquad (1.14)$$

where ϵ' and ϵ'' are the real and imaginary parts of the
dielectric constant. The time-lag between the response
and stimulus is given by the phase angle δ, such that

$$\tan \delta = \frac{\epsilon''}{\epsilon'} \qquad (1.15)$$

The time dependence of ϵ'' and ϵ' are characterised by the

relaxation time, τ, which follows Arrhenius-type equation

$$\tau = \tau_o \exp(\Delta E/kT) \qquad (1.16)$$

In terms of frequency and time

$$\varepsilon' = \varepsilon_\infty + \frac{\varepsilon_s - \varepsilon_\infty}{1 + \omega^2\tau^2} \qquad (1.17)$$

$$\varepsilon'' = \frac{\omega\tau(\varepsilon_s - \varepsilon_\infty)}{1 + \omega^2\tau^2} \qquad (1.18)$$

and $\tan \delta = \dfrac{\omega\tau(\varepsilon_s - \varepsilon_\infty)}{\varepsilon_\infty\omega^2\tau^2 + \varepsilon_s} \qquad (1.19)$

Here ε_s and ε_∞ are static (low frequency) and optical (high frequency) dielectric constants respectively.

From the relations given earlier, we obtain

$$P = \frac{N\alpha E}{(1 - N\alpha/3\varepsilon_v)} \qquad (1.20)$$

The electric susceptibility is therefore given by

$$\chi_e = \frac{P}{\varepsilon_v E} = \frac{N\alpha/\varepsilon_v}{(1 - N\alpha/3\varepsilon_v)} = \varepsilon_r - 1 \qquad (1.21)$$

We see that when $N\alpha/3\varepsilon_v = 1$, both polarization and susceptibility tend to infinity. At a critical temperature, T_c, called the Curie temperature, the randomising effect of

temperature is balanced by the orienting effect of the internal field. Under such conditions

$$\mathcal{X}_e = \varepsilon_r - 1 = \frac{3T_c}{T - T_c} \qquad (1.22)$$

This equation called Curie-Weiss law, is similar to the one in ferromagnetism. Below T_c, the internal field increases the polarization and vice versa, and the material becomes spontaneously polarized or ferroelectric. Above T_c, dipole directions are randomised because of thermal agitation and the material is paraelectric, while below T_c dipoles exhibit parallel alignment. The Curie-Weiss law is generally written in the form

$$\varepsilon = \varepsilon_\alpha + \frac{C}{T - T_c} \qquad (1.23)$$

where the Curie constant, C is given by $Np^2/3\varepsilon_v k$.

(A detailed description of ferroelectricity is given in the following section).

1.4   Ferroelectricity and Ferroelectrics

Ferroelectrics are substances which below a certain temperature (Curie point - T_c) or over a certain temperature range between two Curie points, are subject to spontaneous polarization. The direction of this polarization can be changed by applying an external electric

field. The properties of ferroelectrics can be summarised as follows:

1. They possess a dielectric hysterisis loop, indicating reversible polarization.

2. They show dissappearance of hysterisis at a certain temperature.

3. They have a domain structure, which may be visible in polarized light.

4. They have a high dielectric constant, rising to a peak at the transition point.

5. The falling-off of their dielectric constant above the Curie point follows a Curie-Weiss law.

6. They possess a pseudosymmetric structure.

7. Their symmetry places them in a polar class.

8. They have a transition at the Curie point leading to a higher symmetry.

9. The Curie point is raised (or a lower Curie point is lowered) by the application of a biassing field.

10. There is a sudden dissappearance of surface charges at the transition.

Of these, item (1) is strongly characteristic of ferroelectrics and hence this property is usually used to identify them.

1.4.1 Thermodynamics of ferroelectric transitions

According to Landau's theory [77], a ferroelectric transition can be described in terms of an order parameter whose appearance at T_c breaks the symmetry of the paraelectric phase. The order parameter vanishes above T_c and is nonzero below T_c. The order parameter in ferroelectric transitions is the spontaneous polarization; in antiferroelectric transitions it is the sublattice polarization. Landau's theory was applied to ferroelectrics by Devonshire [78,79].

Following Landau, the expression for free energy density is given by

$$g(T,P) = g_0(T) + \tfrac{1}{2}a(T)P^2 + \tfrac{1}{4}b(T)P^4 + \tfrac{1}{6}c(T)P^6 \qquad (1.24)$$

where P is the spontaneous polarization along the ferro-electric axis. The equilibrium value of spontaneous polarization, P_0, at temperature T is obtained by minimising g:

$$\left(\frac{\partial g}{\partial P} \right)_{P=P_0} = 0 \qquad (1.25)$$

Thus, $P_0[a(T) + b(T)P_0^2 + c(T)P_0^4] = 0 \qquad (1.26)$

One of the solutions of this equation is $P_0 = 0$, applicable to the paraelectric phase. The other solution is $P_0 \neq 0$ is for the ferroelectric phase. The stable solution corresponding

to a minimum in g is

$$\left(\frac{\partial^2 g}{\partial P^2}\right)_{P_0} > 0 \tag{1.27}$$

Since $(\partial g/\partial P) = E$, the stability condition is equivalent to $\chi^{-1} > 0$.

Taking the second derivative of $g(T,P)$, we obtain

$$\chi^{-1} = a(T) + 3b(T)P_0^2 + 5c(T)P_0^4 > 0 \tag{1.28}$$

For the paraelectric phase $(P_0 = 0)$, the above equation becomes

$$\chi^{-1} = a(T) > 0 \tag{1.29}$$

Near the stability limit T_0,

$$a(T) \approx a'(T - T_0) \text{ and } a' = (\partial A/\partial T)_{T=T_0} > 0 \tag{1.30}$$

This gives rise to the Curie-Weiss law of dielectric susceptibility of the paraelectric phase,

$$\chi_T = \frac{C}{T - T_0} \tag{1.31}$$

where $C = \frac{1}{a'}$ and $T > T_0$.

Since $b(T)$ and $c(T)$ would only vary slightly with temperature

around the transition point, we may treat them as constants.

$$b(T) = b(T_c) = b \quad \text{and} \quad c(T) = c(T_c) = c \qquad (1.32)$$

Here c can be taken as positive, while b can be positive or negative.

A phase transition will be of second order if b > 0 and first order if b < 0. The order parameter will be a continuous function of T in a second-order transition and a discontinuous function in first-order transition. The equilibrium properties of ferroelectrics and anti-ferroelectrics have been discussed in detail by Fatuzzo and Merz [80] as well as Blinc and Zeks [81].

1.4.2 Improper ferroelectrics

In the ferroelectrics discussed above, the order parameter was the spontaneous polarization and anomalies in dielectric properties were due to increased correlations in the fluctuations of order parameters at T_c. Such ferroelectrics are considered to be proper ferroelectrics. There are ferroelectrics where the order parameter is not the spontaneous polarization. Because of the coupling between these two quantities, they exhibit a nonvanishing order parameter accompanied by spontaneous polarization at T_c. These ferroelectrics are called improper ferroelectrics.

Two class of improper ferroelectrics can be visualized:

(1) Where P and the order parameter have different symmetry properties (eg. $Gd_2(MoO_4)_3$) and (2) where the two have the same symmetry (eg. KH_2PO_4). Thermodynamic properties of these two classes have been reviewed by Blinc and Zerks [81].

1.4.3 Piezo-and pyroelectrics

Of the 32 crystal classes, 11 are centrosymmetric while 21 are noncentrosymmetric. Of the 21 noncentrosymmetric classes, 20 are piezoelectrics, which exhibit electric polarity when subjected to stress. Ten of the 20 piezoelectric classes possess a unique polar axis and are pyroelectrics which show change in polarization with temperature. Pyroelectrics whose polarity can be reversed by the application of electric fields are ferroelectrics. Thus all ferroelectric materials are also piezoelectric, although the converse is not true. Various types of ferroelectric materials have been discovered and the subject has been reviewed extensively in the literature [82,83].

1.5   Ionic Conductivity

The subject of ionic conductivity has become extremely relevant in recent years. The current revival of interest in electric automobiles and solid-state batteries has led to the production of high conductivity solid

electrolites. These new high conductivity materials such as $RbAgI_5$ [84,85] have greatly expanded the range over which ionic transport phenomena in solids have been utilized.

The foundations upon which our understanding of ionic conductivity are built, were laid down before 1940 by the early work of Schottky [86], Wagner [87] and Mott and Littleton [88,89]. It was found that the transference of mass and charge occurring in alkali halide crystals is mainly by means of ionic processes. Later the subject of ionic conductivity was expounded at length by Lidiard [90-92], Fuller [93-98], Barr [99-100], Franklin [101] etc. In addition to these some other notable works [102-119] can also be found in the literature.

The alkali halides are an important and much investigated class of ionic crystals. The results of Kelting and Witt [120] are typical for conductivity as a function of temperature. The principal features of their results are a straight line variation of log σ against 1/T for the high temperature high purity case and an approximate straight line for the low temperature highly doped case. The first of these region is referred to as the intrinsic region since the conduction properties are those of chemically pure crystal; the second region is called extrinsic since the conductivity depends on the nature and concentration of

impurities. An approximate emperical relation for the conductivity can be written as

$$\sigma = \sigma_e + \sigma_i \qquad (1.33)$$

$$= \sigma_{Oe} \exp(-E_e/kT) + \sigma_{Oi} \exp(-E_i/kT) \qquad (1.34)$$

where E_e and E_i are the conduction activation energies for the extrinsic and intrinsic regions respectively. The constant σ_{Oe} depends on the impurity content while σ_{Oi} depends only on the host crystal. One would therefore expect σ_{Oe}/σ_{Oi} to be much less than unity, and of the order of impurity fraction; this is borne out experimentally. It is also found from experiment that $E_e/E_i \simeq \frac{1}{2}$; this is explained by noting that E_e should be the activation energy for motion of extrinsically introduced defects, while E_i contains in addition the activation energy for creation of the defect within the originally perfect crystal.

1.5.1 Point defects in ionic solids

The simplest type of thermally generated lattice defects which are used to explain the conductivity of ionic solids are Frenkel and Schottky defects. The difference between these two defects are schematically shown in Fig. 1.3. In the formation of a Frenkel defect an ion

Fig.1.3 Model of a perfect alkali halide crystal pertubed by five kinds of defects

26

which originally at a site of the perfect lattice moves to an interstitial position; the net result of the process is to generate two imperfections—a vacant lattice site and an interstitial ion. A Schottky defect is formed by the migration of an ion which was originally at a site of the perfect lattice to a surface position; the net result of this is to generate only one imperfection—the vacant lattice site. The other type of defects usually found in ionic crystals are: impurity ions, impurity-vacancy complexes and impurity-vacancy pairs; the formation these are schematically shown in Fig.1.5.

1.5.2 Simple theory of ionic conductivity

Consider an one dimensional model in which a vacancy migrating in a crystal does so by a series of jumps of distance 'a' from one position to the next over a potential barrier. The potential barriers are all the same and equilibrium positions are equivalent. It can be shown from 1s classical statistical mechanics [90] that the probability per unit time for a vacancy to make the transition to a neighbouring equilibrium position is given by

$$\omega = \nu_0 \exp(-\Delta g/kT),$$
(1.35)

where ν_0 is a frequency which is interpreted as the vibrational frequency of the ions surrounding the vacancy
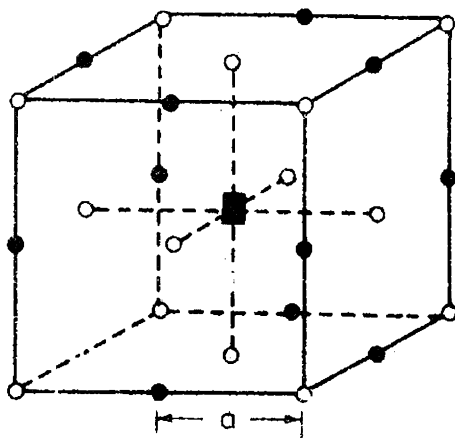
■ Cation vacancy ● Cation positions ○ Anion positions

Fig.1.5 DIAGRAM ILLUSTRATING THE JUMPS POSSIBLE FOR A CATION VACANCY TO NEAREST - NEIGHBOUR CATION POSITIONS IN AN NaCl - TYPE LATTICE
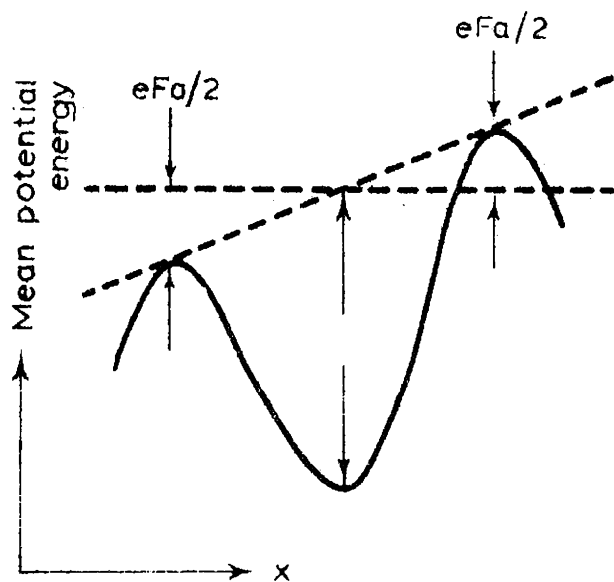

Fig.1.4 A SCHEMATIC REPRESENTATION OF THE MEAN POTENTIAL ENERGY OF A CATION VACANCY WITH AN ELECTRIC FIELD IN THE X - DIRECTION

and Δg is the Gibbs free energy of activation. The Gibbs

free energy can be written in terms of the corresponding

enthalpy Δh and entropy ΔS as

$$\Delta g = \Delta h - T \Delta S \tag{1.36}$$

Now consider the case of a cation vacancy (effective

charge $-e$) moving from one equilibrium position to another

in the presence of a uniform field F directed along the x-axis

(Fig. 1.4); the effect of the field is to add a term eFa

to the potential energy. A jump in the direction of the field

now takes place with a decreased probability.

$$\omega' = \nu_0 \exp[-(\Delta g + eFa/2)/kT] \tag{1.37}$$

and jump against the field with increased probability

$$\omega'' = \nu_0 \exp[-(\Delta g - eFa/2)/kT] \tag{1.38}$$

The mean drift velocity u (in the direction of positive

current flow) is therefore given by

$$u = a (\omega'' - \omega')$$

$$= a \nu_0 \exp(-\Delta g/kT) \times 2\sinh (eFa/2kT) \tag{1.39}$$

For low field strength, we assume $eFa \ll kT$ and we get

$$u = (a^2 e \nu_0 F/kT) \exp(-\Delta g/kT) \tag{1.40}$$

which corresponds to a mobility

$$\mu = (a^2 e \, v_0/kT) \, \exp(-\Delta g/kT) \qquad (1.41)$$

Equation (1.40) holds for an one dimensional model; for the motion of a cation vacancy in a three dimensional model we refer to Fig. 1.5. Consider the electric field to be applied in (100) direction; the central cation vacancy can jump to any one of the twelve nearest neighbour cation sites, each of which is distant $a\sqrt{2}$ away from the vacancy. The electric field makes no change in the energy requirements for a jump in the transverse direction, but neither do these jumps cause any flow of current. Of the remaining eight possible jumps, four are in the field direction; the only change in the equations (1.39),(1.40) and (1.41) is therefore the appearance of a factor 4.

Hence the last equation will now read

$$\mu = (4a^2 e \, v_0/kT)\exp(-\Delta g/kT) \qquad (1.42)$$

Now the discussion on the density of mobile species falls into two parts; viz. those corresponding to intrinsic and extrinsic regions of conduction.

If n_{AV} and n_{CV} be the densities of the anion and cation vacancies respectively and let N be the density

of possible vacancy sites, then from statistical thermo-
dynamics

$$(n_{AV}/N)(n_{CV}/N) = \exp(-g_S/kT) \qquad (1.43)$$

where g_S is the Gibbs free energy of formation of a pair of
Schottky defects.

Then the intrinsic conductivity can be written as

$$\sigma_i = n_{AV}e\mu_{AV} + n_{CV}e\mu_{CV} \qquad (1.44)$$

$$= \frac{4Na^2e^2}{kT} \exp(-g_S/kT) \; x$$

$$x \; [\; \nu_{AV}\exp -(\Delta g_{AV}/kT) + \nu_{CV}\exp -(\Delta g_{CV}/kT)]$$

$$(1.45)$$

Considering $\Delta g_{CV} \ll \Delta g_{AV}$, so that to a high degree of
approximation only the cation vacancies move; then making
appropriate definitions of Gibbs free energy in terms of
enthalpy and entropy

$$g_S = h_S - TS_S \qquad (1.46)$$

and $\quad \Delta g_{CV} = \Delta h_{CV} - T\Delta S_{CV} \qquad (1.47)$

we have

$$\sigma_i = \frac{4Na^2e^2\gamma_{CV}}{kT} \times \exp[(\Delta S_{CV} + S_S/2)/k]$$

$$\times \exp[(\Delta h_{CV} + h_S/2)/kT] \qquad (1.48)$$

Here the following comments on this result are to be noted:

1. The equation is valid only for cubic crystals of alkali halide type.

2. If both anions and cations are mobile, then the approximation made in deriving equation (1.48) from (1.45) is not valid.

3. In comparison with the experimental data, it should be borne in mind that possible contributions to current from all sources except Schottky defects have been ignored.

1.5.3 Ionic conductivity of crystals containing aliovalent impurities

In ionic crystals, there is an opportunity to create a rather unique defect complex by the introduction of aliovalent impurities, ie., impurity ions which differ in charge from the corresponding solvent ion. When such impurities are introduced, additional defects (either vacancies or interstitial ions) must accompany the aliovalent ion in order to achieve charge compensation, the defect possessing an effective charge equal and opposite to that of impurity ion.

We shall consider the effect of divalent cationic impurities in an ionic crystal of the alkali halide type. The conductivity in the impurity sensitive region can be called extrinsic conductivity (σ_e). In equation (1.43), n_{AV} and n_{CV} are no longer equal but are subject to the condition

$$n_{CV} = n_{AV} + n_I \tag{1.49}$$

where n_I is the density of divalent cationic impurities. Hence knowing equation (1.43)

$$\frac{n_{CV}}{N} \frac{(n_{CV} - n_I)}{N} = \exp(-g_S/kT) \tag{1.50}$$

which is a quadratic equation in n_{CV} whose solution is

$$n_{CV} = \frac{n_I}{2} \left[1 + \left\{ 1 + \frac{4N^2 \exp(-g_S/kT)}{n_I^2} \right\}^{\frac{1}{2}} \right] \tag{1.51}$$

The conductivity is therefore given by

$$\sigma_e = n_{AV} e \mu_{AV} + n_{CV} e \mu_{CV} \tag{1.52}$$

$$= Ne(\mu_{AV} + \mu_{CV}) \exp(-g_S/2kT) \times$$

$$\times \left[\left\{ 1 + \frac{n_I^2}{4N^2 \exp(-g_S/kT)} \right\}^{\frac{1}{2}} + \right.$$

$$\left. + \frac{n_I}{2N \exp(-g_S/kT)} \frac{\mu_{CV} - \mu_{AV}}{\mu_{CV} + \mu_{AV}} \right] \tag{1.53}$$

from equations (1.50) and (1.51).

Recalling that the intrinsic conductivity (1.45) is equivalent to

$$\sigma_i = Ne(\mu_{AV} + \mu_{CV}) \exp(-g_S/kT),$$ (1.54)

we have from (1.53)

$$\sigma_e = \sigma_i \frac{n_I}{N \exp(-g_S/2kT)} \frac{\mu_{CV}}{\mu_{CV} + \mu_{AV}}$$ (1.55)

In deriving equation (1.55) we assumed that

$$n_I \gg 2N \exp(-g_S/2kT)$$

If we assume that $\mu_{CV} \gg \mu_{AV}$, equation (1.55) reduces to

$$\sigma_e = n_I e\mu$$ (1.56)

which is a quite obvious result in view of approximations. Using equations (1.42) and (1.56) we obtain

$$\sigma_e = \frac{4n_I a^2 e^2 \nu_{CV}}{kT} \exp\left(\frac{\Delta S_{CV}}{k}\right) \exp(-\Delta h_{CV}/kT)$$

(1.57)

which is approximately of the emperical form

$$\sigma_e = \sigma_{0e} \exp(-E_e/kT)$$

Comments on the result are as follows:

1. A comparison of equations for the intrinsic and extrinsic conductivities (equations (1.48) and (1.57)) is very much useful for explaining the experimentally observed orders of magnitude of the ratios σ_{Oe}/σ_{ie} and E_e/E_i.

2. The field dependence of conductivity cannot be explained on this simple basis.

1.6 Thermally Stimulated Discharge (TSD) Processes

The thermally stimulated discharge (TSD) is a technique that has contributed significantly to the current understanding of charge-storage and charge-decay in solids especially in electrets. The features that have contributed to its popularity are its high sensitivity and resolving power. Although TSD has a relatively short history it has already evolved into a basic tool for the identification and evaluation of dipole reorientation process. Its rapid growth is spurred on by the fact that charge-trapping and charge-transport phenomena are not only of vital importance for electrets, but also for other materials.

At room temperature charge-decay measurements are rather time consuming because of at such low temperatures the dipoles and charges remain virtually immobile [121-125]. However, when an electret is heated, the dipoles and charges

quickly regain their freedom of motion. Thermal stimulation
of the discharge therefore shortens the measurements consi-
derably. During such a heat stimulated discharge, an electret
connected to two electrodes generates a weak current that
shows a number of peaks when recorded as a function of
temperature. The shape and location of these peaks are
characteristics of the detailed information of the dipoles
(density, relaxation time, activation energy) and trapping
parameters (energies, concentration and capture cross section
of traps).

The method has its analogues in various branches
of solid state physics, viz. thermally stimulated conductivity
and thermally stimulated phosphorescence (thermoluminescence)
[126-130]. It was first applied systematically by Bucci and
his group [131], although some studies using the same
principle were done as early as 1936 [132-135]. Using the
new technique Bucci et al. investigated the dielectric
relaxation of impurity-vacancy complexes in ionic crystals.
They called their method ITC (Ionic Thermo-Current). Other
investigators use still different names [136-138], such as
electret thermal analysis [139], thermally stimulated
currents [140], thermally stimulated dielectric relaxation
[141], thermally assisted discharging, thermally activated
depolarization [142] and dielectric depolarization spectro-
scopy [143]. The variety of names illustrates the widening
interest that TSD has aroused in this field.

1.6.1 TSD in inorganic solids

Of the inorganic materials, the ionic crystals, and in particular the alkali halides, have been investigated extensively with TSD. This work was initiated by Bucci and his group [131]. They concentrated their work on the impurity-vacancy (I-V) dipoles formed when divalent impurities are added to monovalent crystals. Thermally stimulated currents arising from a nonuniform distribution of space charge have also been studied by Kessler and Caffyn [136]. The currents arising due to the reorientation of I-V dipoles and due to the nonuniform distribution of space charges in ionic crystals are generally called ionic thermo-currents (ITC). Recently ITC method has been accepted as a very effective and sensitive method for the investigation of various phenomena in ionic materials [144-154].

A detailed description of the principle, experimental methods and theoretical background of ITC is given in chapter VII. The chapter also explains how ITC method can be effectively utilised in studying phase transitions in ionic crystals.

1.7   Applications

According to Goodenough [155], applications of phase transitions may be classified into four groups:

1. the formation and/or motion of mobile boundaries
between two or more phase existing below a critical
temperature T_c,

2. changes in physical properties as the temperature
approaches T_c,

3. changes in properties at T_c, and

4. metastable phase obtained by control of the kinetics
of nucleation or diffusion required for the transformation
to stable phases.

Under the first category (phase transitions at
$T < T_c$), where one makes use of changes in the net material
properties by control of nucleation or movement of domain
boundaries of materials like ferroelectrics, ferroelastics,
ferromagnets, liquid crystals and superconductors. Liquid
crystals have been found useful for optical display, detect-
ion of temperature uniformity and impurities. These propert-
ies are related to the orientational order of molecules in
the temperature region between T_c and the melting point.
Superconductors (type II) can be used to create high
magnetic fields at low pressure; the ability of type I
superconductors to trap magnetic flux within the domains
of the normal material also have applications.

Two important properties which change near T_c are softening of an optical vibration mode before a displacive transition, and temperature dependence of spontaneous magnetisation in ferromagnets below T_c. These properties are used in dielectric and pyromagnetic detectors respectively. Device applications of soft-mode anomalies have been discussed by Fleury [156].

Coming to properties at T_c, we can conceive of uses being made of the latent heat of a first order transition. First order magnetic transitions could be used for switching. Semiconductor-metal transitions can be employed as circuit breakers, voltage dividers or optical switches.

The best known examples of metastable materials are glasses and other amorphous materials. Switching properties and other applications of such materials are well known.

Ferroelectrics are being applied on a wide scale. They are extensively used in high and ultrahigh capacitance capacitors, dynamic elements of memory and logical elements of electronic computers, electromechanical converters, capacitance analogues of thermistors and special thermistors with a positive temperature coefficient, high-voltage accumulators, electrets, radiation modulators and regulators of the quality of optical quantum generators, I-R

detectors, ferroelectric energy converters, frequency
multipliers, intermediate frequency filters, dielectric
amplifiers, relaxation oscillators, frequency modulators,
dielectric equipment for the adiabatic cooling method in the
ultra-low temperature range and in measurement of these
temperatures, parametric converters in electrometers and in
temperature autostabilizers. Ferroelectrics are also used
in pulse-generation circuits, devices for controlling lumi-
nescence of electroluminophores, voltage and current
stabilizers, ignition systems of motor cars, remote-control
of radio receivers, key circuits and coincidence circuits,
time relays etc. Recently, substances with both ferro-
electric and ferro- or anti-ferromagnetic properties has
been discovered so that we can expect a further widening
of the field of application of ferroelectrics.

REFERENCES

[1]   A.R. Ubbelohde, Quart. Rev. (London) 11, 246 (1957)

[2]   A.R. Ubbelohde, Reactivity of Solids, ed. J.H. de Boer,
      Elsevier, Amsterdam (1961)

[3]   C.N.R. Rao and K.J. Rao, Progress in Solid State
      Chemistry, ed. H. Reiss Vol.4, Pergamon Press,
      Oxford (1967)

[4]   C.N.R. Rao, Modern Aspects of Solid State Chemistry,
      ed. C.N.R. Rao, Plenum Press, New York (1974)

[5]   P. Ehrenfest, Proc. Amsterdam Acad. 36, 153 (1963)

[6]   L.D. Landau and E.M. Lifshitz, Statistical Physics,
      Pergamon Press, Oxford (1959)

[7]   C.N.R. Rao and K.J. Rao, Phase Transitions in Solid :
      An Approach to the Study of Physics and Chemistry
      of Solids, Mc Graw-Hill Inc. (1978)

[8]   Helen D. Megan, Ferroelectricity in Crystals, Methuen
      and Co. London (1957)

[9]   C.N.R. Rao and M. Natarajan, Crystal Structure Transform-
      ations in Binary Halides, NSRDS-NBS Monograph
      41, Washington D.C. (1972)

[10] C.N.R. Rao and G.V. Subba Rao, Transition Metal Oxides:
      Crystal Chemistry, Phase Transitions and Related
      Aspects, NSRDS-NBS Monograph 49, Washington D.C.
      (1974)

[11] C.N.R. Rao, B. Prakash and M. Natarajan, Crystal
      Structure Transformations in Inorganic Nitrites,
      Nitrates and Chromates, NSRDS-NBS Monograph 53,
      Washington D.C. (1975)

[12] C.N.R. Rao and P. Prakash, Crystal Structure Trans-
      formations in Inorganic Sulphates, Chromates,
      Phosphates and Perchlorates, NSRDS-NBS Monograph
      56, Washington D.C. (1975)

[13] C.N.R. Rao and K.P.R. Pisharody, Progress in Solid
      State Chemistry, Pergamon Press, Oxford, Vol.10
      (1975)

[14] J.B. Goodenough and J.M. Longo, Crystallographic and
      Magnetic Properties of Perovskite and Perovskite
      Related Compounds, Landolt-Bornstein New Series,
      Group III, Vol.4a, Springer-Verlag, Berlin (1970)

[15] H.M. Rietveld, J. Appl. Cryst. 2, 65 (1969)

[16] K.J. Rao and C.N.R. Rao, J. Materials Sci. 1,
      238 (1966)

[17] M. Natarajan, A.R. Das and C.N.R. Rao, Trans. Faraday
      Soc. 65, 3081 (1969)

[18] J.B. Goodenough, Magnetism and Chemical Bond, John
      Wiley, New York (1963)

[19] E. Barthelemy, O. Gorochov and H.McKinzie, Mat. Res.
      Bull. 8, 1401 (1973)

[20] W.J.L. Burgers, G. Dowling, J. Sakurai and R.A. Cowley, Neutron Inelastic Scattering, Proceedings of IAEA Symp. Copenhagen 2, 126 (1968)

[21] D.S. McClure, Excitons, Magnons and Phonons in Molecular Crystals, ed. A.B. Zahlan, Cambridge University Press, London (1968)

[22] J. Chenavas, J.C. Joubert and M. Marezio, Solid State Commun. 9, 1057 (1971)

[23] P. Day et al. Phys. Rev. Lett. 30, 19 (1973)

[24] P. Day et al. Chem. Phys. Lett. 19, 529 (1973)

[25] D.R. Huffmann and R.L. Wild, Phys. Rev. 148,526 (1966)

[26] W.S. Carter and K.W.H. Stevens, Proc. Phys. Soc. B69, 1006 (1956); 76, 969 (1960)

[27] W. Rudorff, G. Walter and J. Stadler, Z. Anorg.u Allgem 297, 1 (1958)

[28] F.J. Morin, Phys. Rev. 78, 819 (1950)

[29] P.H. Carr and S. Foner, J. Appl. Phys. Suppl. 31, 3445 (1960)

[30] T. Shinjo and K. Kosuge, J. Phys. Soc. Japan 21, 21, 2622 (1966)

[31] K. Dwight, R.W. German, N. Menyuk and A. Wold, J. Appl. Phys. 33, Suppl. 3, 1341 (1962)

[32] B. Van Laar, Phys. Rev. 156, 654 (1967)

[33] K. Dwight, N. Menyuk and J.A. Kafalas, Phys. Rev. B2, 3630 (1970)

[34] T.J.A. Popma, C. Haas and B. Van Laar, J. Phys. Chem.
     Solids 32, 581 (1971)

[35] H.F. Franzen, D.M. Strachen and R.G. Barnes, J. Solid
     State Chem. 7, 374 (1973)

[36] J.P. Delamaire, H. Le Brusq and F. Marion, Acad.
     Sci. C272, 2144 (1971)

[37] F. Gronvold, H. Heraldsen, B. Pedersen and T. Tufte,
     Rec. Chim. Min. 6, 215 (1969)

[38] A.B. De Vries and C. Hass, J. Phys. Chem. Solids 34,
     651 (1973)

[39] C.B. Van den Berg, Ferroelectrics 4, 117 (1972)

[40] J.B. Goodenough, Phys. Rev. 164, 785 (1967)

[41] H.B. Mathur, Solid State Chemistry ed. C.N.R. Rao,
     Marcel Dekker, New York (1974)

[42] D.G. Wickham and W.J. Croft, J. Phys. Chem. Solids
     7, 351 (1958)

[43] E.J.W. Verwey et al. J. Chem. Phys. 15, 174 (1947)

[44] T. Riste and L. Tenzer, J. Phys. Chem. Solids 19,
     117 (1961)

[45] M.T. Evans, E. Warming and G.L. Squires, Neutron
     Inelastic Scattering : Proc. of the Grenoble
     Symp. IAEA (1972)

[46] W. Kudig, H. Bommel, G. Constabaris and R.H.Lindquist,
     Phys. Rev. 142, 327 (1966)

[47] W. Kudig and R.S. Hargrove, Solid State Commun.
       7, 223 (1969)

[48] J.B. Goodenough, J. Appl. Phys. 39, 403 (1968)

[49] J.M. Pollock and M. Sharan, J. Chem. Phys. 51,
       3604 (1969)

[50] E.J. Murphy, J. Appl. Phys. 35, 2609 (1964)

[51] V. Hugo Schmidt, J. Chem. Phys. 38, 2783 (1963)

[52] Y.V.G.S. Murti and P.S. Prasad, Physica   77, 543
       (1974)

[53] Y.V.G.S. Murti and P.S. Prasad, Physica   79B, 243 (1975)

[54] J. Appel, Solid State Phys. 21, 193 (1968)

[55] D.B. McWhan and J.P. Remeika, Phys. Rev. B2, 3734 (1970)

[56] B.K. Chakravarty, J. Solid State Chem. 12, 376 (1975)

[57] C.N.R. Rao and G.V. Subba Rao, Phys. Stat. Solidi(a)
       1, 597 (1970)

[58] A.K. Cheetam and C.N.R. Rao, Acta Cryst. B32, 1579
       (1976)

[59] N.F. Mott, Metal Insulator Transitions, Taylor and
       Francis, London (1974)

[60] D.B. McWhan and T.M. Rice, Phys. Rev. Lett. 22, 887
       (1969)

[61] D. Adler, J. Feinleib, H. Brooks and W. Paul, Phys.
       Rev. 155, 851 (1967)

[62] J. Feinleib and W. Paul, Phys. Rev. 155, 841 (1967)

[63] N.F. Mott, Rev. Mod. Phys. 40, 677 (1968)

[64] J.B. Goodenough, Mat. Res. Bull. 2, 37 (1967)

[65] L.K. Keys and L.N. Mulay, Phy. Rev. 154, 453 (1967)

[66] C.N.R. Rao, S. Ramdas, R.E. Lochman and J.M. Honig,
      J. Solid State Chem. 3, 83 (1971)

[67] M. Marezio, J. Solid State Chem. 6, 213 (1973)

[68] S. Kachi, K. Kosuge and H. Okinaka, J. Solid State
      Chem. 6, 258 (1973)

[69] C.N.R. Rao, G.R. Rao and G.V.S. Rao, J. Solid State
      Chem. 6, 258 (1973)

[70] A. Jayaraman, V. Narayanamurti, E. Bucher and
      R.G. Mains, Phys. Rev. Lett. 25, 368 (1970)

[71] A. Chatterjee, A.K. Singh, A. Jayaraman and E. Bucher,
      Phys. Rev. Lett. 27, 1571 (1971)

[72] A Jayaraman, E. Bucher, P.D. Dernier and L.D.
      Longinotti, Phys. Rev. Lett. 31, 700 (1973)

[73] A. Jayaraman, Narayanamurti, E. Bucher and R.G. Maines,
      Phys. Rev. Lett. 25, 430 (1970)

[74] C.N.R. Rao, J. Indian Chem. Soc. 51, 979 (1974)

[75] D.S. Rajoria, V.G. Bhide, G.R. Rao and C.N.R. Rao,
      J. Chem. Soc. Faraday II, 70, 512 (1974); See
      also Phys. Rev. B8, 5028 (1973)

[76] V.G. Jadhao, R.M. Singru, G.N. Rao, D. Bahadur and
      C.N.R. Rao, J. Phys. Chem. Solids 37, 113 (1975);
      See also J. Chem. Soc. Faraday II, 71, 1885 (1975)

[77] L.D. Landau, Collected Papers of L.D. Landau
ed. D. ter Haar, Gordon and Breach, New York
(1954)

[78] A.F. Devonshire, Phil. Mag. 40, 1040 (1949)

[79] A.F. Devonshire, Phil. Mag. 42, 1065 (1951)

[80] F. Fatuzzo and W.J. Merz, Ferroelectricity,
John Wiley, New York (1967)

[81] R. Blinc and B. Zerks, Soft Modes in Ferroelectrics
and Antiferroelectrics, North Holland,
Amsterdam (1974)

[82] E.C. Subba Rao, Solid State Chemistry ed. C.N.R.Rao,
Marcel Dekker, New York (1974)

[83] J. Villain and S. Aubry, Phys. Stat. Solidi 33,
337 (1969)

[84] P B. Owens and G.R. Argune, Science 157, 308 (1967)

[85] G.G. Bentle, J. Appl. Phys. 39, 4037 (1968)

[86] W. Schottky, Z. Phys. Chem. Abt. B29, 335 (1935)

[87] C. Wagner, Z. Phys. Chem. Abt. B38, 325 (1938)

[88] N.F. Mott and M.J. Littleton, Trans. Faraday
Soc. 34, 485 (1938)

[89] N.F. Mott and R.W. Gurney, Electronic Process
in Ionic Crystals, 2nd ed. Oxford Press,
London (1948)

[90] A.B. Lidiard, Handbuch der Physik, Vol.20, p.246
(1957)

[91] A.B. Lidiard, Phys. Rev. 94, 29 (1954)

[92] I. Boswara and A.B. Lidiard, Phil. Mag. 16, 805 (1967)

[93] R.G. Fuller, C.L. Marquardt, M.H. Reilly and

J.C. Wells Jr., Phys. Rev. 176, 1036 (1968)

[94] R.G. Fuller and H.B. Rosenstock, J. Phys. Chem.

Solids, 30, 2105 (1969)

[95] R.G. Fuller and M.H. Reilly, Phys. Rev. Lett.

19, 113 (1967)

[96] R.G. Fuller, Bull. Am. Phys. Soc. 15, 384 (1970)

[97] R.G. Fuller and M.H. Reilly, J. Phys. Chem. Solids

30, 457 (1969)

[98] R.G. Fuller and F.W. Pattern, J. Phys. Chem. Solids

31, 539 (1970)

[99] L.W. Barr and A.B. Lidiard, Defects in Ionic Crystals,

in Physical Chemistry An Advanced Treatise Vol.X

Academic Press, New York (1970)

[100] D.K. Dawson and L.W. Barr, Phys. Rev. Lett. 19,

844 (1967)

[101] W. Franklin, Phys. Rev. 180, 682 (1969)

[102] G. Shennon, Diffusion in Solids, McGraw-Hill,

New York (1963)

[103] H.R. Glyde, Rev. Mod. Phys. 39, 373 (1954)

[104] E. Pitts, Proc. Roy. Soc. A217, 43 (1953)

[105] C. Ramasastry and Y.V.G.S. Murti, Proc. Roy. Soc.

305, 441 (1968)

[106] F.A. Kroeger, J. Chem. Phys. 51, 4025 (1969)

[107] S. Chandra and J. Rolfe, Can. J. Phys. 48, 397
       (1970)

[108] S. Chandra and J. Rolfe, Can. J. Phys. 48, 412
       (1970)

[109] V.C. Nelson and R.J. Friauf, J. Phys. Chem. Solids
       31, 825 (1970)

[110] P.L. Read and E. Katz, Phys. Rev. Lett. 5, 466
       (1960)

[111] Y.V.U.S. Murti and P.S. Prasad, Proc. Nuclear Phys.
       and Solid State Phys. Symp. (India) 17C, 67 (1974)

[112] T.M. Herrington and L.A.K. Stavely, J. Phys. Chem.
       Solids 25, 921 (1964)

[113] Y.V.G.S. Murti and C.S.N. Murthy, J. de Physique
       34, C9 (1973)

[114] D. Mapother, H.N. Crooks and R.J. Maurer, J. Chem.
       Phys. 18, 1231 (1950)

[115] D. Patterson, J.A. Morrison and G.S. Rose Phil.
       Mag. 1, 393 (1956)

[116] G. Arai and J.G. Mullen Phys. Rev. 143, 663 (1966)

[117] A.M. Karo and J.R. Hardy, Phys. Rev. B3, 3418 (1971)

[118] H. Rabin and C.C. Klick, Phys. Rev. 117, 1005 (1960)

[119] N.L. Peterson and S.J. Rothman, Phys. Rev. 177,
       1329 (1969)

[120] H. Kelting and H. Witt, Z. Phys. 126, 697 (1949)

[121] A. Chowdry, C.R. Westgate, J. Phys. D 7, L149 (1974)

[122] V.M. Fridkin and I. Zheludev, Photoelectrets and
       Electrographic Process, Consultant Bureau, New
       York (1961)

[123] V.M. Fridkin, Photoferroelectrics, Springer Series
       in Solid State Sci. Vol.9, New York (1979)

[124] B. Gross, Charge Storage in Solid Dielectrics,
       Elsevier, Amsterdam (1964)

[125] M. Latour, Ann. Phys. (Paris) 7, 115 (1972)

[126] R.H. Bube, Photoconductivity of Solids, Wiley,
       New York (1960)

[127] P. Braunlich, Thermoluminescence and Thermally
       Stimulated Luminescence of Geological Materials,
       ed. D.J. McDougall, Academic Press, New York
       (1968)

[128] A.G. Milnes, Deep Impurities in Semiconductors,
       Wiley-Interscience, New York (1973)

[129] G.F.J. Garlick, Luminescence in Handbuch der Physik,
       Vol.26 ed. S. Flugge, Springer (1958)

[130] D. Curie, Luminescence in Crystals, Wiley, New York
       (1963)

[131] C. Bucci, R. Fieschi and G. Guidi, Phys. Rev. 148,
       816 (1966)

[132] H. Frei, G. Groetzinger, Phys. Z. 37, 720 (1936)

[133] O.G. Von Althein, Ann. Phys. (Leipzig) 35, 417
(1939)

[134] B. Gross, R.J. de Moraes, J. Chem. Phys. 37, 710
(1962)

[135] A.N. Gubkin, B.N. Matsonashvili, Sov. Phys. Solid
State 4, 878 (1962)

[136] A. Kessler and J.E. Caffyn, J. Phys. C5, 1134 (1972)

[137] R. Chen, J. Mater. Sci. 11, 1521 (1976)

[138] L. Brehmer, Faserforsch. Textiltech. 28, 43 (1977)

[139] Takamatsu, E. Fukada, Polym. J. 1, 101 (1970)

[140] M.M. Perlman, J. Electrochem. Soc. 119, 892 (1972)

[141] J.G. Simmons, G.W. Taylor, Phys. Rev. B6, 4804
(1972)

[142] P.R. Moran, D.E. Fields, J. Appl. Phys. 45, 3266
(1974)

[143] P. Hedvig, Dielectric Spectroscopy of Polymers,
Hilger, Bristol (1977)

[144] M. Puma, E. Laredo, M.E. Galavis and D.R. Figueroa,
Phys. Rev. B22, 5791 (1980)

[145] D. Kostopoulos, P. Varotsos and S. Mourikis,
J. Phys. C 13, 3003 (1980)

[146] E. Laredo, M. Puma and D. Figueroa, Phys. Rev.
B19, 2224 (1979)

[147] D.L. Kirk and R.M. Innes, J. Phys.C 11, 1105 (1978)

[148] G.E. Matthews and J.H. Crawford Jr. Phys. Rev. B15,
       55 (1977)

[149] J. Prakash and F. Fischer, Phys. Stat. Solidi (a)
       39, 499 (1977)

[150] A.M. Hor, P.W.M. Jacobs and K.S. Moodie, Phys. Stat.
       Solidi (a) 38, 293 (1976)

[151] B.P.M. Lenting, J.A.J. Numan, E.J. Bijvank and
       H.W. den Hartog, Phys. Rev. B14, 1811 (1976)

[152] A. Kessler, Solid State Commun. 12, 697 (1973)

[153] R. Capelletti and R. Fieschi, Electrons, Charge
       Storage and Transport in Dielectrics ee MM
       Perlman, Princeton : Electrochem. Soc. (1973)

[154] Bucci and Riva, J. Phys. Chem. Solids 26, 363
       (1965)

[155] J.B. Goodenough, in Phase Transitions, ed.
       H. Henisch, R. Roy, L.E. Cross, Pergamon Press,
       New York (1973)

[156] P.A. Fleury, in Phase Transitions, ed. H. Henisch,
       R. Roy, L.E. Cross, Pergamon Press, New York
       (1973)

CHAPTER II

EXPERIMENTAL TECHNIQUES AND METHODS OF MEASUREMENTS

Abstract

The general experimental techniques and the
methods of measurements used for the present investi-
gation are given. The different sections contain
descriptions of the methods of sample preparation,
different types of furnaces and cells fabricated and
used for various temperature regions and the methods
of measurements of electrical conductivity, dielectric
constant and ionic thermo-currents in crystals.

2.1   Introduction

An extensive and elaborate experimental programme was necessary to complete the investigations presented in this thesis. Only brief descriptions of the general experimental techniques adopted have been given in the present chapter. Any variation from the general experimental procedure required in the context of specific problems has been indicated at appropriate places.

The different sections of this chapter deal mainly with the various aspects of experimental arrangements. They include the technique for growing the crystals used in these studies, the methods of sample preparation, descriptions of the different type of furnaces and cells for various temperature regions and the methods of measurements of d.c. electrical conductivity, dielectric constant and of ionic thermocurrent in crystals.

2.2   Sample Preparation

2.2.1 Crystal growth

2.2.1.1. Growth from melt: Good quality single crystals were grown from melt as well as from solution. Eventhough most of the crystals studied here have been grown from solution, melt grown crystals (pure and doped $NaNO_3$) were used for standardising the measuring set-up using the already available

results [1]. For this purpose a crystal growing furnace was
fabricated using the Bridgeman-Stockbarger technique [2] with
some modifications. The schematic diagram and the photograph
of the furnace are shown in Figs. 2.1 and 2.2 respectively.
The furnace has two temperature zones with separate control.
Thick walled corning glass tube was used as the inner compart-
ment of the furnace. Uniform temperatures in the two separate
zones have been ensured by inserting two brass tubes inside
the glass tube with a corning glass ring as the separator.
This glass ring serves two purposes: 1. it provides a proper
gradient in between the two uniform temperature zones and
slight changes in the gradient can be made by varying the
diamensions of this glass ring; 2. this serves as a window
through which the different stages of growth can be observed
visually. Samples were contained in evacuated and sealed
corning glass tubes with tapered bottom. Very slow drawing/
pulling rates have been achieved by using a clock-work motor
mechanism. The furnace was used for growing crystals with
melting point less than $350^\circ C$. The photograph of   fairly
large single crystals of $NaNO_3$ grown by using this furnace is
shown in Fig. 2.3.

2.2.1.2. Growth from solution: Growth from a saturated
solution has many practical advantages in the case of crystals
containing ammonium groups,   since most of them begins to
decompose near their melting point. Almost all the crystals

Fig.2.2   Photograph of the furnace used for growing
crystals from melt.

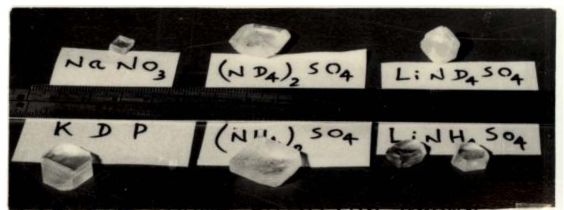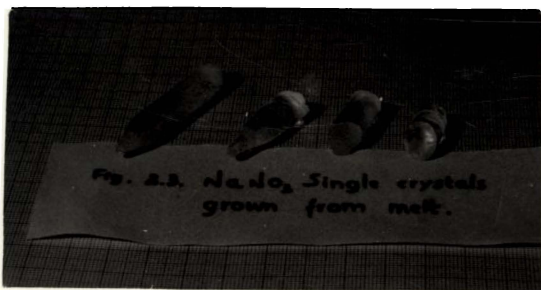Fig. 2.3. NaNO₃ Single crystals
grown from melt.

Fig.2.4   Some solution grown
single crystals.

used in this work were grown by slow evaporation at constant temperature of a saturated solution prepared with triply distilled water. A constant temperature water bath having a stability of ± 0.01°C in the temperature range 30 to 60°C was used for this purpose. Pure as well as doped single crystals of $LiNH_4SO_4$, $(NH_4)_2SO_4$, $(NH_4)_3H(SO_4)_2$, KH_2PO_4, $NaNO_3$,$LiND_4SO_4$ and $(ND_4)_2SO_4$ of fairly large size were grown by this method (photographs shown in Fig. 2.4).

2.2.2 Doping of the crystals

Doping of the crystals with various amount of divalent cationic impurities like Sr^{2+}, Ba^{2+}, Zn^{2+}, Mn^{2+}, Cu^{2+} etc. was carried out by adding proper amount of the corresponding salts with the same anions into the solution. For example, the doping of Cu^{2+} ions in $(NH_4)_2SO_4$ can be done by adding proper amount of $CuSO_4$ in to $(NH_4)_2SO_4$ solution. In the case of crystals grown from melt the dopants have been added to the bulk material before melting.

2.2.3 Deuteration

Crystals like $LiND_4SO_4$ and $(ND_4)_2SO_4$ were obtained by repeated recrystallisation (five times) of $LiNH_4SO_4$ and $(NH_4)_2SO_4$ respectively using heavy water of isotopic purity 99.8%. Single crystals of these were grown from a saturated solution using heavy water by slow evaporation. Nearly complete deuteration has been verified by using an IR spectrometer (Beckman IR20).

2.2.4 Estimation of impurities

The pure crystals used in this study were obtained after five recrystallisations of extrapure BDH Analar grade salt using triply distilled water. The purity of the Samples were tested by an atomic absorption spectrometer (Perkin Elmer 306) and it has been confirmed that the inherent impurity levels in the pure samples were below the detection limit of the instrument. The nominal concentrations of the added divalent cationic impurities like Cu^{2+} and Zn^{2+} were also estimated by the same instrument.

2.2.5 Preparation of samples from large single crystals

Large single crystals grown from solution, were cleaved/cut (using a wet thread) along the three crystallographic axes, as evidenced by their natural faces (in the case of melt grown crystals measurements were made only along their growth axis). Thin plate specimens having typical size 5 x 5 x 1 mm^3 with the edges along the three crystallographic axes were prepared by polishing the cut samples using zero grade emery and ground glass. The broad faces of the samples were coated with quick drying silver conducting paint which served as the electrodes.

2.3   Sample Holders

Several type of sample holders were used for studying the various electrical properties both in the low and high temperature regions. In all these cases spring loaded
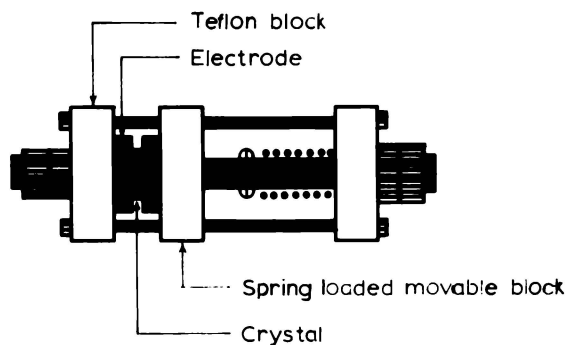
Fig. 2.5 a A GENERAL TYPE OF CRYSTAL HOLDER
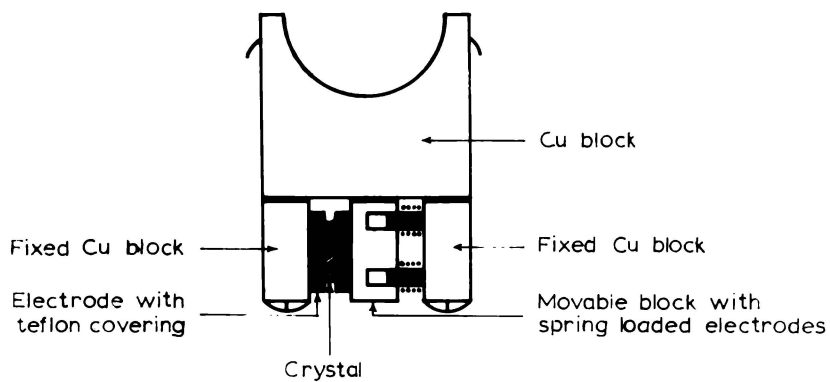USED FOR HIGH TEMPERATURE STUDIES

Fig. 2.5 b A GENERAL TYPE OF CRYSTAL HOLDER
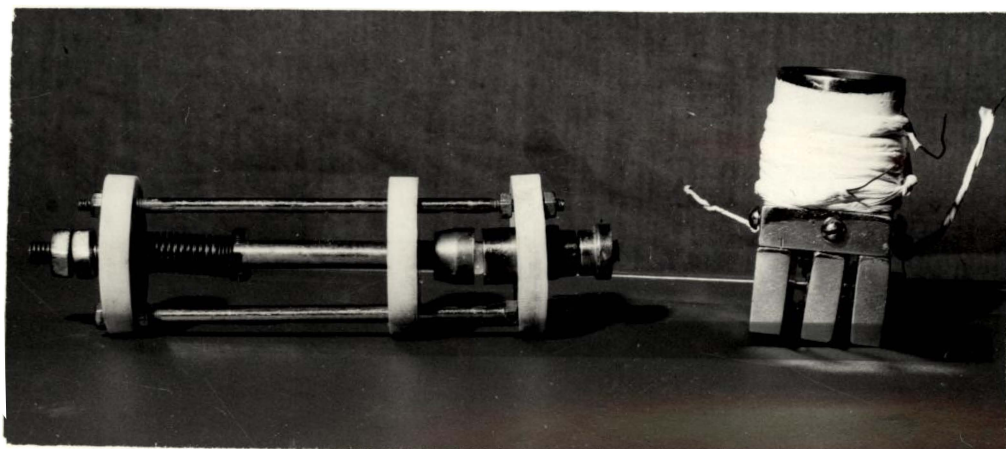USED FOR LOW TEMPERATURE STUDIES

Fig.2.6 Photograph of the crystal holders used in the low- and high-temperature regions.
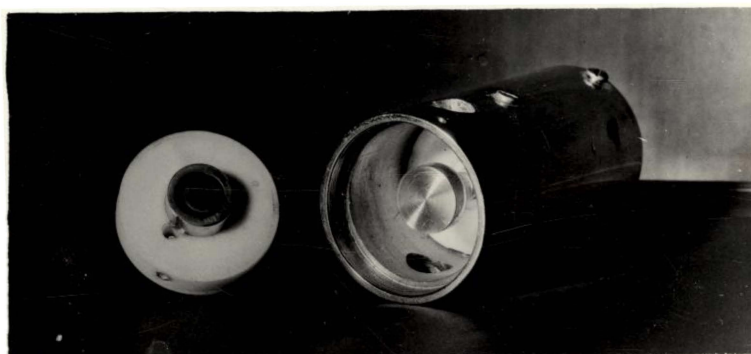

Fig.2.7 Sample holder with guarded electrode.

61

copper blocks provided with teflon insulations were used for holding the crystals. Schematic diagrams and photographs of two typical sample holders for the low and high temperature regions are shown in Figs. 2.5 and 2.6 respectively. In addition to these, some of the measurements were carried out using sample holders with guarded electrodes (Fig. 2.7). Also several low temperature measurements were made using a sample holder which had been built on to the measuring cell itself (Fig. 2.8).

2.4 Furnaces and Cells for Temperature Variation Studies

2.4.1 Furnace for high temperature studies

Figs. 2.9 and 2.10 show the schematic diagram and photograph of a corning glass furnace fabricated and used for studying the temperature variation of the different electrical properties in the high temperature region $(30-350^{\circ}C)$. This horizontal cylindrical furnace can be evacuated to a low pressure of 10^{-3} torr using a rotary pump or it can be filled with an inert gas. The stray electrical disturbances have been completely eliminated by a metallic shielding. The electrical leakage current through the mount has been by-passed to earth by grounding the mount. Heating tapes with fibreglass insulation was used as the heater. The power to this heater is provided from a servo-controlled stabilizer unit and the temperature is varied by
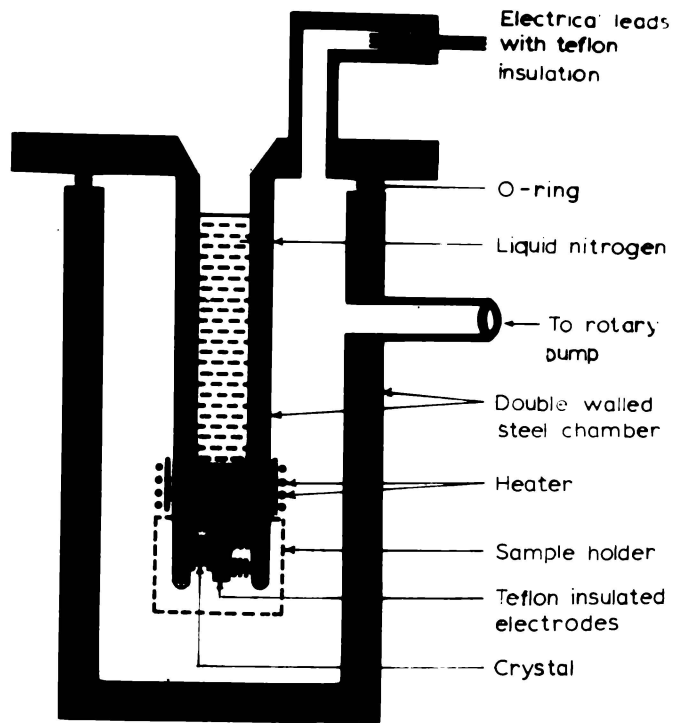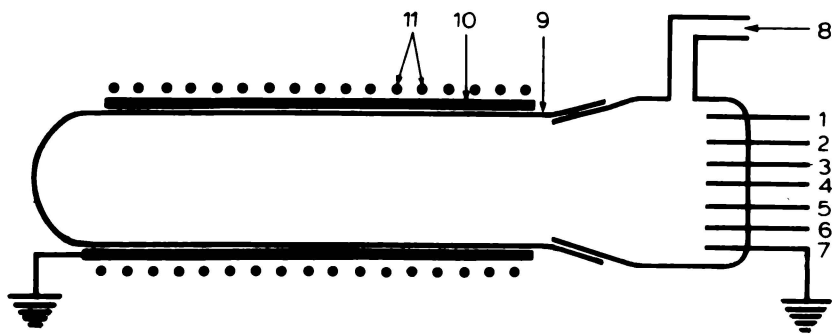
Electrical leads with teflon insulation

O-ring

Liquid nitrogen

To rotary pump

Double walled steel chamber

Heater

Sample holder

Teflon insulated electrodes

Crystal

Fig. 2.8 METAL CELL USED FOR LOW TEMPERATURE STUDIES

1,2,3 and 4. Thermocouple leads   9. Corning glass furnace

5 and 6. Leads from the electrodes   10. Metalic shelding

7. Lead from the sample holder chasis   11. Heating tape

8. To rotary pump

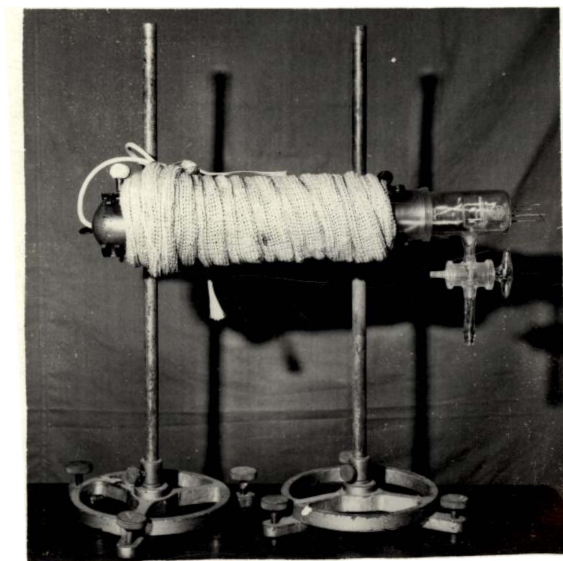**Fig. 2.9   FURNACE USED FOR HIGH TEMPERATURE (30-350°) STUDIES**

Fig.2.10   Photograph of the glass cell used for high-temperature studies.

using a dimmerstat which is calibrated to give the temperature
of the furnace as well as the rate of heating. A variation of
± 2µV in the thermocouple voltage is indicated by a lab-made
unit which is counter checked with a digital microvoltmeter.
Temperature measurements were carried out by two thermocouples
(Cu-Co/Fe-Co) arranged just above and below the specimen. Using
this set-up the temperature of the crystal could be controlled
with a stability and accuracy better than ± 0.1°C and ± 0.5°C
respectively.

2.4.2 Cell for low temperature studies (glass)

The schematic diagram and photograph of the low
temperature cell made of corning glass fabricated and used for
the measurements below room temperature to liquid nitrogen
temperature are shown in Figs. 2.11 and 2.12 respectively. The
cell consists of a double walled corning glass container for
liquid nitrogen having a male-female joint in its lower
portion. The inner tube has a narrow shape in this region
and ends in a hemispherical form. A sample holder (Fig. 2.8)
built in a massive copper block having a similar hemispherical
socket smoothly fits in the hemispherical end of the inner
tube and is tightly held in position with the help of
springs. The electrical leads are taken outside through a
side tube. A 50W (24V) heater with power supplied from a
highly stabilised d.c. source has been used for varying the
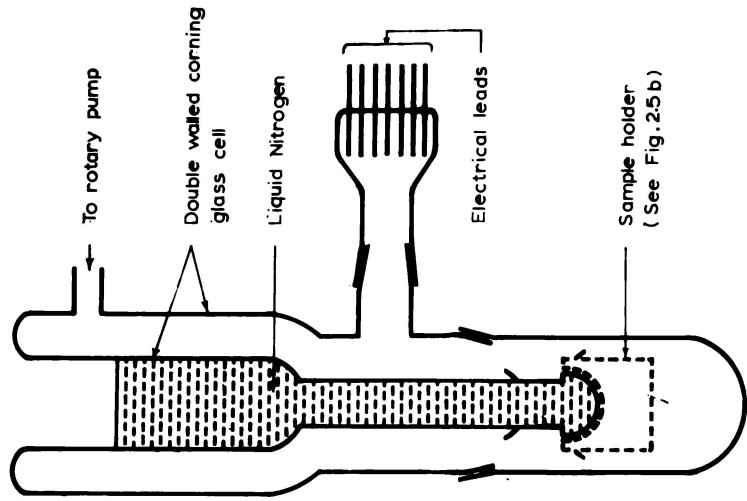temperature. Here also two thermocouples were used for

Fig.2.12 Photograph of the glass cell used for low-temperature studies.

To rotary pump

Double walled corning glass cell
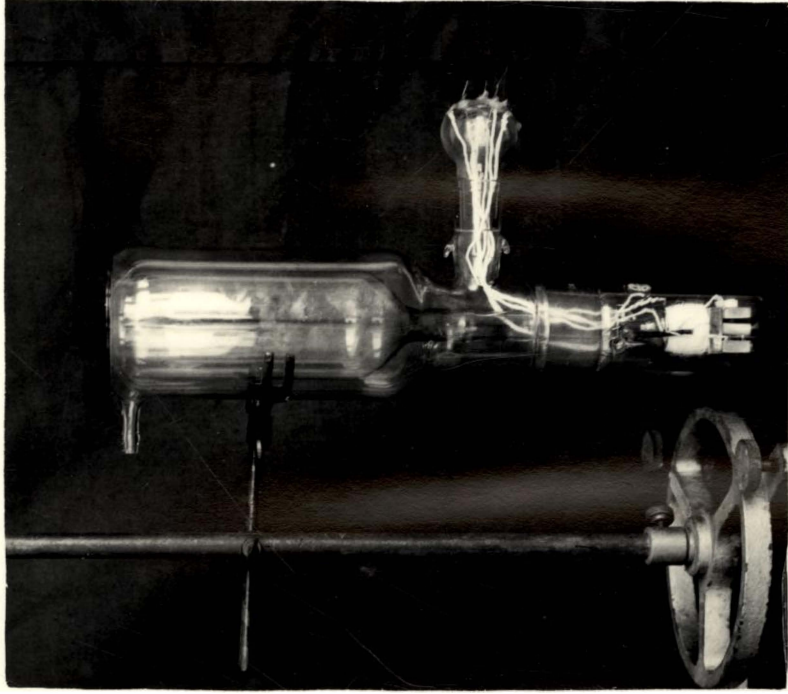
Liquid Nitrogen

Electrical leads

Sample holder (See Fig.2.5 b)

Fig. 2.11 GLASS CELL USED FOR LOW TEMPERATURE STUDIES

temperature measurements and as before, the temperature could
be controlled with a stability and accuracy better than $\pm$ 0.1°C
and $\pm$ 0.5°C respectively.

2.4.3   Cell for low temperature studies (metal)

Fig.2.8 shows the schematic diagram of the metal
(mild steel) cell fabricated and used for the low temperature
electrical properties, mainly for the ionic thermo-current
studies. As in the case of the glass cell, here the metal
cell also consists of a double walled cylindrical chamber
made of mild steel. The inner tube was welded to a large
plate and the outer enclosure was made leak proof by using
a neoperene 'O'-ring as shown in Fig. 2.8. As the radius
of the liquid nitrogen reservoir (inner tube) is so small
and the outer tube has a very large radius, the temperature
of the 'O'-ring will be almost at room temperature itself.
A sample holder similar to one used in the glass cell was
fitted (using screws) on to the bottom of the inner tube.
A 100W (24V) heater with stabilised d.c. source has been
used for temperature variations. The electrical leads
were taken out through teflon insulation. The method of
measurement of temperature is the same as described
earlier (Sec.2.4.2). Using this cell it is also possible
to keep the sample upto a temperature of 250°C.

The metal cell is found to be more suitable for studying the ionic thermo-currents, since it requires sudden quenching from high temperatures to liquid nitrogen temperature.

2.5   Methods of Measurements

2.5.1 Electrical conductivity

Since most of the crystals used in this study are normal ionic, these materials obviously have very low conductivity at and below room temperature. Several of them have a conductivity value less than 10^{-13} ohm^{-1}cm^{-1} near room temperature. Hence low current measuring instruments like Electrometer (ECIL EA815) or D.C. Microvoltmeter (Marconi TF2655) had to be used for conductivity measurements. A steady potential difference (ranging from 10 to 100V depending on the crystal) was applied across the prepared crystal samples kept in the conductivity mount and the resulting current was measured. Dry batteries are found to be more suitable for applying the steady voltage across the crystal than some of the highly stabilised power supplies working on the mains.

Eventhough the conventional method of measuring ionic conductivity is by the use of alternating currents in order to avoid polarization effects, the later studies [3-8] show that direct current methods are also very effective in
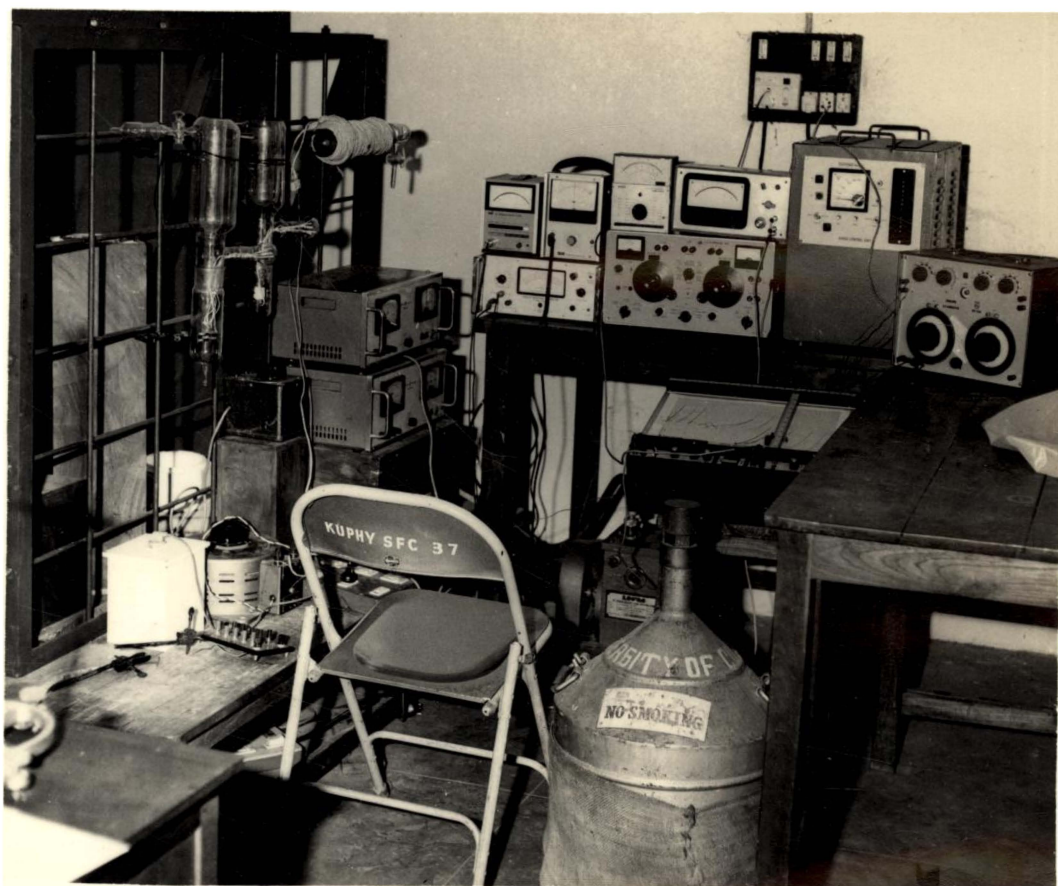
Fig.2.13   Experimental set-up for studying electrical
conductivity, dielectric constant and ionic
thermo-currents in crystals from liquid
nitrogen temperature to 350°C.

this regard. The effect of polarization can be avoided to a greater extent by the proper selection of the magnitude of the current through the crystal.

Occasionally when very low rate of heating was used, an X-Y recorder (Digital Electronics 2000) was employed to study the current variation through the sample especially near a phase transition point. In the low temperature region all the crystals show very low conductivity and in this region the heating was done by direct current. The stray electrical disturbances were eliminated by proper shielding. The electrical leakage current through the mounts were by-passed to earth by grounding its chassis so that the meter reading gives only the crystal current

2.5.2 Dielectric constant

The dielectric constant of all the crystals studied here have been obtained by measuring the capacitance of a parallel plate condenser with the crystal sample (typical size 8 x 8 x 1 mm^3) as the dielectric. The main problem in determining the dielectric constant of a crystal plate is to obtain the capacitance of the dielectric filled test capacitor from the measured total capacitance. The lead and fringe capacitances should be taken into account for this purpose. The conventional method generally employed is to reset the capacitor after removing the crystal to an air gap equal to the thickness of the crystal using a precision

micrometer arrangement [9,10]. The fringe capacitance can
also be reduced by using a guard ring. As these methods have
serious limitations, we have adopted the method due to
Ramasastry and Syamasundara Rao [11] for accounting the effect
of lead and fringe capacitances. The method generally employs
the use of a number of samples with different A/d values
(A- area, d- thickness). The total capacitance of each of
these sample is measured accurately by any one of the capaci-
tance measuring instrument. When the measured capacitance is
plotted against A/d, a straight will be obtained; the inter-
cept of which will give the sum of the lead and fringe capaci-
tances. Some of the measurements have also been done using
a sample holder with guarded electrodes.

The capacitance measurements have been performed
using a direct reading L.C. meter (Vasavi Electronics VLC1)
which has the following advantages in the measurement of
crystal capacitance.

1. The capacitance can be directly read from the meter with-
out making repeated adjustments as in the case of a bridge.
This enables one to take accurate readings even in the
vicinity of the transition points of crystals.

2. The effect of lead and fringe capacitance can be elimi-
nated using the offset provision of the instrument.

3. The conductivity of the test sample does not significantly
interfere with the measurement of capacitance.

4. The instrument has a maximum sensitivity of 0.05 PF with
very good stability.

The capacitance measurements have also been counter-
checked using a Marconi Universal bridge (TF 2700) and the
readings are found to be same as obtained from the L.C. meter
except at the transition points of the crystal where the
bridge is found to be not as suitable as the direct reading
instrument.

2.5.5 Ionic Thermo-currents (ITC)

An X-Y recorder together with an Electrometer/D.C.
Microvoltmeter has been used for the measurement of ionic
thermo-currents. The detailed method of measurements has
been given in chapter VII.

CHAPTER III

D.C. ELECTRICAL CONDUCTIVITY IN $LiNH_4SO_4$ AND $LiND_4SO_4$

Abstract

The results of the measurements of d.c. electrical conductivity of pure, doped, quenched and deuterated samples of $LiNH_4SO_4$ from liquid nitrogen temperature to $290^{\circ}C$ are presented in this chapter. $\wedge$-type conductivity anomalies are observed at 10 and $186.5^{\circ}C$ in the case of $LiNH_4SO_4$ and at -1.5 and $191^{\circ}C$ for $LiND_4SO_4$ respectively. The mechanisms of the phase transitions and of electrical transport process in the various phases of the crystal are discussed.

3.1   Introduction

Lithium ammonium sulphate (LAS) is an extremely
interesting room temperature ferroelectric material exhibiting
two phase transitions of the first order [1-9]. It is known
to have an orthorhombic symmetry with pseudohexagonal
structure belonging to the space group $Pna2_1$ with a = 5.280,
b = 9.140, c = 8.786 $\overset{o}{A}$ and Z = 4 [2]. On cooling it exhibits
a first order change to a polar monoclinic structure in the
vicinity of $10\,^{o}C$ at atmospheric pressure [1]. The second
transition which occurs at $186.5\,^{o}C$ has been reported by
Mitsui et al [3] and they showed that the crystal is ferro-
electric along the a-axis between the two transition points.
The three phases, space groups and the nature of the crystal
appearing successively while lowering the temperature are
denoted by phase I (Pnam) (paraelectric) $\xrightarrow{186.5\,^{o}C}$ phase II
$(Pna2_1)$ (ferroelectric) $\xrightarrow{10\,^{o}C}$ phase III $(P2_1/a)$ (ferro-
elastic). The Raman [10] as well as the infrared [11]
spectrum of this material has been studied in detail. Recent
studies include the NMR investigations of the effect of high
pressure [12,13].

In this chapter we discuss the results of our
investigations on the d.c. electrical conductivity of pure,
doped, quenched and deuterated samples of LAS from liquid
nitrogen temperature to $290\,^{o}C$.

3.2   Experimental

Single crystals of $LiNH_4SO_4$ and $LiND_4SO_4$ (DLAS)

were grown over a period of about three weeks from a saturated

solution by slow evaporation at a constant temperature of

33 ± 0.01^{o}C using triply distilled water and heavy water of

isotopic purity 99.8%. Doping of the crystals with Zn^{2+},

Cu^{2+} and Fe^{2+} ions has been done by adding proper amount of

the corresponding sulphates into the solution. The details

of the purification methods, estimation of impurities, sample

preparation and measurement of conductivity have already been

described in chapter II [14]. A steady potential difference

of 100V from dry batteries was applied across the crystal

samples of typical size 5x 5 x 1 mm^3. The rate of the

temperature change was 1°C/hr in the vicinity of the transi-

tion points and 5°C/hr in the other regions.

3.3   Experimental Results

3.3.1 For pure $LiNH_4SO_4$

The conductivity data were obtained on raising the

temperature from that of liquid nitrogen to 290°C and also

on cooling. The results were found to be very well reproduci-

ble for different samples as well as for different heating

and cooling runs. Curves denoted by (a) in Figs. 3.1 and 3.2

respectively show the conductivity plots for LAS along

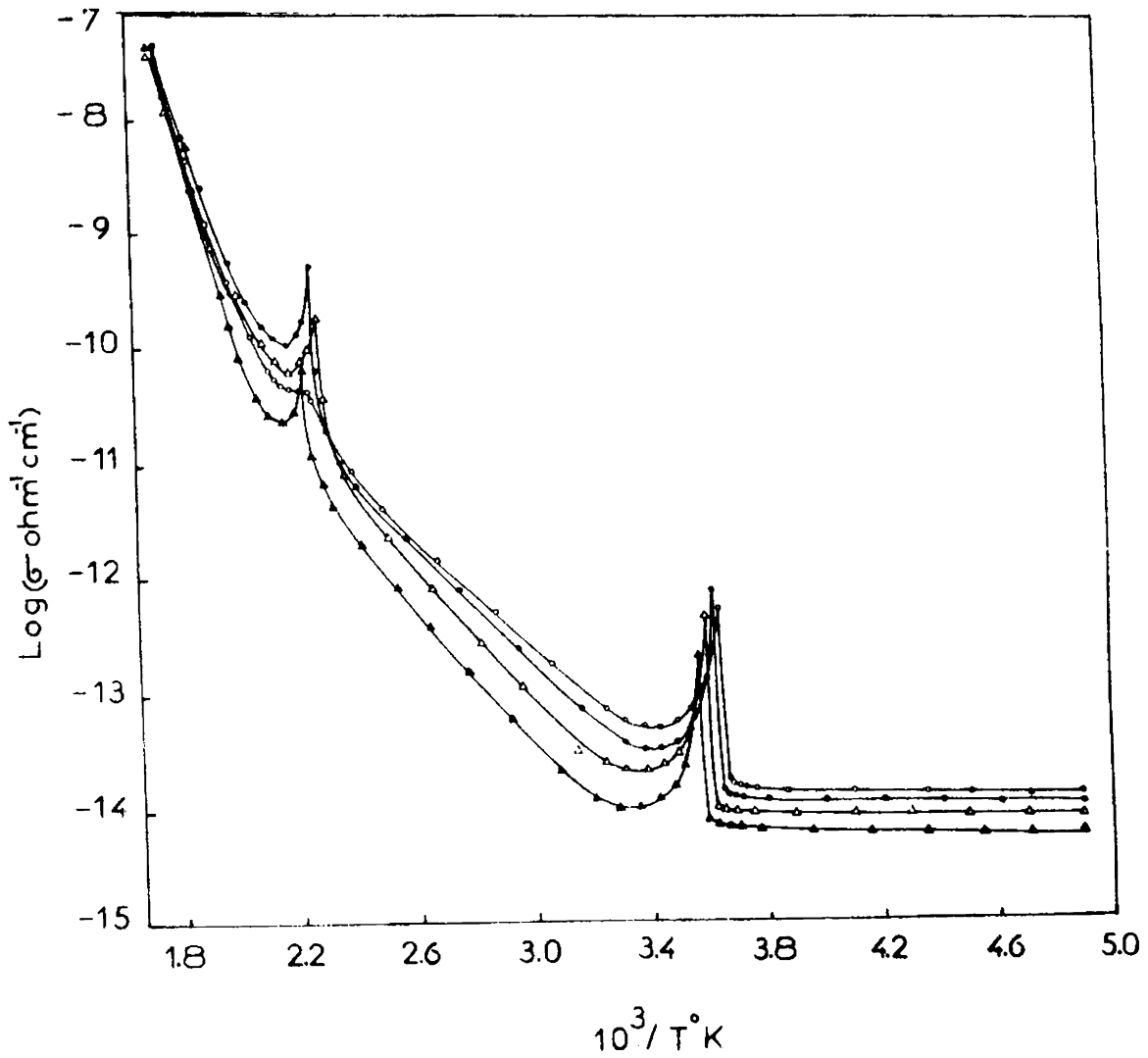a- (ferroelectric) axis and that along b-axis. The curve

Fig.3.1 Log σ vs $10^3/T$ plot for $LiNH_4SO_4$ single crystals along the ferroelectric axis (a-axis): —•—•— (a) pure sample, —○—○— (b) quenched from the upper transition temperature ▲—▲ (c) doped with Zn^{2+}, —○—○— (d) doped with Cu^{2+}.
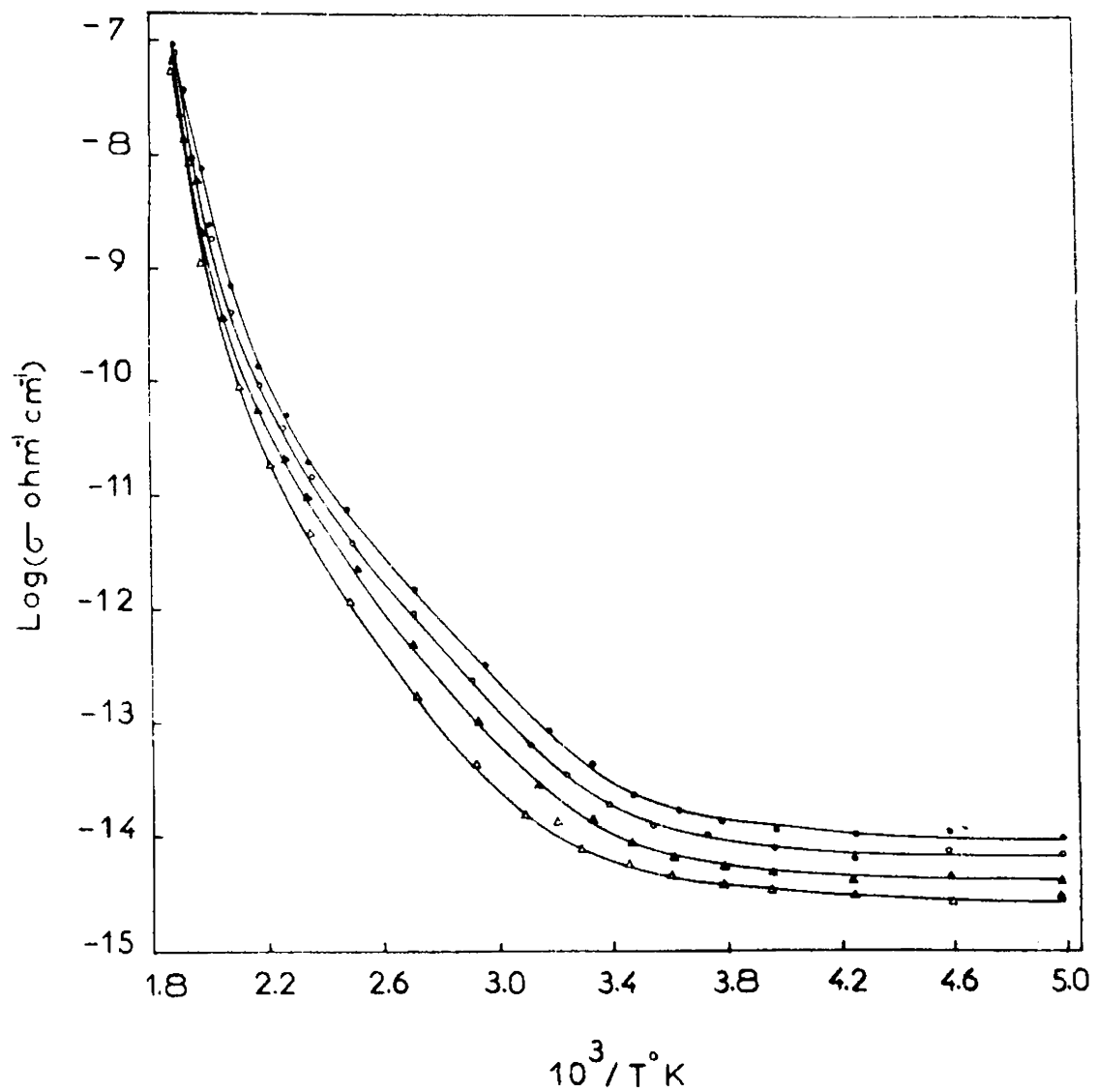
Fig.3.1 Log σ vs $10^3/T$ plot for $LiNH_4SO_4$ single crystals along the b-axis: —•—•— (a) pure sample, —○--○— (b) doped with Fe^{2+}, —▲—▲— (c) doped with Zn^{2+}, —▽--▽— (d) doped with Cu^{2+}.

for the c-axis is almost identical to that for b and hence
it is not shown in the figure. A striking feature of the
present result is that two distinct A-type conductivity
anomalies are observed, one at 10°C and the other at 186.5°C.
The transition at 10°C is quite abrupt and there is an
enormous increase in conductivity of about two orders of
magnitude, while the transition at 186.5°C is rather gradual
and the increase in conductivity is only about an order of
magnitude. It is found that slower rate of variation of
temperature gives sharper peaks. Except in the vicinity of
the transition points the plots have three distinct straight
line regions characteristic of ionic crystals [15]. The
linear regions of the curve denoted by (a) in Fig. 3.1 can
be described by the following equations:

$$\sigma_{LAS}(I) = 1.19 \times 10^6 \exp(-17,265/T), \qquad (3.1)$$

$$\sigma_{LAS}(II) = 1.09 \times 10^{-4} \exp(-6714/T), \qquad (3.2)$$

$$\sigma_{LAS}(III) = 5.01 \times 10^{-14} \exp(-287/T) \qquad (3.3)$$

Thus the conductivity of the whole region except in the
vicinity of the transition points can be written as

$$\sigma_{LAS} = \sigma_{LAS}(I) + \sigma_{LAS}(II) + \sigma_{LAS}(III) \qquad (3.4)$$

The slopes of the three linear regions give activation
energies 1.51, 0.58 and 0.025 eV in phases I, II and III of
the crystal respectively. In phase III the rate of variation

of conductivity is extremely small and the curve extends

almost parallel to the x-axis (region below $-70^{\circ}C$ is not shown

in figure).

3.3.2 Effect of doping

Electrical conductivity measurements were extended

to samples doped with divalent cationic impurities like

Zn^{2+}(105 ppm), Cu^{2+} (108 ppm) and Fe^{2+}(220 ppm) with a view

to explain the mechanism of electrical conduction in the

crystal. The conductivity plots corresponding to these doped

samples are also shown in Figs. 3.1 and 3.2. It is found that

these impurities have in general the effect of reducing the

conductivity of the crystal. The effect is more pronounced in

phase II. In phase III doping reduces the conductivity slightl

while in phase I it has a lower value upto $270^{\circ}C$ when compared

to the conductivity values for pure crystals. Above $270^{\circ}C$, the

curves for both pure and doped crystal merge into one another.

The activation energies of the doped crystals show a significan

increase in phase II and I while it has no change in phase III.

3.3.4 Effect of quenching (LAS)

In order to identify the type of carriers released

at the high temperature transition point of the crystal,

measurements have been made on pure samples quenched from the

upper transition temperature. The quenching has been performed

by keeping the sample at 186.5°C in vacuum for about 2 hrs and suddenly exposing it to a dry air jet. The plot denoted by (b) in Fig. 3.1 corresponds to such a quenched sample. It is found that this plot shows a higher conductivity in phase II, corresponding to a low activation energy of about 0.1 eV. A noticeable result is that quenching reduces the height of the high temperature /\-peak.

3.3.5 Effect of deuteration

Fig. 3.3 shows the log σ vs. $10^3/T$ plot for DLAS single crystals along the a-axis from liquid nitrogen temperature to 290°C. Here the corresponding variation for LAS is also shown alongside for comparison. As in the case of LAS, DLAS also exhibits two prominent /\-type conductivity anomalies occurring at -1.5°C and at 191°C. (No such anomalies are observed along b or c-axes and hence the plots are not given here. Also no measurable thermal hysterisis is noted in the heating and cooling runs). It is to be noted that for DLAS there is an upward shift of the high temperature transition point by 4.5°C and a downward shift of the low temperature transition point by 11.5°C when compared to the transitions in LAS. The height of the peak at the low temperature transition point is found to be unaffected by deuteration; but that for the high temperature transition point is reduced significantly. Also, the magnitude of electrical conductivity along all the axes in DLAS is found to be much lower than those in LAS in
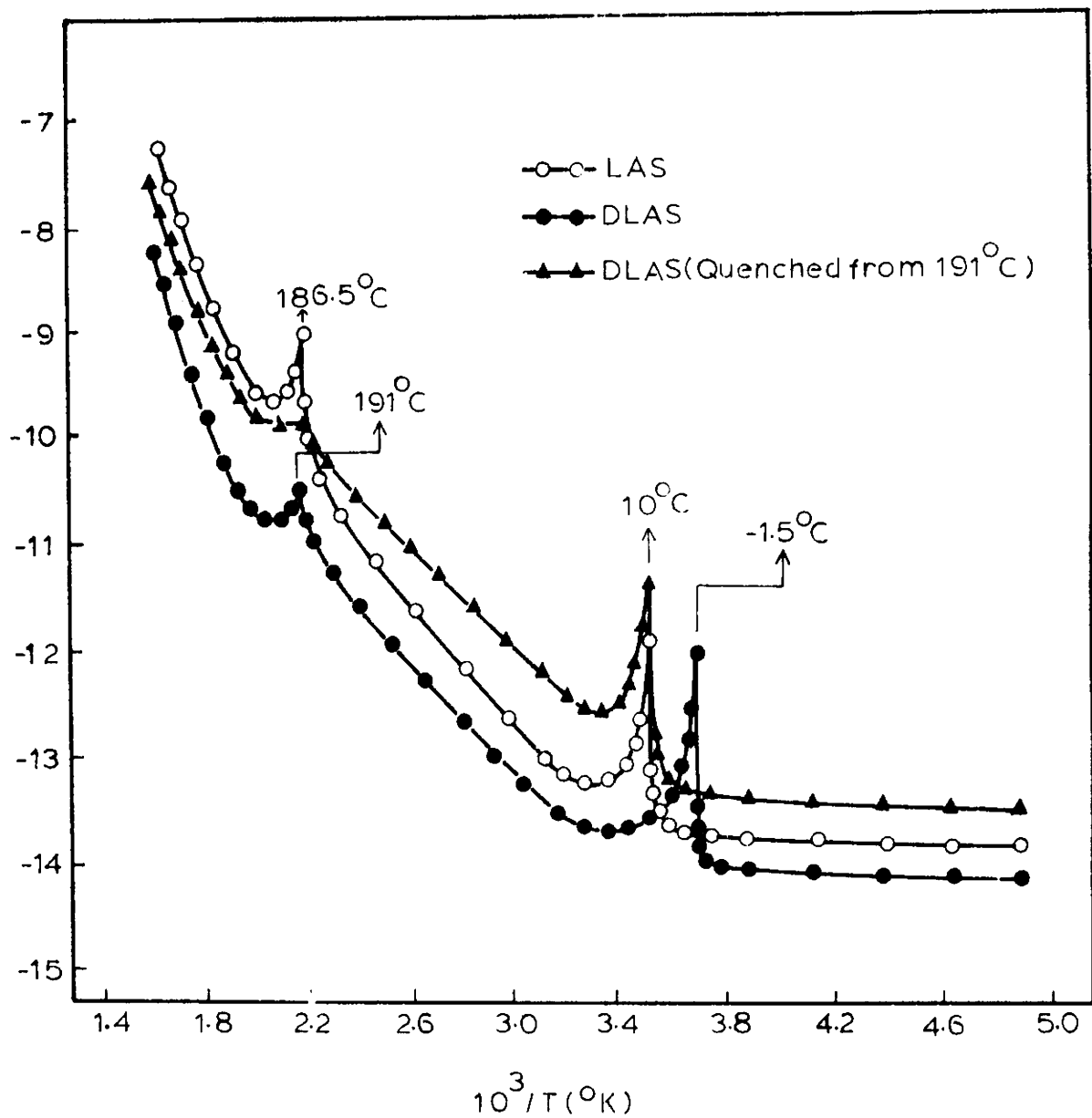
Fig.7.3 Effect of deuteration on the electrical conductivity and phase transition points in $LiNH_4SO_4$ (LAS).

all the three phases, wheree : the general shape of the conducti-
vity plots are the same. The conduction activation energies for
the DLAS sample show only a very slight variation in all the
phases (1.60, 0.57 and 0.025 for DLAS compared with 1.51, 0.58
and 0.025 eV for LAS in phases I, II and III respectively). The
distinct straight line regions corresponding to the conductivity
plots along a-axis for DLAS representing the three different
phases of the crystal can be described by the following equations:

$$\sigma_{DLAS}(I) \quad = 8.50 \times 10^4 \ \exp(-18573/T), \quad\quad (3.5)$$

$$\sigma_{DLAS}(II) \quad = 2.45 \times 10^{-5} \ \exp(-6598/T), \quad\quad (3.6)$$

$$\sigma_{DLAS}(III) = 2.82 \times 10^{-14} \ \exp(-267/T) \quad\quad (3.7)$$

From these equations it is evident that the lower value of
conductivity observed in all the three phases of DLAS is mainly
due to the decrease in the value of the pre-exponential factors
for conduction (8.50×10^4 2.45 $\times 10^{-5}$ and 2.82 $\times 10^{-14}$ for
DLAS against 1.19×10^6, 1.09×10^{-4} and 5.01 x 10^{-14} for LAS
in phases I, II and III respectively). The values of pre-
exponential factors for b or c axes are 2.3×10^4, 7.5×10^{-6}
and 1.1×10^{-14} in phases I, II and III respectively. (Acti-
vation energies are the same as for the a-axis).

3.3.6   Effect of quenching in $LiND_4SO_4$

The plot corresponding to a DLAS sample quenched
from $191^\circ C$ (the high temperature transition point) shows a

higher conduction than for the as grown sample in phases II
and III. In phase II this increase in conductivity due to
quenching is more than one order of magnitude with only a very
slight decrease in the activation energy. Furthermore quench-
ing has the effect of flattening the peak at $191^{\circ}C$ as in the
case of LAS, while the peak at $-1.5^{\circ}C$ is unaffected.

3.4   Discussion

3.4.1 Mechanism of electrical conduction in $LiNH_4SO_4$

It is well known that the electrical conduction in
ionic crystals is a defect controlled property. The defect
concentration increases exponentially with rise of temperature
and hence the electrical conduction enhances correspondingly.
In ionic crystals containing ammonium groups the possible type
of point defects are normal ionic and electronic defects as
found in alkali halides and conventional semiconductors and
protonic defects [16]. As a result conductivity may be ionic,
electronic and/or protonic. Generally in ionic crystals, the
electronic defects viz., electrons and holes are very small
in number. The protonic defects are the hydrogen ions removed
from the ammonium groups or the mixing hydrogen ions. In LAS
the ionic defects are lithium, ammonium and sulphate ions
(both vacancies and interstitials). Our experimentally well
confirmed result shows that the doping of the crystals with
divalent cationic impurities has a general effect of reducing

the electrical conductivity. To compensate the excess charge
of the added divalent positive ion impurities (Z^{2+}), positive
ion vacancies (V_p^-) or negative ion interstitials (X^-), may be
created in the crystal lattice. If the mechanism of electrical
conduction in the crystal is by the migration of either of
these defects, the conductivity must be enhanced. To account
for the observed decrease in conductivity, we should consider
the effect of the above increase in number of the negative
carriers on the concentration of other defects such as negative
ion vacancies (V_n^+) and positive ion interstitials (X^+). The
concentration of positive ion vacancy [V_p^-], exists in equali-
brium with the concentration of negative ion vacancy [V_n^+], and
also with the concentration of positive ion interstitials [X^+].
Similarly the concentration of negative ion interstitials [X^-],
exists in equalibrium with that of negative ion vacancy [V_n^+].
These may be expressed by the following equations [15,17]:

$$[V_p^-][V_n^+] = \exp\,(-g_S/kT) = x_S^2 \qquad (3.8)$$

$$[V_p^-][x^+] = \exp\,(-g_F/kT) = x_F^2 \qquad (3.9)$$

$$[X^-][V_n^+] = \exp\,(-g_{AF}/kT) = x_{AF}^2 \qquad (3.10)$$

Where S, F and AF stand for Schottky, Frenkel and AntiFrenkel
defects respectively, g for the free energy of formation of
defects and x for the concentration of either defects in pure
crystal. It is understood from the expressions (3.8) to (3.10)

that increase in $[V_p^-]$ or $[X^-]$ results in the decrease of $[V_n^+]$ and/or $[X^+]$. That is, the addition of divalent positive ion impurities into the lattice has the effect of decreasing the negative ion vacancies and/or positive ion interstitials. The conductivity will decrease if the process is mainly contributed by either anion vacancies or cation interstitials. On account of the larger size of the sulphate (Sulphur-Oxygen bond length in sulphate ion is 1.44 $\overset{o}{A}$ with oxygen having an ionic radius of 1.40 $\overset{o}{A}$) and ammonium ions (ionic radius 1.43 $\overset{o}{A}$), occurrence of interstitial ammonium and sulphate ions is less likely [18]. Also the mobility of the above interstitials and their vacancies is far less. Therefore the only ionic defect which can take part in the electrical conduction process is the interstitial lithium ions (with ionic radius 0.68 $\overset{o}{A}$). Now a comparison of the magnitude of conductivity in deuterated and undeuterated samples shows that the former one has a lower conductivity in all the phases than the latter. This leads to the conclusion that protons in LAS contribute significantly to the electrical transport process in LAS. Hence we can come to a final conclusion that the electrical conduction process in the crystal is mainly contributed by the migration of interstitial lithium ions along with the protonic defects.

The method of purification used in the case of LAS was of repeated recrystallisation (five times)using triply distilled water. Even this sample contains some amount of

divalent positive ion impurities (Z^{2+}) and divalent negative

ion impurities (Z^{2-}). One should therefore consider the effect

of association of these impurity ions with the more significant

charge compensators, viz., (V_p^-) and (X^+) to form complexes

$(Z^{2+}V_p^-)$ and $(Z^{2-}X^+)$. In phase I most of these complexes will

be entirely in dissociated states providing a greater number of

mobile defects resulting in a higher conductivity. In phase II

these complexes are only partially dissociated and hence the

conductivity will be comparatively smaller. In phase III the

existing impurity content may exceed the solubility limit and

the impurity may precipitate out as a separate phase. This

leads to a large reduction of carriers which explains the

lower portion of the electrical conductivity plot (Figs. 3.1

and 3.2).

The part of the electrical conductivity plot for LAS

(Figs. 3.1 and 3.2) above 270°C can be considered as the

intrinsic region since the curves corresponding to all the

samples merge into one another in this portion. Although the

actual values of conductivity are different along a- and

b-(c-) directions, the activation energies themselves are found

to be independent of direction. Thus it appears that the

mechanism of electrical conduction is the same for the differ-

ent directions in the crystal.

3.4.2 Explanation of the /\-type peaks based on the results
on quenched and deuterated samples

3.4.2.1. The high temperature /\-peaks. As in the case of
NH_4Cl [19,20], the $(NH_4)^+$ ions in LAS may be assumed to change
from a state of torsional oscillation to one of free rotation
while the crystal undergoes phase transition from phase II to
I. This may generate an enormous amount of protonic defects
giving rise to the conductivity anomaly at $186.5^\circ C$. Quenching
of the crystal from the transition point leads to freeze the
excess carriers produced at the transition point and these
frozen-in defects [15] may be responsible for the increase in
conductivity of the quenched sample. Hence the observed
decrease in activation energy value of 0.1 eV should corres-
pond to the migration of these frozen carriers. Murti et al
[21] estimated the activation energy of protons in NH_4Cl to be
0.08 eV by a plastic deformation experiment. A reasonable
assumption that the activation energy of protons in LAS is
not widely different from this value leads to the conclusion
that protonic conduction can be the phenomenon responsible for
the conductivity anomaly at $186.5^\circ C$.

The experimental results on the electrical conducti-
vity in DLAS samples conclusively show that DLAS also under-
goes two phase transitions at -1.5 and $191^\circ C$ corresponding to
the two transitions in LAS at 10 and $186.5^\circ C$. The transition
at $10^\circ C$ in LAS is a structural one (accompanied by a unit cell

doubling along the a-direction) which has already been studied in detail [6,7]. On the other hand no attempt was so far been made in studying the mechanism involved in recently observed high temperature transition in this crystal. Here the quenching experiment suggests that the conductivity anomaly at $186.5^\circ C$ in LAS is due to the sudden release of protons as a result of the onset of free rotation of the $(NH_4)^+$ ions in the crystal. Again the experimentally well confirmed result that the high temperature transition point shifts upwards in DLAS is completely in agreement with this suggestion and the observed increase in transition temperature by $4.5^\circ C$ corresponds to the additional energy required in the case of $(ND_4)^+$ ions to change over into a state of free rotation in DLAS. Also the earlier proposal that the sudden release of a large number of protonic defects generated due to the unrestricted rotation of the $(NH_4)^+$ ions leading to the high temperature conductivity anomaly in LAS is confirmed here by the experimental result that in deuterated samples, the peak height corresponding to the high temperature transition point has a much lower value as expected because of the lower mobility of the deuterons.

The quenching of the DLAS sample from $191^\circ C$ leads to the freezing of the newly generated carriers (the deuterons) produced at the transition point. This is also evident from the flattening of the peak in quenched sample. These frozen-in defects are responsible for the increase in conductivity of the quenched sample.

3.4.2.2. The low temperature Λ-peaks: Since the transition at $10^{\circ}C$ is a structural one, the sharp rise in conductivity at the transition point from phase III to II may be due to the large scale availability of the carriers released during the rearrangement process of the crystal lattice or due to the loosening of the same. The downward shift of the low temperature transition point in DLAS can be explained as follows. The pressure-temperature phase diagram of LAS [12] shows that the low temperature transition point of the crystal shifts downwards with increase in pressure. In many hydrogen bonded crystals substitution of deuterons in the place of protons reduces the mean amplitude of vibration and thereby alters the effective lengths of the hydrogen bonds in the crystal [22]. This effect can be considered as equivalent to an increase in the internal pressure. Hence one may expect a downward shift of this transition temperature on deuteration.

3.5   Conclusions

1. The measurement of d.c. electrical conductivity of $LiNH_4SO_4$ single crystal from liquid nitrogen temperature to $290^{\circ}C$ shows that two Λ-type conductivity anomalies exist in the log σ vs. $10^3/T$ plot for this crystal at 10 and $186.5^{\circ}C$.

2. The conductivity plots falls into three straight line regions except in the vicinity of the transition points showing the characteristics of ionic crystals.

3. Measurements made on $LiND_4SO_4$ reveal that this crystal also undergoes two phase transitions at -1.5 and $191^\circ C$ corresponding to the two transitions at 10 and $186.5^\circ C$ in $LiNH_4SO_4$.

4. The experimental results on doped and deuterated $LiNH_4SO_4$ samples reveal that the dominant mechanism of electrical transport in the crystal is the migration of interstitial lithium ions along with protonic defects.

5. Axiswise activation energy measurements show that the above mechanism of electrical transport in $LiNH_4SO_4$ is the same for the different directions in the crystal.

6. The conductivity anomaly at $10^\circ C$ in $LiNH_4SO_4$ is suggested to be due to the large scale availability of the carriers released during the rearrangement process of the crystal lattice or due to the loosening of the same. The downward shift of this transition temperature in $LiND_4SO_4$ is attributed to an increase in internal pressure arising from the substitution of deuterons in the place of protons.

7. The high temperature phase transition in $LiNH_4SO_4$ can be attributed to the onset of free rotation of the $(NH_4)^+$ ions in the crystal and the high temperature conductivity anomaly is suggested to be due to the sudden release of protons, when the $(NH_4)^+$ ions start free rotation from a state of torsional oscillation. The upward shift of this transition temperature by $4.5^\circ C$ in $LiND_4SO_4$ corresponds to the additional energy required in the case of $(ND_4)^+$ ions to change over into a state of free rotation.

REFERENCES

[1] R. Pepinsky, K. Vedam, Y. Okaya and S. Hoshino,
     Phys. Rev. 111, 1467 (1958)

[2] W.A. Dollase, Acta Crystallogr. B25, 2298 (1969)

[3] T. Mitsui, T. Oka, Y. Shiroishi, M. Takashige, K. Iio
     and S. Swada, J. Phys. Soc. Japan 39, 845 (1975)

[4] A.I. Kruglik, K.S. Aleksandrov and M.A. Simonov
     Kristallografia 23, 2 (1978)

[5] B.O. Hildman, Th. Hahn, L.E. Cross and R.E. Newnham,
     Appl. Phys. Lett. 27, 103 (1975)

[6] K.S. Aleksandrov, I.P. Aleksandrova, A.I. Kruglik,
     A.I. Krupnyi, S.V. Melnikova, V.E. Shneider
     and L.A. Shuvalov, Izv. Akad. Nauk SSR,
     Ser. fiz 39, 943 (1975)

[7] I.P. Aleksandrova, I.S. Kabanov, S.V. Melnikova,
     T.I. Chekmasova and V.I. Yuzvak Krystallografia
     22, 321 (1977)

[8] I.M. Iskornev and I.N. Flyorov, Fiz. tvered. Teta
     19, 1040 (1977)

[9] V.I. Yuzvak, L.I. Zerebstova, V.B. Shkuryaeva and
     I.P. Aleksandrova, Kristallografia 19, 773
     (1974)

[10] A.V.R. Warrier, Spectra of Crystals, Ph.D. Thesis
     Indian Institute of Science, Bangalore (1966)

[11] P. Kumara Acharya and P.S. Narayanan, Indian J. Pure and Appl. Phys. 11, 514 (1973)

[12] T.I. Chekmasova, I.S. Kabanov and V.I. Yuzvak, Phys. Stat. Solidi (a) 44, K155 (1977)

[13] T.I. Chekmasova and I.P. Aleksandrova, Phys. Stat. Solidi (a) 49,K185 (1978)

[14] U. Syamaprasad and C.P.G. Vallabhan, Solid State Commun. 34, 899 (1980)

[15] A.B. Lidiard, Handbuch der Physik 20, 246 (1957)

[16] F.A. Kroeger, J. Chem. Phys. 51, 4025 (1969)

[17] C. Ramasastry and Y.V.G.S. Murti, Proc. Roy. Soc. A305, 441 (1968)

[18] N.F. Mott and R.W. Gurney, Electronic Process in Ionic Crystals, 2nd edn (1964)

[19] Y.V.G.S. Murti and P.S. Prasad, Physica, 79B, 243 (1975)

[20] Y.V.G.S. Murti and P.S. Prasad, Proc. Nuclear Phys. and Solid State Phys. Symp. 17C, 67 (1974)

[21] Y.V.G.S. Murti and P.S. Prasad, Solid State Commun. 15, 1619 (1974)

[22] D. Hadzi, Hydrogen Bonding (Pergamon Press, New York 1959)

CHAPTER IV

ELECTRICAL CONDUCTIVITY AND PHASE TRANSITIONS
IN $(NH_4)_2SO_4$ AND $(ND_4)_2SO_4$

Abstract

This chapter presents the results of the studies on d.c. electrical conductivity of pure, doped, quenched and deuterated $(NH_4)_2SO_4$ single crystals. Anomalous variations in conductivity with temperature are observed in this crystal around $150^{\circ}C$ suggesting a new phase transition. Further an extension of the measurement of conductivity of $(NH_4)_2SO_4$ upto liquid nitrogen temperature shows that the crystal exhibits two phase transitions, instead of one at temperatures -49.5 and $-58^{\circ}C$; these transition temperatures remain unaltered in $(ND_4)_2SO_4$. Explanation based on rotations (for the high temperature transition) and successive distortions (for the low temperature transitions) of the nonequivalent $(NH_4)^+$ ions are given. The mechanisms of electrical conduction in the crystal also is discussed.

4.1   Introduction

The results of electrical conductivity studies on LiNH$_4$SO$_4$ (chapter III) [1-3] have conclusively shown that in the case of crystals of this type d.c. conductivity measurement is a simple and very sensitive tool for detecting phase transitions. In this chapter we have substantiated this point by extending these studies to ammonium sulphate (AS) which is a very well known material. Quite surprisingly these studies have revealed the existence of two more phase transitions in the crystal which have not been detected earlier.

Unlike lithium ammonium sulphate, $(NH_4)_2SO_4$ has two nonequivalent ammonium ions in a unit cell [4]. It is known to undergo a first order ferroelectric phase transition at -49.5°C. The symmetry of the crystal changes from D_{2h}^{16}- Pnam in the paraelectric phase to C_{2v}^9- Pna2$_1$ in the ferroelectric phase (T $<$ -50°C). The nature of this transition is rather unique and it has many features which are different from those of usual ferroelectrics. The peculiarity of this transition has been the subject of a large number of investigations which include structural [4], mechanical [5], dielectric [6-17], magnetic resonance [18-26] as well as infrared and Raman spectral studies [27-31]. On the other hand, the paraelectric phase of this material is not so well studied. Also, no detailed investigation on the electrical transport properties of this material and its

deuterated analogue have so far been made. The only conductivity measurement reported in the literature is that due to Hugo Schmidt [32] who apparently obtained a linear conductivity plot throughout the paraelectric region and a peak at $-50^\circ C$ corresponding to the ferroelectric transition point of this material. In the following sections, we present some of the interesting results of our studies on the electrical conductivity of $(NH_4)_2SO_4$ and $(ND_4)_2SO_4$.

4.2 Experimental

Single crystals of $(NH_4)_2SO_4$ and $(ND_4)_2SO_4$ (DAS) were grown from solution over a period of about one month at $34 \pm 0.01^\circ C$ using triply distilled water and heavy water of isotopic purity 99.8%. The details of the method of purification of the material, doping, sample preparation and measuring techniques are the same as described in chapter II [33]. A potential difference of 10-20V was applied across the crystal sample of typical size 5 x 5 x 1 mm^3. No polarization effect was observed in this voltage range. The rates of temperature variation used was $1^\circ C/hr$ in the vicinity of the transition points and $5^\circ C/hr$ in the other regions.

4.3 Experimental Results

4.3.1 Electrical conductivity in the paraelectric phase of $(NH_4)_2SO_4$

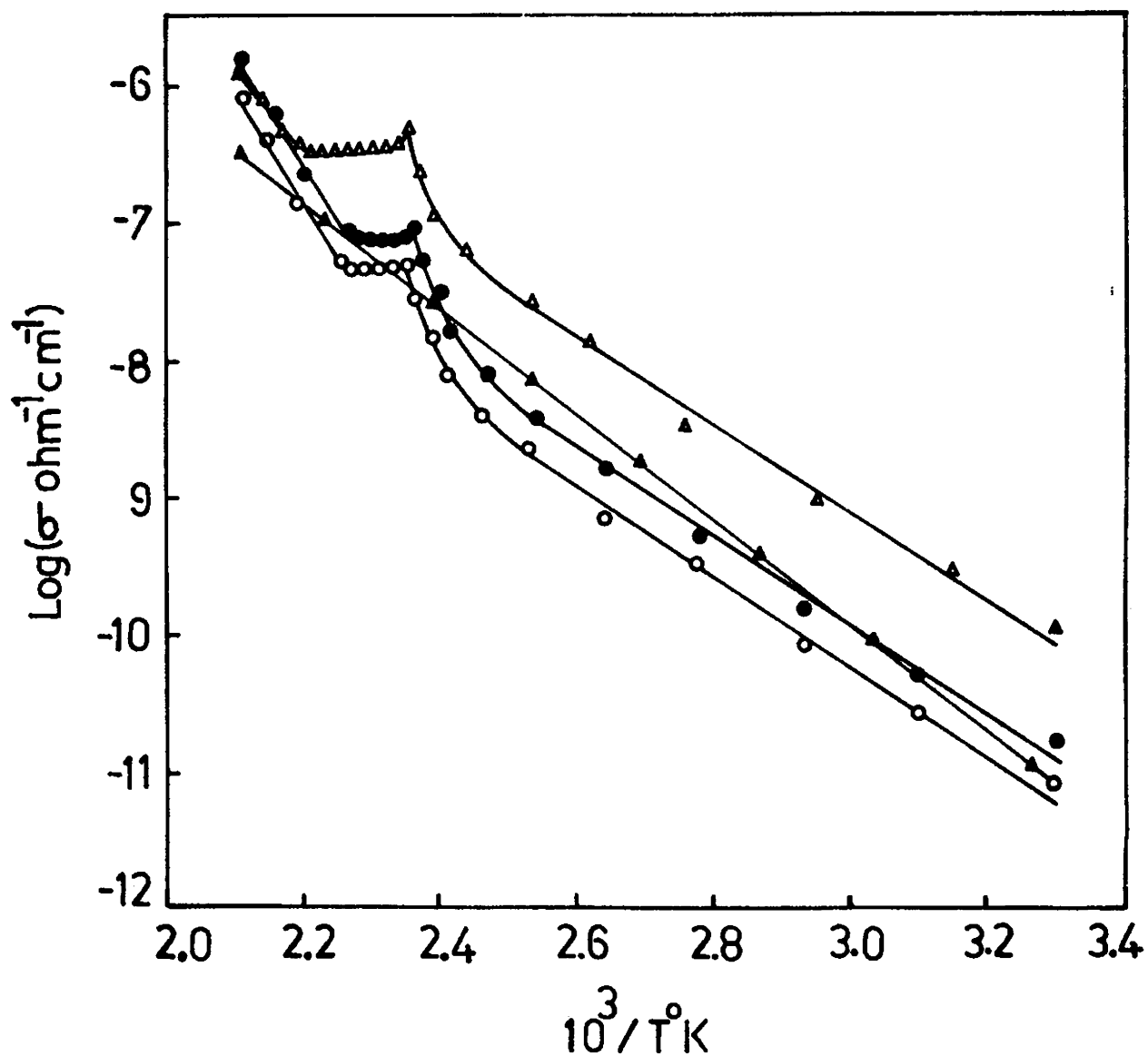4.3.1.1. Pure sample: The results of electrical conductivity

Fig.4.1 Conductivity plots for $(NH_4)_2SO_4$ single crystals: —•—•—along the c-axis, —o—o— along a or b-axis, —▲—▲—result reported previously. —△—△— result for a second run of the measurement after a very slow cooling rate (along the c-axis).

measurements on pure A S single crystals along the three
different crystallographic axes are shown in Fig. 4.1. It
can be seen that contrary to the previous results [32], the
present plot has two straight line regions in the paraelectric
phase characteristic of ionic crystals. The magnitude of
conductivity along the c-axis (σ_{33}) is found to be higher
than that along a (σ_{11}) and b (σ_{22}) by a factor of two. A
significant aspect of the present result is that in between
the straight line regions (in the vicinity of $150^{\circ}C$) the
curves exhibit a definite anomalous behaviour. In this region
the conductivity increases to a maximum value and then de-
creases by a small amount forming a peak and remains constant
afterwards corresponding to an increase in temperature of
about $15^{\circ}C$. For the second run of the measurement on the
same sample, after a very slow cooling rate (about $5^{\circ}C/hr$)
this anomalous effect becomes more pronounced with a subsequent
rise in conductivity of about one order of magnitude in the
lower straight line region (Fig. 4.1). The third run shows
no appreciable change from the second one. The linear regions
of the curve corresponding to the pure crystal along the
c- (ferroelectric) axis can be described by the following
equations:

$$\sigma_e = 1.05 \text{ x exp } (-7627/T), \tag{4.1}$$

$$\sigma_i = 8.01 \text{ x exp } (-17219/T) \tag{4.2}$$
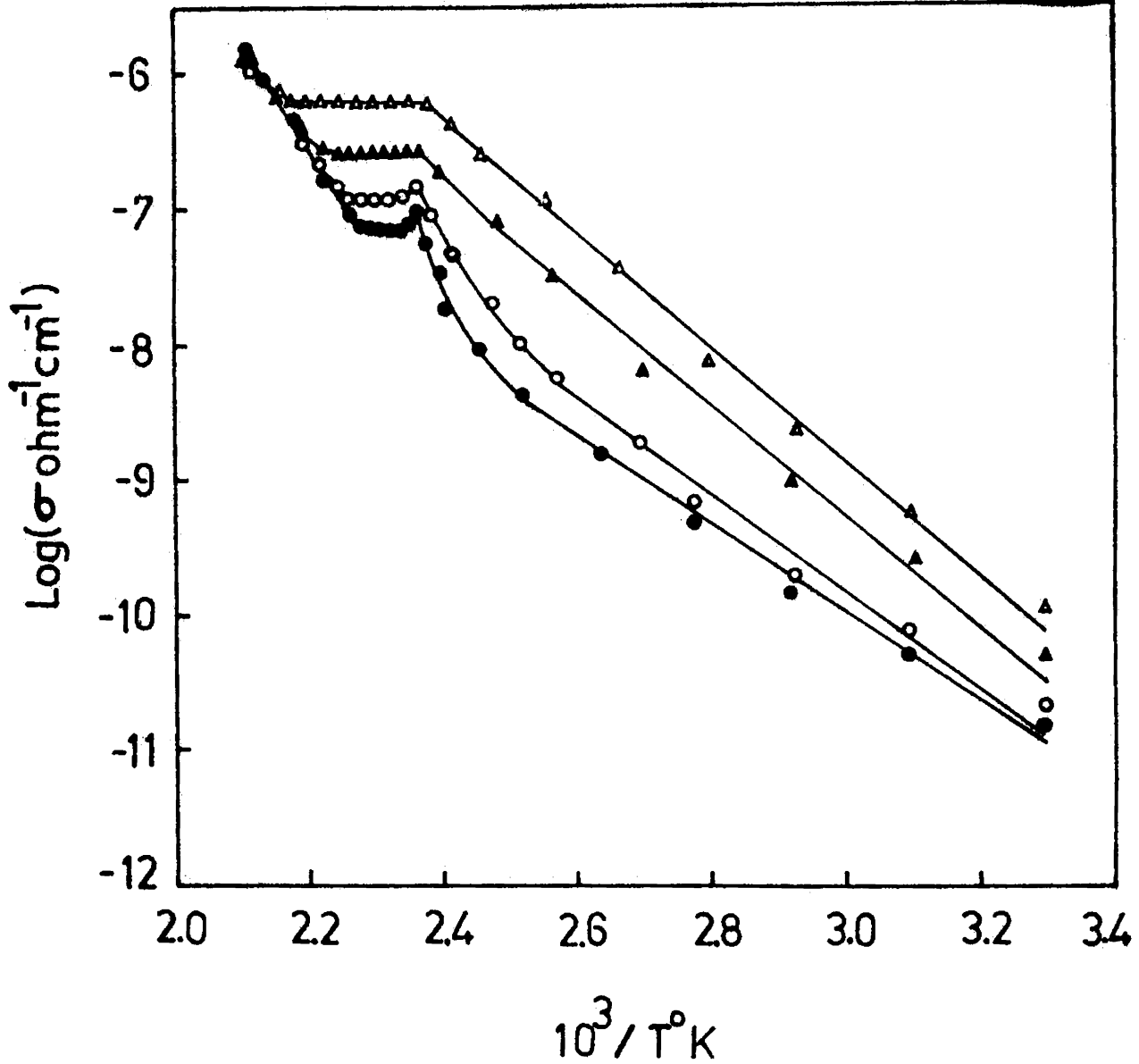
Fig.4.2   Conductivity plots for doped $(NH_4)_2SO_4$ single
crystals along the c-axis: —●●— Undoped,
—o—o— sample doped with Mn^{2+}, —▲▲— doped with
Cu^{2+}, —△△— doped with Zn^{2+}.

99

So the conductivity of the pure crystal along the c-axis in the whole paraelectric region except in the vicinity of the anomalous part can be expressed as

$$\sigma_{33} = \sigma_e + \sigma_i \qquad\qquad (4.3)$$

The activation energies corresponding to the lower and higher regions are given by 0.67 and 1.50 eV respectively. These activation energy values are found to be independent of the axis of the crystal.

4.3.1.2. Effect of doping: Conductivity measurements were extended to samples doped with divalent cationic impurities, Zn^{2+}(420 ppm), Cu^{2+}(350 ppm) and Mn^{2+}(265 ppm) (Fig. 4.2) with a view to explain the mechanism of electrical conduction in the crystal. It is found that these impurities have in general the effect of increasing the conductivity and activation energy in the lower linear part. The effect is more pronounced in the case of Zn^{2+} doped samples which show an increase in conductivity of about one order of magnitude. The activation energy in this case increases by 0.2 eV. The doped samples also exhibit the conductivity anomaly with a difference that the constant conductivity region increases in these cases.

4.3.1.3. Effect of quenching: To understand the mechanism of electrical conduction in the anomalous and in the upper straight line regions, measurements were carried out on
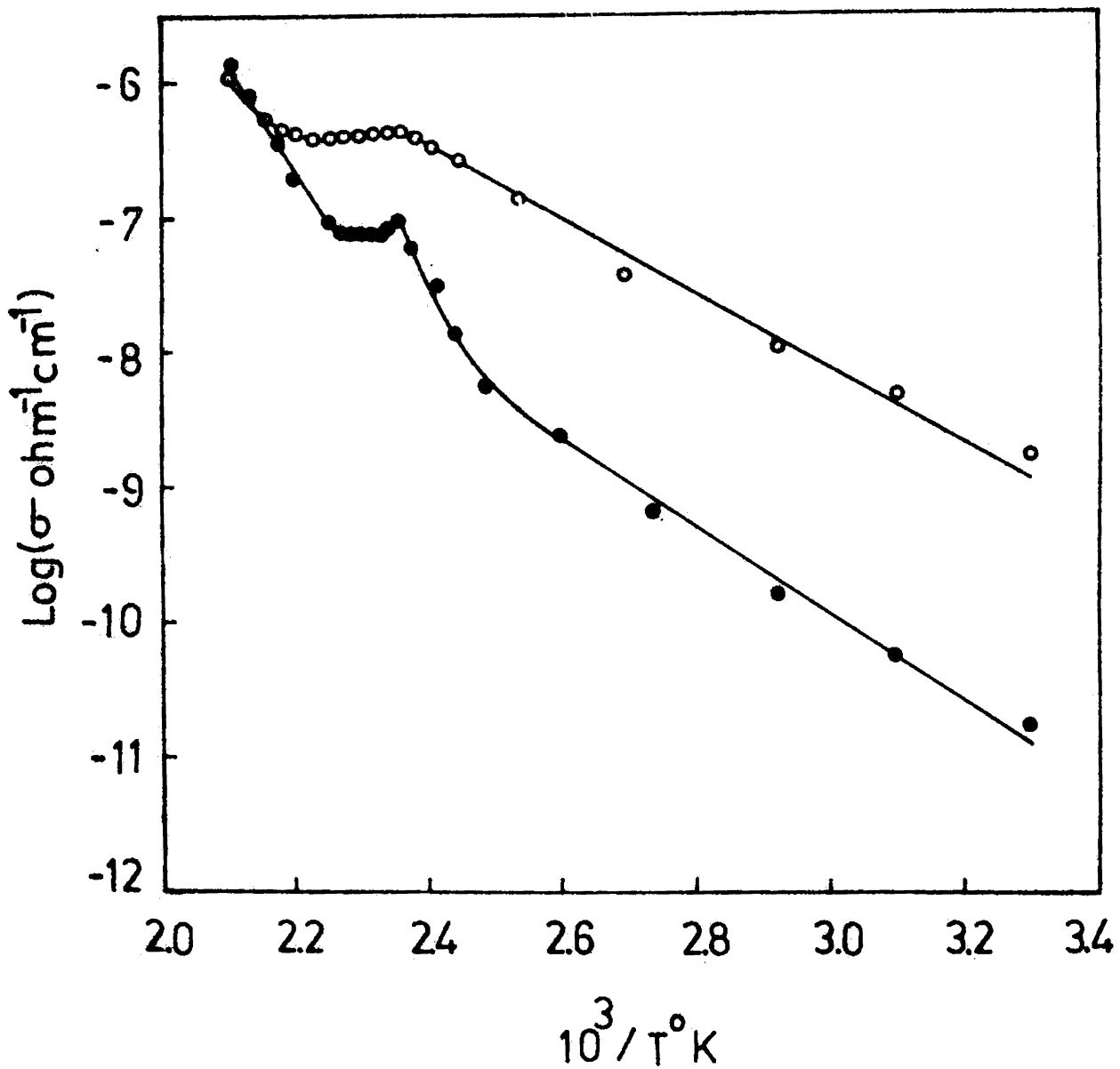
Fig.4.3 Conductivity plots along c-axis for a pure
sample (●—●) and for a sample quenched
from 150°C (o—o).

101

crystals quenched from higher temperatures to room temperature

(Fig. 4.3). Three types of quenched samples were used: (1)

crystal quenched from 150°C corresponding to the anomalous

region, (2) those quenched from 190°C and (3) samples quenched

from 140°C. The quenching was done by keeping the sample

in vacuum at the appropriate quenching temperature for 2 hrs

and suddenly exposing it to a dry air jet at room temperature.

Measurements reveal that the conductivity of the first type

of samples increases by more than two orders of magnitude

with a decrease in activation energy by 0.11 eV (Fig. 4.3),

while the second type of samples shows a still higher condu-

ctivity with a decrease in activation energy by 0.3 eV. The

third type of samples shows a slight increase in conductivity

with a decrease in activation energy of 0.04 eV.

4.3.2 Electrical conductivity and the low temperature phase transitions in $(NH_4)_2SO_4$

Recently Yoshihara et al.[12] observed a very

small anomaly in the thermal behaviour of dielectric constant

in AS along the different crystallographic axes at temperatures

ranging from 6 to 12°C below the well known ferroelectric phase

transition occurring in this crystal at -49.5°C. Since condu-

ctivity measurements seem to be a very sensitive technique for

the detection of a phase transition in this type of crystals,

the above observation by Yoshihara et al. prompted us to carry

out a detailed study of the electrical conductivity of this

material and its deuterated and doped analogues giving special importance to the region of the newly observed anomaly. Our measurements show that a distinct conductivity anomaly does indeed exist in AS at a definite temperature of $-58^{\circ}C$ and this is found to be independent of the crystallographic axes and heating or cooling rate; which is a result not exactly in agreement with that of Yoshihara et al. The details of the results of the low temperature conductivity measurements on pure, doped and deuterated samples of AS are given in the following sections [34].

4.3.2.1. Pure $(NH_4)_2SO_4$ and $(ND_4)_2SO_4$: Fig. 4.4 shows the conventional log σ vs. $10^3/T$ plots for AS and DAS along the c- and b- axes from 50 to $-115^{\circ}C$. The plot for the a-axis is almost identical with that for b and hence it is not shown here. Beyond $-115^{\circ}C$ the plots insignificantly extends upto liquid nitrogen temperature and this region also is not shown in Fig. 4.4. Using the heating rate as mentioned in the experimental section of this chapter, it is found that there is no noticeable change in the value of conductivity both in the heating and cooling runs and hence the average values of these are plotted. Furthermore no thermal hysterisis is observed. The notable feature of the present result is that all the curves exhibit two well defined $\wedge$-type conductivity anomalies one at $-49.5^{\circ}C$ corresponding to the well known ferroelectric phase transition and the other at $-58^{\circ}C$. It
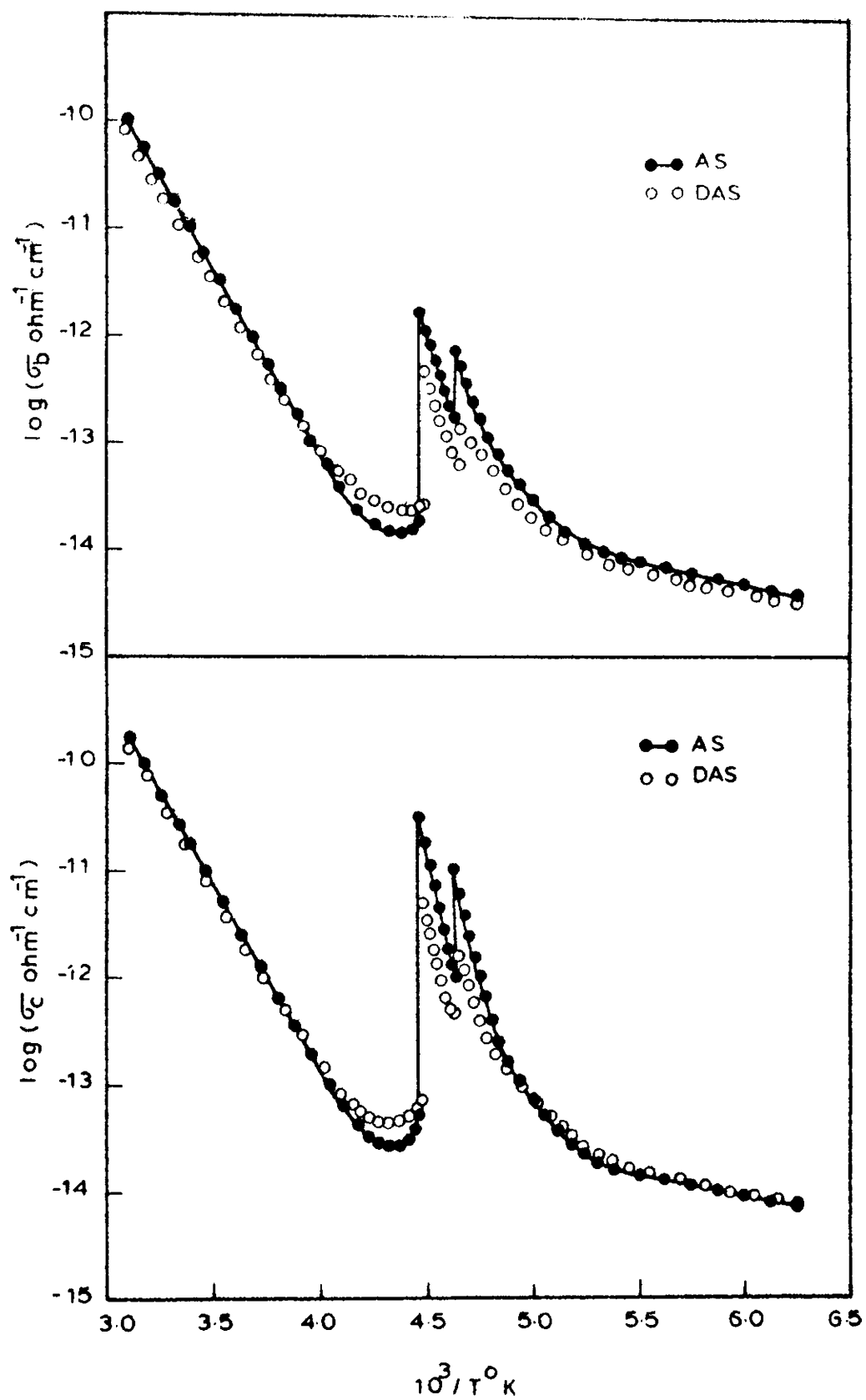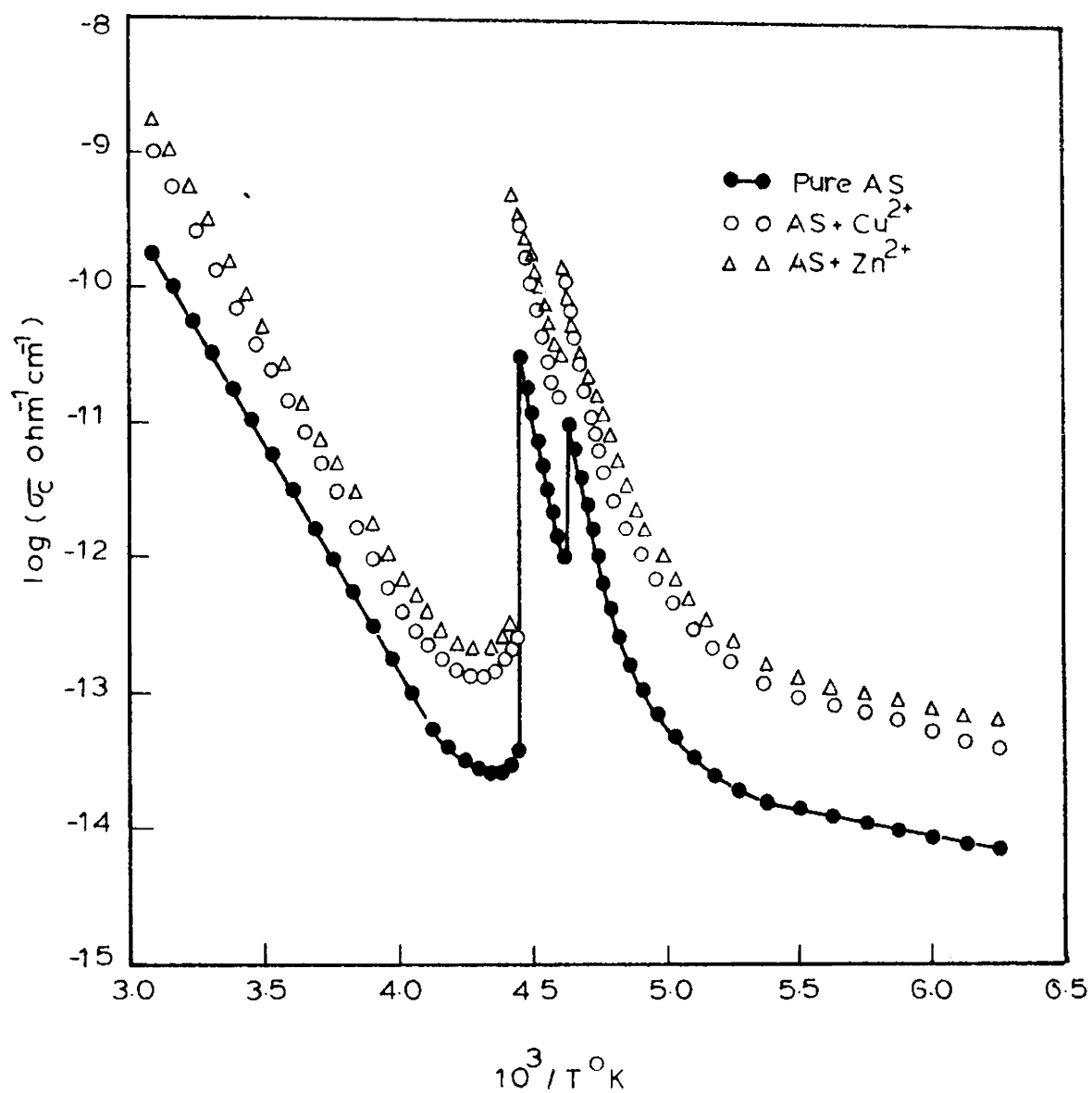
Fig.4.4   Low-temperature electrical conductivity plots
for $(NH_4)_2SO_4$ (AS) and $(ND_4)_2SO_4$ (DAS).

may be recalled that this additional peak went unnoticed in
an earlier conductivity study [32]. For AS along the c-axis,
the conductivity increases by about three orders of magnitude
at -49.5 and -58°C. The heights of the peaks are considerably
reduced in the case of plots corresponding to b- or a-axes
(Fig. 4.4(b)). For DAS the variation of electrical conducti-
vity with temperature is found to be exactly the same as
for AS. It is worth mentioning that no measurable shift in
the transition temperatures is observed in the case of
deuterated sample for both these transitions. Except in the
vicinity of the anomalous part the curves have two distinct
straight line regions below room temperature. The linear
regions of the curve corresponding to the c-axis of AS can
be described by the following equations:

$$\sigma_{para} = 0.71 \times \exp\left(-7556/T\right) \tag{4.4}$$

$$\sigma_{ferro} = 2.46 \times 10^{-12} \exp\left(-938/T\right) \tag{4.5}$$

The activation energies corresponding to these regions are
0.66 and 0.081 eV respectively, of which the former value
remains unchanged for AS upto its high temperature transition
point. Hence along with the results obtained from the high
temperature region, it can be concluded that the nature of
electrical conduction in AS in the temperature range 200 to
-196°C is ionic. Also, in this temperature range the con-
ventional electrical conductivity plot falls into three

ig.4.5 Effect of doping on the low-temperature electrical conductivity of $(NH_4)_2SO_4$ (AS).

distinct straight line regions with a high temperature anomaly at 150°C and a well defined pair of peaks at low temperature occurring at -49.5 and -58°C respectively.

4.3.2.2. Effect of doping: Fig. 4.5 shows the effect of divalent cationic impurities, Cu^{2+}(350 ppm) and Zn^{2+}(420 ppm) on the low temperature electrical conductivity of AS. As noted earlier in the high temperature region, these impurities have the effect of increasing the conductivity both in the ferroelectric and paraelectric phases of the crystal. For Zn^{2+} doped (420 ppm) sample the enhancement of electrical conductivity is about one order of magnitude throughout the range. The activation energies of the doped samples show a considerable increase in the paraelectric phase, while in the ferroelectric phase these remain almost the same as that for pure samples. It is found that these impurities ($\cong$ 500 ppm) do not affect either the height of the peaks or their position.

4.4   Discussion

4.4.1 Mechanism of electrical conduction

Several mechanisms have been suggested by various authors for the electrical conduction in ionic crystals containing ammonium groups [1-3,32-41]. The conductivity data for pure AS single crystals in the paraelectric region fall into two straight line regions with activation energies 0.67 and 1.50 eV showing that more than one defect mechanism is

involved in the conduction process. Unlike the typical ionic

crystals AS has two ions of larger size (for ammonium ion,

ionic radius is 1.43 $\overset{o}{A}$, the sulphur-oxygen bond length in

sulphate ion is 1.44 $\overset{o}{A}$ with oxygen having an ionic radius

1.40 $\overset{o}{A}$). On account of the larger size of these ions, the

probabilities of occurrence of interstitial ammonium and

sulphate ions and their vacancies are very low. Also the

mobilities of these defects are much less. Hence ammonium

and sulphate ions and their vacancies cannot contribute to the

conduction process in any significant manner. Eventhough the

starting material is recrystallised five times using triply

distilled water, it is known to contain a certain amount of

cationic and anionic impurities ($\simeq 10^{-6}$ molar fraction).

Our experimentally well confirmed result is that addition of

divalent cationic impurities into the crystal enhances the

conductivity. Hence we can readily conclude that the condu-

ction process in AS in the structure sensitive region is

dominated by the inherent cations. The experimental results

on pure and doped samples in the low temperature region

reveal that the above mechanism of electrical conduction in

the crystal continues to be operative until the low tempera-

ture anomaly is reached. In the ferroelectric phase, the

activation energy of AS drops considerably to a very low

value (0.081 eV). This small activation energy value observed

in the lower linear region may be due to the precipitation of

the existing impurities leading to a large reduction in the number of mobile species.

4.4.2 Evidence for a new high temperature phase transition in $(NH_4)_2SO_4$

Anomalous effects in conductivity were reported [1-3,33,35,36] in various ammonium containing ionic crystals viz. NH_4Cl, NH_4Br and $LiNH_4SO_4$ at their high temperature phase transition point. In AS no such high temperature phase transition has been reported so far. Now the observed conductivity anomaly at $150^{\circ}C$ may indicate in all possibility of a new phase transition taking place in AS. The studies which are presented in chapter III [1-3] in this line show that conductivity study is a very effective method for the detection of a phase transition in crystals which come under the class of improper ferroelectrics. Apparently this anomalous phenomena on the d.c. conductivity of AS went unnoticed in a measurement which has reported previously [32]. We believe that this may be due to a higher heating rate that might have been employed in that experiment.

The anomalous part of the conductivity plot can be explained as follows. As in the case of NH_4Cl [35,36] and $LiNH_4SO_4$ [1,2], the ammonium ions in AS can be assumed to be in a state of torsional oscillation, from which it changes to a state of free rotation around $150^{\circ}C$. This free rotation might

cause the generation of a large number of protonic defects giving rise to an increase in conductivity. Part of the generated protonic defects may be suddenly reabsorbed by the surrounding lattice and when the temperature corresponding to the constant conductivity part is reached, the concentration of the generated and reabsorbed defects become almost equal. The quenching of the crystal from the anomalous region ($150^{\circ}C$) leads to freeze the excess carriers produced at the transition point and these frozen-in defects can be responsible for the increase in conductivity of the quenched sample. Hence the decrease in activation energy of 0.11 eV should evidently correspond to the migration of these frozen-in defects. The activation energy of protons in NH_4Cl [43] is found to be 0.08 eV. A reasonable assumption that the activation energy of protons in AS is not widely different from this value leads to the conclusion that protonic conduction can be the phenomenon responsible for the conductivity anomaly at $186.5^{\circ}C$. Above $170^{\circ}C$ the plot for all the type of samples coincide and hence the region above this temperature can be considered as the intrinsic region. The conductivity at this region can be attributed to one of a mixed nature due to the following defects: (1) protonic defects, (2) inherent cationic defects and (3) ions dissociated from impurity-vacancy complexes.

(As the high temperature conductivity peak is not sharp, the study on the effect of deuteration on this phase transition has not been carried out by electrical conductivity method. The effect has been studied by dielectric method and is presented in chapter VI).

4.4.3 Ferroelectric phase transition in $(NH_4)_2SO_4$ as a double transition

In spite of the numerous investigations, the nature of the ferroelectric phase transition of AS has not been clearly explained so far. It is well known that in AS there are two nonequivalent ammonium ions in a unit cell which are denoted as $(NH_4)_I^+$ and $(NH_4)_{II}^+$ along with $(SO_4)^{2-}$ ions. The neutron diffraction study [4] reveals that in the paraelectric phase, the ammonium ions are highly distorted with H - N - H angles varying from 104.7° to 118.5° in one ammonium ion and 100.2° to 116.2° in the other ammonium ion. In the ferroelectric phase, the ammonium ions are much less distorted with H - N - H angles varying from 106.1° to 111.6° in one ammonium ion and 104.7° to 114.1° in the other. The O - S - O angles show no appreciable change during the passage through the transition. The results of deuteron magnetic resonance [17] and pulsed nitrogen double resonance [18] studies also support the existence of highly distorted ammonium ions in AS. Hence it is evident that the $(SO_4)^{2-}$ ions carry a smaller dipole moment while the major contribution

to the spontaneous polarization comes from $(NH_4)_I^+$ and

$(NH_4)_{II}^+$. The ESR study [23] reveal that the different

ammonium ions giving rise to the spontaneous polarization

show different temperature dependences at and below the

transition point. The proposal by Unruh et al.[44] that,

two or more kinds of dipoles may be involved in the total

polarization in AS, is also in favour of this conclusion.

Hence the ions $(NH_4)_I^+$ and $(NH_4)_{II}^+$ which can be considered as

two dipoles with unequal values of dipolemoment and with

different temperature dependences of spontaneous polarizations

need not undergo distortions all at the same temperature

viz. $-49.5^\circ C$, contrary to what has been believed so far. Here

the experimentally observed double peak in the electrical

conductivity plots shows that in AS, the nonequivalent ammonium

ions viz. $(NH_4)_I^+$ and $(NH_4)_{II}^+$ undergo sudden distortions at two

differing temperatures of $-49.5^\circ C$ and $-58^\circ C$ and thus leading to

the occurrence of two separate transitions.

The fact that the deuteration of AS does not affect

both these transition points is in accordance with the above

conclusion that the abrupt distortions of the different

ammonium ions are responsible for these transitions. On the

other hand if the transitions were due to the motional effects

(reorientation or free rotation) of the ammonium ions, an

upward shift in the corresponding temperatures should have been

observed in DAS. It may be noted that the high temperature

transition points of $LiNH_4SO_4$ [3] and AS [45] (discussed in chapters III and VI) undergo such upward shifts of 4.5^oC and 10.5^oC respectively and hence these transitions have been attributed to the onset of free rotation of the ammonium ions.

4.5 Conclusions

1. The migration of inherent cationic impurities is suggested to be the dominant mechanism of electrical transport in single crystals of $(NH_4)_2SO_4$ in the extrinsic region which extends to 170^oC from low temperature. The mechanism is the same along the different crystallographic axes, since the activation energy values are independent of directions.

2. Anomalous variations in d.c. electrical conductivity with temperature are observed in $(NH_4)_2SO_4$ single crystals, suggesting a new phase transition around 150^oC. (This suggestion has been confirmed by dielectric studies and the results of which are presented in chapter VI).

3. The intrinsic region of $(NH_4)_2SO_4$ starts from 170^oC and in this region the dominant carriers are protonic defects, inherent cationic defects and ions dissociated from impurity-vacancy complexes.

4. A very careful measurement of electrical conductivity of $(NH_4)_2SO_4$ along the different crystallographic axes in the low temperature region shows that in this crystal, there

exists one more phase transition at $-58^\circ C$ close to the well known ferroelectric phase transition occurring at $-49.5^\circ C$. (This result is also confirmed by dielectric studies and the details of which are presented in chapter VI). These low temperature transition points are unaffected by deuteration of the samples. The existence of such a pair of peaks is attributed to the sudden distortions occurring successively in the two different type of ammonium ions in the crystal.

REFERENCES

[1] U. Syamaprasad and C.P.G. Vallabhan, Solid State
    Commun. 34, 899 (1980)

[2] U. Syamaprasad and C.P.G. Vallabhan, National Acad.
    Sci. Lett. (India) 3, 364 (1980)

[3] U. Syamaprasad and C.P.G. Vallabhan (Communicated)

[4] E.O. Schlemper and W.C. Hamilton, J. Chem. Phys.
    44, 4498 (1966)

[5] Y. Makita, A. Swada and Y. Takagi, J. Phys. Soc.
    Japan 41, 67 (1976)

[6] S. Hoshino, K. Vedam, Y. Okaya and R. Pepinsky,
    Phys. Rev. 112, 405 (1958)

[7] R. Guillien, Compt. rend. 208, 980 (1939)

[8] L. Conture et al. Compt. rend. 243, 1804 (1956)

[9] B.T. Mathias and J.P. Remeika, Phys. Rev. 103,
    262 (1956)

[10] H.G. Unruh, Solid State Commun. 8, 1951 (1970)

[11] A.T. Anistratov and U.G. Martynov, Sov. Phys.
     Crystallogr. 15, 256 (1970)

[12] A. Yoshihara, T. Fujimura and K.I. Kamiyoshi, Phys.
     Stat. Solidi (a) 34, 369 (1976)

[13] T. Ikeda, K. Fujibayashi, T. Nagai and J. Kobayashi,
     Phys. Stat. Solidi(a) 16, 279 (1973)

[14] K. Ohi, J. Osaka and H. Uno, J. Phys. Soc. Japan
        44, 529 (1978)

[15] A. Onodera, Y. Sugata and Y. Shiozaki, Solid State
        Commun. 27, 243 (1978)

[16] H.G. Unruh, E. Sailer, H. Hussinger, O. Ayere
        Solid State Commun. 25, 871 (1978)

[17] D.E. O'Reilly and T. Tsang, J. Chem. Phys. 46,
        1291 (1967)

[18] R. Blinc, M. Mali, O. Osredkar, A. Prelesnik,
        J. Seliger and I. Zupancic, Chem. Phys.
        Lett. 14, 49 (1972)

[19] R. Blinc and I. Levstek, J. Phys. Chem. Solids
        12, 295 (1960)

[20] R.E. Richards and T. Schaefer, Trans. Faraday
        Soc. 57, 210 (1961)

[21] A. Watton, A.R. Sharp, H.E. Petch and M.M. Pintar
        Phys. Rev. B5, 4281 (1972)

[22] D.W. Kydon, M. Pintar and H.E. Petch, J. Chem.
        Phys. 47, 1185 (1967)

[23] N. Shibata, R. Abe and I. Suzuki, J. Phys. Soc.
        Japan 41, 2011 (1976)

[24] K. Hirabayashi and R. Abe, J. Phys. Soc. Japan
        48, 520 (1980)

[25] R. Abe, N. Shibata and K. Dejima, Ferroelectrics
        20, 217 (1978)

[26] K.V. Ramanathan and R. Srinivasan, Chem. Phys. Lett. 22, 572 (1973)

[27] B.H. Torrie, C.C. Lin, O.S. Binbrek and A. Anderson, J. Phys. Chem. Solids 33, 697 (1972)

[28] Y.S. Jain, H.D. Bist and G.C. Uproti, Chem. Phys. Lett. 22, 572 (1973)

[29] J. Petzelt, J. Grigas and I. Mayerova, Ferroelectrics 6, 225 (1974)

[30] C.J.H. Schutte and A.M. Heyns, J. Chem. Phys. 52, 864 (1970)

[31] Z. Iqbal and C.W. Cristoe, Solid State Commun. 18, 269 (1976)

[32] V. Hugo Schmidt, J. Chem. Phys. 38, 2783 (1963)

[33] U. Syamaprasad and C.P.G. Vallabhan, Solid State Commun. 38, 555 (1981)

[34] U. Syamaprasad and C.P.G. Vallabhan, Solid State Commun. (In Press)

[35] Y.V.G.S. Murti and P.S. Prasad, Physica 79B, 243 (1975)

[36] Y.V.G.S. Murti and P.S. Prasad, Proc. Nuclear Phys. and Solid State Phys. Symp. (India) 17C, 67 (1964)

[37] T.M. Herrington and L.A.K. Stavely, J. Phys. Chem. Solids 25, 921 (1964)

[38] F.A. Kroeger, J. Chem. Phys. 51, 4025 (1969)

[39]   A. Kessler, Solid State Commun. 12, 697 (1973)

[40]   Y.V.G.S. Murti and C.S.N. Murthy, J. dePhys.
       34, C9-339 (1973)

[41]   Y.V.G.S. Murti and P.S. Prasad, Physica 77,
       543 (1974)

[42]   N.F. Mott and R.W. Gurney, Electronic Process in
       Ionic Crystals, 2nd ed (1964)

[43]   Y.V.G.S. Murti and P.S. Prasad, Solid State Commun.
       15, 1619 (1974)

[44]   U.G. Unruh and V. Rudiger, J. Phys. (France)
       33, C2-77 (1972)

[45]   U. Syamaprasad and C.P.G. Vallabhan, J. Phys. C
       (to appear in Vol.14 1981)

CHAPTER V

ELECTRICAL CONDUCTIVITY AND PHASE TRANSITIONS
IN $(NH_4)_3H(SO_4)_2$

Abstract

The d.c. electrical conductivity measurements of $(NH_4)_3H(SO_4)_2$ single crystals show that, there exist four distinct peaks in σ_c* vs T^{-1} plot between 200 and $-196^{\circ}C$ for this material corresponding to four different phase transitions occurring in the crystal. Of the four transitions, the one occurring at $-26^{\circ}C$ is observed for the first time. Data on doped samples reveal the charge transport mechanism in the crystal.

119

5.1   Introduction

Among the double salts of ammonium sulphate,
triammonium hydrogen disulphate (TAHDS) is known to exhibit
a maximum number of phase transitions. The crystal at room
temperature is monoclinic with the space group $A2/a$ and the
lattice parameters are: $a = 10.153$, $b = 5.854$, $c = 15.410 \overset{o}{A}$
and $\beta = 101.76°$[1]. Pepinsky et al [2] reported that, this
material shows dielectric anomalies at -26 and $-130°C$ and
they suggested that the material might be antiferroelectric
within this temperature range. A detailed dielectric measure-
ment and differential thermal analysis of this material have
been done by Gesi [3]. He observed three phase transitions
in this crystal below room temperature at -8, -132 and $-140°C$.
He also noticed that the dielectric constant of TAHDS along
the c^*-direction (Fig. 5.1) shows breaks at -8, and $-132°C$
while it shows a discontinuous change accompanied by a thermal
hysterisis for the transition at $-140°C$. In addition to the
above mentioned transitions, a broad maximum of dielectric
constant was found at about $-28°C$ along the c^*-direction.
However no thermal anomalies were observed at this tempera-
ture (Fig. 5.2) and the broad peak of dielectric constant
has not been attributed to a phase transition. Adding up
the one polymorphic transition [4,5] occurring in this
crystal at $140°C$, it can be seen that TAHDS has four phase
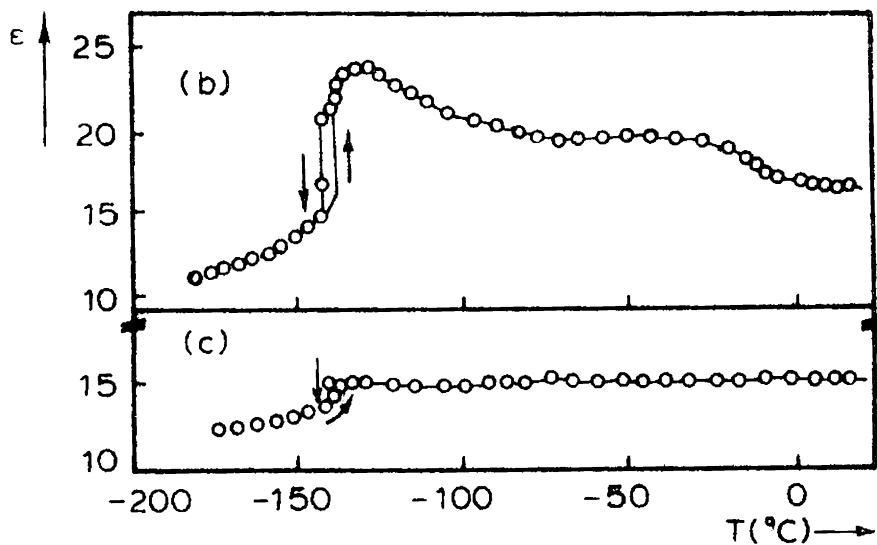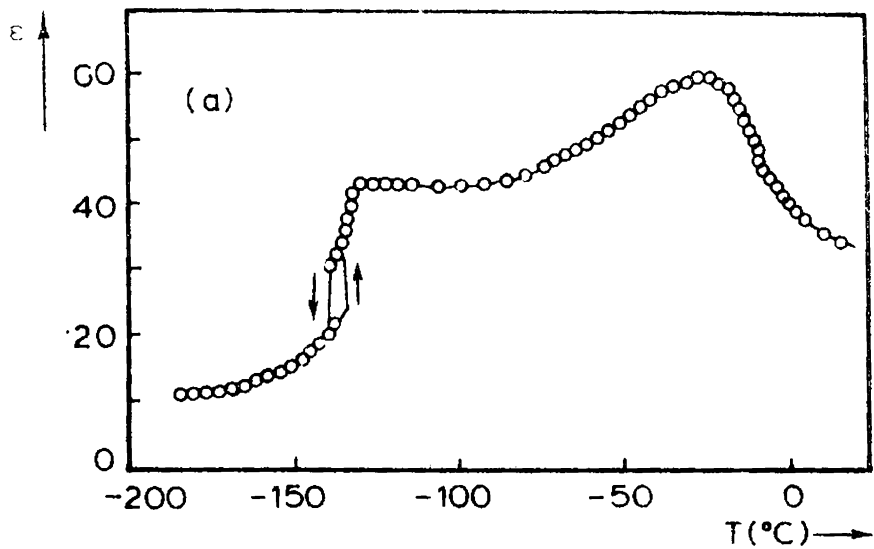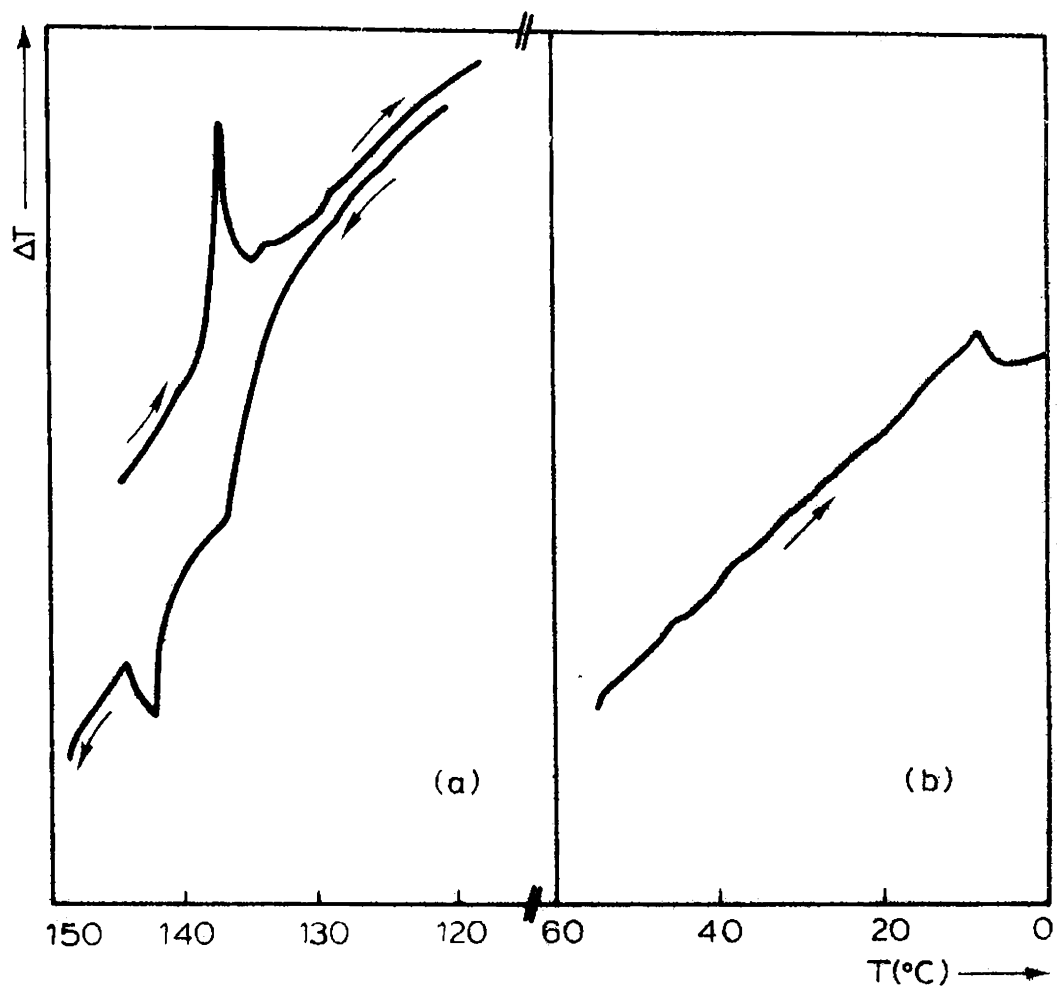transitions and five phases above liquid nitrogen temperature.

Fig.6.1 Temperature dependence of the dielectric
constant of $(NH_4)_3H(SO_4)_2$: (a) along the
c^*-direction (perpendicular to the c-plane),
(b) along the a-direction and (c) along the
b-direction (due to Gesi [3]).

g.6.2   DTA signals: (a) around the -132 and -140°C-
         transitions and (b) around the -8°C-transition
         (Gesi [3]).

However no ferroelectricity has been observed for any of these phases. Later it has been found by Gesi [6,7] that the broad peak of dielectric constant can be increased and sharpened by hydrostatic pressure and then it splits into two peaks between which a ferroelectric phase appears. This pressure induced ferroelectric phase is considered to be 6th phase of TAHDS. It is noted further that there is another ferro-electric phase denoted as the 7th phase located below the 6th phase of TAHDS.

Later it has been found [8] that the deuterated analogue of this crystal viz. $(ND_4)_3D(SO_4)$ has also two ferro-electric phases above liquid nitrogen temperature and shows a similar dielectric behaviour with that observed for the normal TAHDS crystal under high pressure. This indicates a large isotope effect on the ferroelectric activity. In order to clarify the details of the isotope effect as a function of deuterium concentration (x), the dielectric properties of the system $[(NH_4)_3H(SO_4)_2]_{1-x}[(ND_4)_3D(SO_4)_2]_x$ has been studied by Osaka et al.[9] and found indirectly by obtaining the phase diagram of the system that the normal crystal, TAHDS itself, undergoes a ferroelectric phase transition at about $-210^{o}C$. Very recently it has been found by Gesi [10] that TAHDS under-goes a phase transition at $-227^{o}C$ on cooling and at $-195^{o}C$ on warming, having a mean transition temperature $-211^{o}C$. However, no ferroelectric hysterisis loop was observed below

124

the transition temperature. Eventhough some structural,
dielectric, calorimetric and dilatometric [11] studies of this
very interesting crystal with much exhotic properties have
been made, many of its other details still remain to be
investigated. The present chapter deals with the electri-
cal conductivity studies of pure and doped single crystals
of TAHDS from liquid nitrogen temperature to $200^{\circ}C$. The
behaviour of electrical conductivity at the different phase
transition points, and the mechanism of electrical condu-
ction in the various phases of the crystal are discussed.
The detection of a new phase transition in this crystal
at $-26^{\circ}C$ without applying any external pressure is also
reported [12].

5.2   Experimental

Single crystals of TAHDS were grown by slow evapora-
tion of an aqueous solution containing 3:1 molar fraction of
$(NH_4)_2SO_4$ and H_2SO_4. Doping of the crystals with Cu^{2+} and
Zn^{2+} was done by adding specific amount of $CuSO_4$ and $ZnSO_4$
in the solution. Crystals obtained were plates of pseudo-
hexagonal shape with predominant (001) faces. Quick drying
silver conducting paint was applied on these faces as electrodes
and the electrical conductivity perpendicular to the (001)
plane (σ_c^*) was measured by a set-up as described in chapter II.
A steady d.c. voltage of 10-100V was applied to samples of

typical size 5 x 5 x 0.5 mm^3. The rate of temperature
variation used was $2^{\circ}C/hr$ in the transition regions and
$5^{\circ}C/hr$ in the other regions. No polarization effect was
observed for the current densities used here. The crystals
were annealed at $100^{\circ}C$ for 3 hrs in vacuum (10^{-3}torr) before
each measurement and all the measurements were carried out
in the same vacuum condition.

5.3   Experimental Results

5.3.1 Conductivity of pure $(NH_4)_3H(SO_4)_2$ single crystals

The temperature variation of electrical conducti-
vity of pure and doped TAHDS single crystals is shown in
Fig. 5.3. Curves a and b in Fig. 5.3 show the variation of
σ_c* with temperature for pure TAHDS single crystal in the
heating and cooling runs respectively. In both the heating
and cooling runs the curves have four unmistakable peaks
occurring respectively at 140, -26, -132 and $-140^{\circ}C$ and these
evidently correspond to the four distinct phase transitions
occurring in the crystal. The corresponding five phases
obtained here are denoted as phases I, II, III, IV and V in
the order of decreasing temperature. The transition at $-140^{\circ}C$
is accompanied by a thermal hysteresis of $4^{\circ}C$ during heating
and cooling cycles whereas no thermal hysterisis is observed
for the other transitions. The detailed shape of each of
the electrical conductivity peaks obtained at the different
transition points in the heating cycle is separately shown
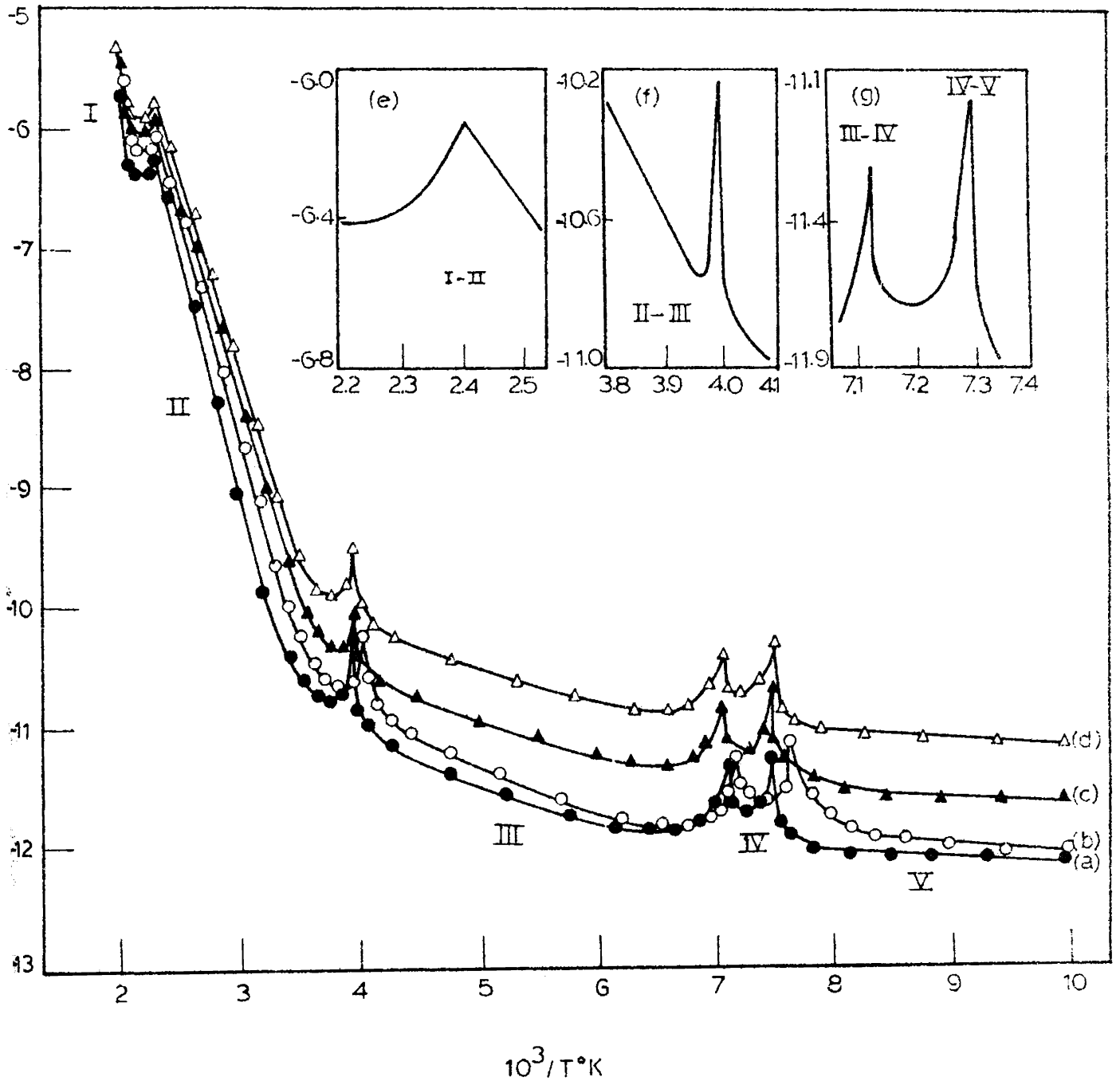
6.3 D.C. electrical conductivity plots for $(NH_4)_3H(SO_4)_2$ single crystals along the c^*-direction: a — for pure sample in the heating run, b — for pure sample in the cooling run, c — for Zn^{2+} doped sample, d — Cu^{2+} doped sample; curves e, f and g show the details of the conductivity peaks corresponding to the different phase transitions.

126

by curves e, f and g given as the inset of Fig. 5.3. In
contrast to the dielectric results reported by Gesi [3,6],
we have here obtained a very sharp peak at -26°C without
applying any external pressure (the contact pressure applied
to the crystal was only about 300 gram/cm^2). On the other
hand no conductivity anomaly was observed at -8°C eventhough
a temperature variation of 1°C/hr was used in this region.
Except in the vicinity of the transition points, the plots
have straight line regions characteristic of ionic crystals
[13]. Obviously, these straight line regions represent the
different phases of the crystal. Phase IV is so narrow that
no linear region can be perceived here. By taking the average
values in the heating and cooling runs, the straight line
regions for the pure crystal can be represented by the follow-
ing equations:

$$\sigma(I) \quad = 9.97 \times 10^8 \exp (-16442/T) \qquad (5.1)$$

$$\sigma(II) \quad = 1.07 \times 10^2 \exp (-8101/T) \qquad (5.2)$$

$$\sigma(III) = 1.34 \times 10^{-10} \exp (-714/T) \qquad (5.3)$$

$$\sigma(V) \quad = 2.63 \times 10^{-12} \exp (-133/T) \qquad (5.4)$$

These equations give activation energy values 1.43, 0.71,
0.062 and 0.012 eV corresponding to phases I, II, III and V
respectively.

5.3.2 Effect of doping

Conductivity measurements were extended to samples doped with divalent cationic impurities with a view to explain the mechanism of electrical conduction in the crystal. Curves c and d in Fig. 5.3 are the conductivity plots for Zn^{2+} (350 ppm) and Cu^{2+} (570 ppm) doped samples respectively. It can be seen that doping of the crystal with these impurities has the effect of enhancing the electrical conductivity of the crystal. The effect is more pronounced in phases III, IV and V. The activation energy of the doped samples has no significant change in these phases, while it shows a decrease in value in phase II. In phase I, the conductivity and activation energy of all the samples coincide and this region may be considered as the intrinsic region.

5.4   Discussion

5.4.1 Mechanism of electrical conduction in TAHDS single crystals

Several mechanisms were suggested by various authors for the electrical conduction in ionic crystals containing ammonium groups [14-18]. The conductivity data for pure TAHDS single crystals above -196°C fall into different straight line regions, which show that more than one defect mechanism are involved in the conduction process. Usually in ionic crystals containing ammonium groups, the possible type of

point defects are: normal ionic and electronic defects and
protonic defects. Of these, electronic defects viz. electrons
and holes are very small in number. As noted in the previous
chapters (III and IV), in crystals containing $(NH_4)^+$ and
$(SO_4)^{2-}$ ions, the contribution to the electrical conduction
process by these ions and their vacancies can be neglected on
considerations based on their size. The experimentally well
confirmed result that the addition of divalent cationic impuri-
ties into the crystal enhances the conductivity of the crystal
proves that the positive charge carriers are responsible for
the conduction process thereby eliminating the role of positive
ion vacancies. The positive ion impurities in the sample
obtained after five recrystallisations of extra pure BDH Analar
grade salt using triply distilled water is below the detection
limit of the instrument (A.A. Spectrometer - Perkin Elmer 306)
used for estimation of impurities. But the pure sample is
expected to contain divalent positive and negative ion
impurities below 10^{-6} molar fraction. Hence it is concluded
that the migration of protons in the interstitial position
and of the inherent cationic impurities in the crystal is the
dominant mechanism of electrical transport in TAHDS single
crystals.

We should also consider the effect of association
of inherent impurity ions with the more significant charge
compensators viz. the protonic defects. In phase I, these

complexes will be entirely in dissociated states providing
a greater number of mobile defects resulting in a higher
conductivity. In phase II these complexes are only partially
dissociated and hence the conductivity will be comparatively
smaller. In phase III, IV and V, the existing impurity
content may exceed the solubility limit and the impurity
may precipitate out as a separate phase. This leads to a
reduction in carrier concentration which explains the remain-
ing portion of the curve.

5.4.2 A new phase transition in $(NH_4)_3H(SO_4)_2$

The results of the investigations already presented
in chapters III and IV [19-23] show that conductivity measure-
ment is a very sensitive method for the detection of a phase
transition in improper ferroelectrics containing ammonium
groups, since in such materials, the change in conductivity
at the transition point is much greater than the variation in
dielectric constant (the dielectric results of these materials
are presented in chapter VI). The dielectric and conductivity
results presented here on TAHDS are entirely in accordance
with the above conclusion. The very sharp peak observed at
$-26^\circ C$ should definitely correspond to a new phase transition
in this crystal at atmospheric pressure itself. Eventhough
the details have not been published, Pepinsky et al.[1]
mentioned a dielectric anomaly at $-26^\circ C$ which is in support
with our observation.

5.4.3 The conductivity peaks in $(NH_4)_3H(SO_4)_2$

The anomalies in the conductivity plots can be related to phase transitions of structural as well as re-orientational type. The protonic defects in TAHDS are of two category: the hydrogen ions and their vacancies belonging to the ammonium groups and those associated with the rest of the molecular unit. The onset of free rotation of ammonium groups or the beginning of random reorientation of axes of its torsional oscillation in the crystal can lead to a sudden increase in the concentration of protonic defects of the former type and this can lead to an anomalous rise in conductivity. As the peak at $140^{\circ}C$ is certainly due to a structural phase transition as revealed by earlier studies, it is reasonable to assume that the next peak found at $-26^{\circ}C$ may be due to the motional effects of ammonium groups. Gesi's observation of maximum value of dielectric constant around $-28^{\circ}C$ is in support with this conclusion.

5.5 Conclusions

1. Four distinct peaks are observed at 140, -26, -132 and $-140^{\circ}C$ in the σ_c^* vs. T^{-1} plot between -196 and $200^{\circ}C$ for $(NH_4)_3H(SO_4)_2$ single crystal which correspond to four different phase transitions occurring in this crystal at these temperatures.

2. Of the above four transitions, the one at $-26^\circ C$ is reported here for the first time. This transition is attributed to the motional effects of the ammonium groups in the crystal.

3. Except in the vicinity of the transition points, the plot shows distinct straight line regions representing the different phases of the crystal. Phase IV $(-132 \geq T \geq -140^\circ C)$ is so narrow, that no linear region can be perceived in this phase.

4. The transition at $-140^\circ C$ is accompanied by a thermal hysterisis of $4^\circ C$ during heating and cooling cycles, whereas no measurable thermal hysterisis was observed for the other transitions.

5. No conductivity anomaly was observed at $-8^\circ C$, where a transition has been reported earlier [3], eventhough a temperature variation of $1^\circ C/hr$ was used in this region.

6. The exponential variations of conductivity with temperature in different phases (except phase IV) are given by equations (5.1) to (5.4). The conduction activation energies are 1.43, 0.71, 0.062 and 0.012 eV in phases I, II, III and V respectively.

7. Measurements on crystals doped with divalent cationic impurities show that the mechanism of electrical conduction in $(NH_4)_3H(SO_4)_2$ single crystal is mainly due to the migration of the protons in the interstitial position and of the inherent cationic impurities in the crystal.

REFERENCES

[1] R. Pepinsky, K. Vedam, S. Hoshino and Y. Okaya, Phys. Rev. 111, 1508 (1958)

[2] S. Suzuki and Y. Makita, Acta Crystallogr. B34, 732 (1978)

[3] K. Gesi, Phys. Stat. Solidi(a) 33, 479 (1976)

[4] B. Gossner, Z. Krist. 38, 110 (1904)

[5] P. Fischer, Z. Krist. 54, 528 (1914)

[6] K. Gesi, J. Phys. Soc. Japan 41, 1437 (1976)

[7] K. Gesi, J. Phys. Soc. Japan 43, 1914 (1977)

[8] T. Osaka, Y. Makita and K. Gesi, J. Phys. Soc. Japan 43, 933 (1977)

[9] T. Osaka, Y. Makita and K. Gesi, J. Phys. Soc. Japan 49, 593 (1980)

[10] K. Gesi (to be published in Jpn. J. Appl. Phys. mentioned in ref.[9])

[11] S. Suzuki, J. Phys. Soc. Japan 47, 1205 (1979)

[12] U. Syamaprasad and C.P.G. Vallabhan, J. Phys. C 14, L571 (1981)

[13] A.B. Lidiard, Handbuch der Physik 20, 246 (1957)

[14] T.M. Herrington, L.A.K. Stavely, J. Phys. Chem. Solids 25, 921 (1964)

[15] F.A. Kroeger, J. Chem. Phys. 51, 4025 (1969)

[16] Y. V. G. S. Murti and C. S. N. Murthy, J. de Phys.
    C9-337 (1973)

[17] Y. V. G. S. Murti and P. S. Prasad, Physica 77, 543
    (1974)

[18] Y. V. G. S. Murti and P. S. Prasad, Proc. Nuclear
    Phys. and Solid State Phys. Symp. (India)
    17C, 67 (1974)

[19] U. Syamaprasad and C. P. G. Vallabhan, Solid State
    Commun. 34, 899 (1980)

[20] U. Syamaprasad and C. P. G. Vallabhan, National
    Acad. Sci. Lett. (India) 3, 364 (1980)

[21] U. Syamaprasad and C. P. G. Vallabhan, Solid State
    Commun. 38, 555 (1981)

[22] U. Syamaprasad and C. P. G. Vallabhan, Proc. Nuclear
    Phys. and Solid State Phys. Symp. (India)
    Paper No. SLA10 (1980)

[23] U. Syamaprasad and C. P. G. Vallabhan (Communicated)

CHAPTER VI

DIELECTRIC STUDIES ON AMMONIUM AND LITHIUM AMMONIUM SULPHATES AND ON THEIR DEUTERATED ANALOGUES

Abstract

The results of the dielectric studies on $LiNH_4SO_4$, $(NH_4)_2SO_4$, $LiND_4SO_4$ and $(ND_4)_2SO_4$ single crystals from liquid nitrogen temperature to temperatures well below their melting points are presented in this chapter. Many of the results obtained from the electrical conductivity studies viz. the observation of a new high temperature phase transition and a low temperature double transition in $(NH_4)_2SO_4$ have been confirmed here. The effect of deuteration on the phase transitions in $LiNH_4SO_4$ and in $(NH_4)_2SO_4$ is discussed.

135

6.1   Introduction

The measurement of dielectric constant of an
ammonium containing ionic crystal and its deuterated analogue
as a function of temperature can give direct evidences on the
nature of the phase transitions occurring in the crystal. This
chapter discusses the dielectric measurements made on pure
$LiNH_4SO_4$ (LAS) and $(NH_4)_2SO_4$ (AS) and their deuterated
analogues viz. $LiND_4SO_4$ (DLAS) and $(ND_4)_2SO_4$ (DAS) along the
different crystallographic axes from liquid nitrogen tempera-
ture to temperatures well below their melting or decomposition
points. The results confirm most of the conclusions derived
earlier from electrical conductivity measurements [1-6] which
are presented in chapters III, IV and V. Also these dielectric
measurements give some additional information [5-9] about the
phase transitions occurring in the crystal.

Eventhough LAS has recently been proved to be a room
temperature ferroelectric material by dielectric method [10],
no proper dielectric study of this material has been carried
out so far. Also, no attempt has so far been made to study the
dielectric properties of DLAS.

Extensive studies exist on the dielectric properties
of AS [11-22]. An earlier study of DLAS also can be found in
the literature [11]. The main interest of all these studies
was to reveal the nature of the well-known and unusual phase
transition occurring in AS at $-49.5^{\circ}C$. Hence in all these

investigations, the dielectric measurements were made only in the vicinity of -49.5°C. On the other hand the paraelectric phase of this material is very rarely investigated. The recent observation of anomalous variations in d.c. electrical conductivity [3,4] (chapter IV) in AS around 150°C indicate the possibility of a new phase transition in AS and in DAS in this region. This prompted us to investigate carefully the temperature dependence of dielectric constants of AS and DAS in their paraelectric phase.

Recently Yoshihara et al.[17] observed a small anomaly in the ε vs. T plots for AS along the different crystallographic axes at temperatures ranging from 6 to 10°C below the well known ferroelectric phase transition occurring in this crystal at -49.5°C. The electrical conductivity study of AS and DAS in this temperature region shows that a distinct conductivity anomaly exist in AS at a definite temperature of -58°C and this is found to be independent of the crystallographic axes and heating or cooling rate [8]. Hence we have made a very accurate reinvestigation of the dielectric constant of AS and DAS along the different crystallographic axes in the vicinity of the newly observed anomaly at low temperature.

6.2   Experimental

The methods of preparation of single crystals of AS, DAS, LAS and DLAS have been described in chapters III

and IV. The details of the measurement of dielectric constant

as a function of temperature have been explained in chapter II.

The dielectric measurements were carried out in vacuum using

a direct reading LC meter (its advantages over a bridge are

explained in chapter II) at a fixed frequency of 1 KHz. Samples

of typical size 8 x 8 x 1 mm^3 were used for the measurements.

The rate of variation of temperature was $1^{\circ}C$/hr in the vicinity

of the transition points.

6.3   Experimental Results

6.3.1 Dielectric constants of $LiNH_4SO_4$ and $LiND_4SO_4$

The temperature variation of dielectric constant (ε)

of DLAS along the a-axis at 1 KHz is shown in Fig.6.1(a) in

which two sharp peaks (at -1.5 and $191^{\circ}C$) occur exactly at

the same position of the corductivity peaks (Such anomalies

are absent along the b- and c-axes. Also no measurable thermal

hysteresis occurs for both the transitions). Unlike the

ε vs. T plots for LAS (Fig. 6.1(b)) obtained by Mitsui et al.

we have here observed much larger anomalies at the transition

points of DLAS. This has prompted us to reinvestigate the

dielectric constant of LAS also. As a result we have found

that the dielectric constant of LAS along the a-axis reaches

much higher values (90 and 65 at 10 and $186.5^{\circ}C$ respectively)

than those (12 and 26) indicated in the plot given by
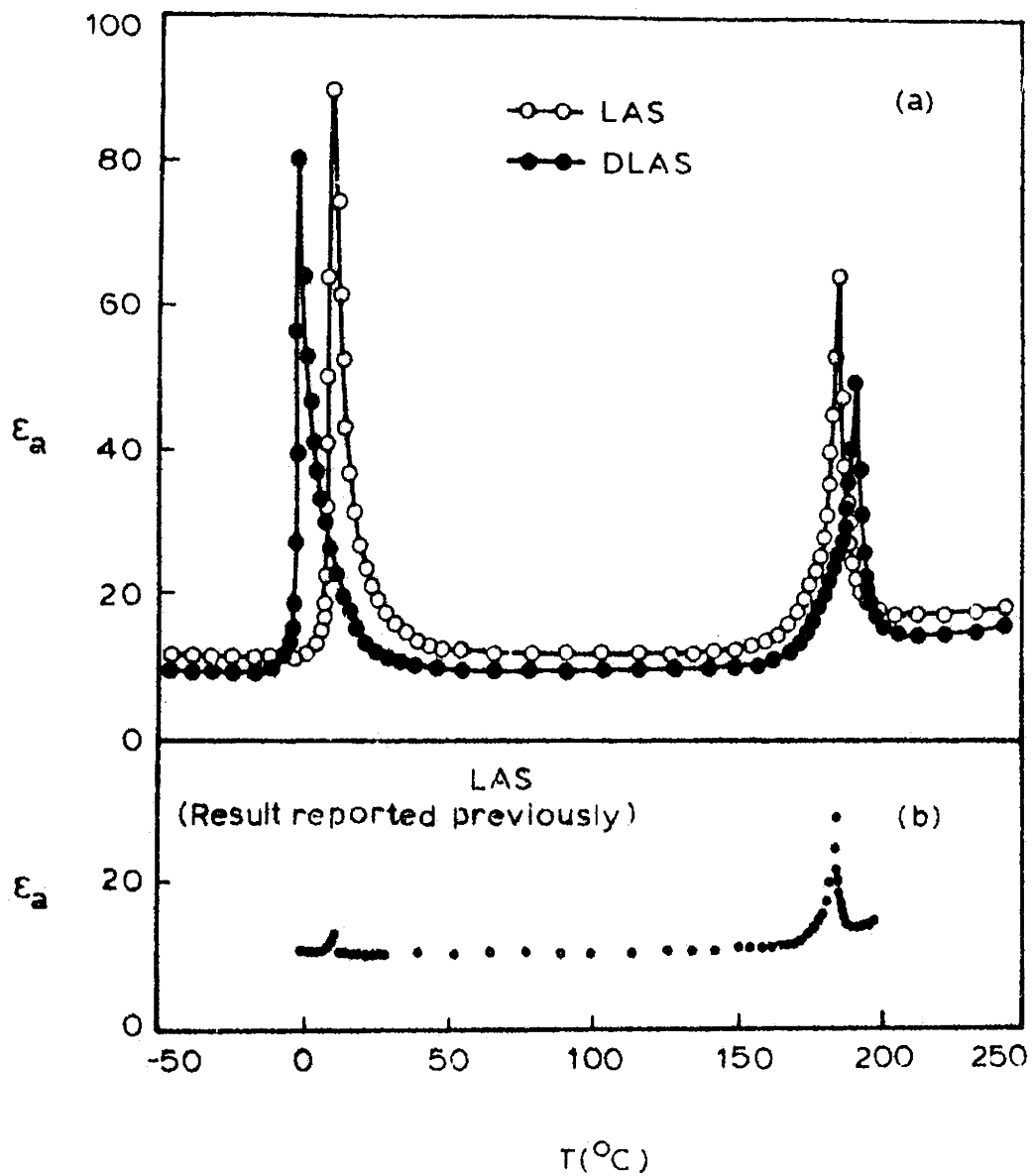
Mitsui et al.[10]. The general dielectric behaviour of DLAS

Fig.6.1 (a) ε vs T plots for $LiNH_4SO_4$ (LAS) and $Li(ND_4)SO_4$ (DLAS), (b) dielectric result on LAS reported previously.

139

with temperature is found to be as that of LAS with the difference that peak heights for the former (85 and 50 at -1.5 and 191°C respectively) are slightly smaller. The value of the room temperature dielectric constant is found to be the same as reported previously [10]. The reason for the low values of dielectric maxima observed at the transition points in the previous study of Mitsui et al.[10] might have been due to a higher heating rate and/or due to the use of a bridge (which requires repeated balancing) instead of a direct reading instrument for capacitance measurement.

6.3.2 Dielectric constants of $(NH_4)_2SO_4$ and $(ND_4)_2SO_4$

6.3.2.1. Paraelectric phase: Fig. 6.2 shows the temperature dependence of the dielectric constants of AS and DAS along the three crystallographic axes measured at a frequency of 1 KHz in the temperature range 100 to 185°C. It is found that all the samples show large and sudden changes in the values of dielectric constant in the heating and cooling runs. In the case of AS in the heating run, the dielectric constant along the c-axis (ε_c) remains almost constant upto 135°C and,at 156°C it reaches a maximum value of 1530 and then levels off beyond this temperature. In the cooling run the above changes reverses with a reproducible thermal hysterèsis of 9°C. The dielectric constants along a- and b-directions also show the same type of anomaly with a
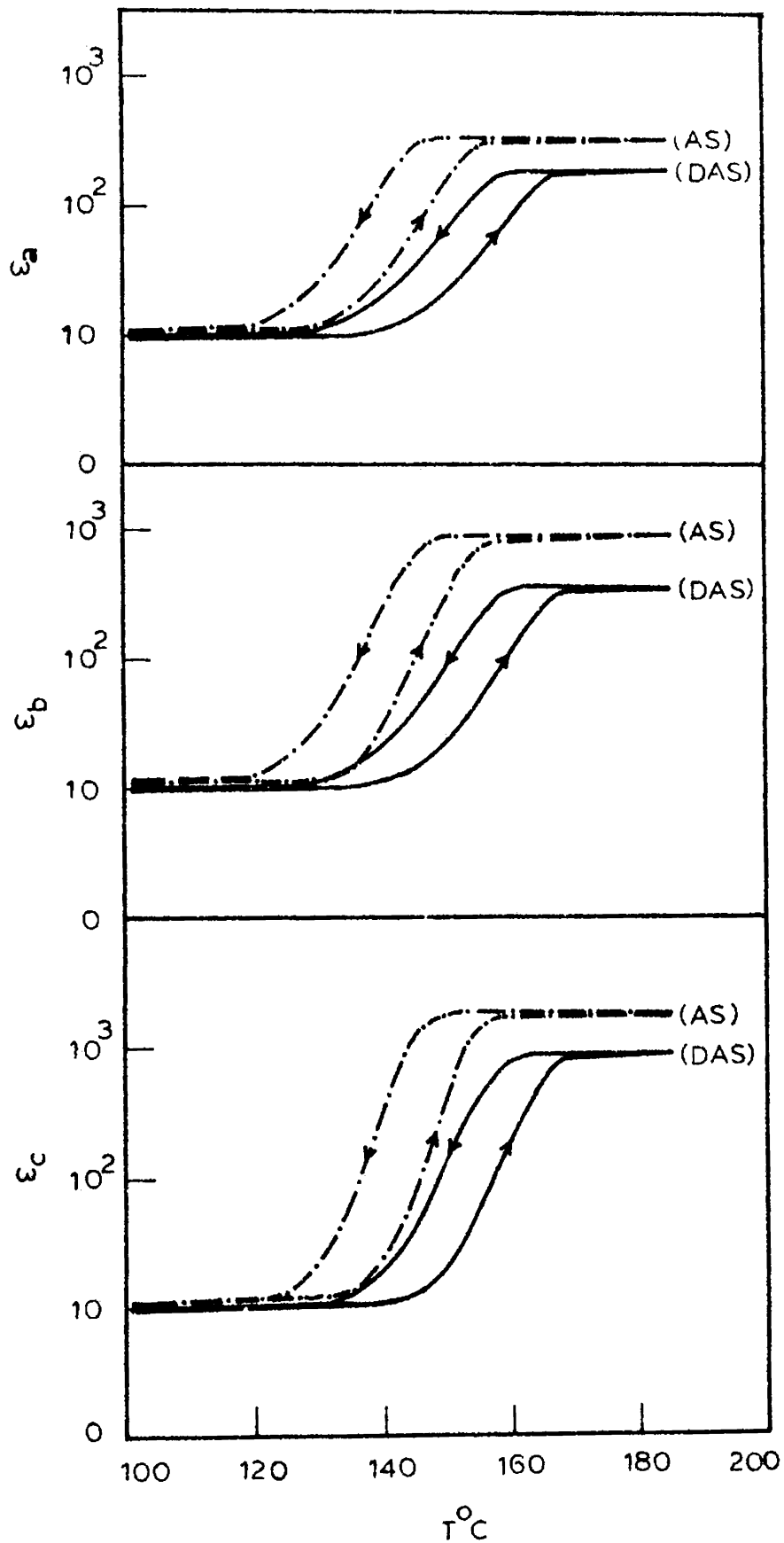
Fig.6.2 Axiswise dielectric plots for $(NH_4)_2SO_4$ (AS) and $(ND_4)_2SO_4$ (DAS) in the high temperature region.

141

difference that the dielectric maxima in these cases have only smaller values (ε_a = 340, ε_b = 890) when compared to the maximum values of ε_c (Fig. 6.2). The results are found to be very well reproducible for different samples as well as for different heating and cooling cycles for the same sample. The values for the room temperature dielectric constants are found to be same as those obtained in the earlier dielectric measurements [11].

In the case of deuterated samples, it is found that the transition point is shifted to a high temperature by 10.5°C. Here the dielectric constant show no appreciable variation upto 140°C and attains a maximum value at 166.5°C and then levels off at ε_c = 810. In the cooling run it shows a thermal hysteresis of 8°C. As shown in Fig. 6.2, deuteration of the sample has the effect of making the transition a more gradual one.

6.3.2.2. Low temperature phase: Eventhough many dielectric measurements on AS have been reported previously [11-22], no anomalous behaviour in the dielectric constant was observed below -49.5°C except that due to Yoshihara et al. [17]. However the faint anomalies observed by them in the temperature range 6 to 12°C below the well known ferroelectric phase transition point had no uniqueness regarding their temperatures with respect to the different crystallographic axes. The results of our dielectric measurements obtained
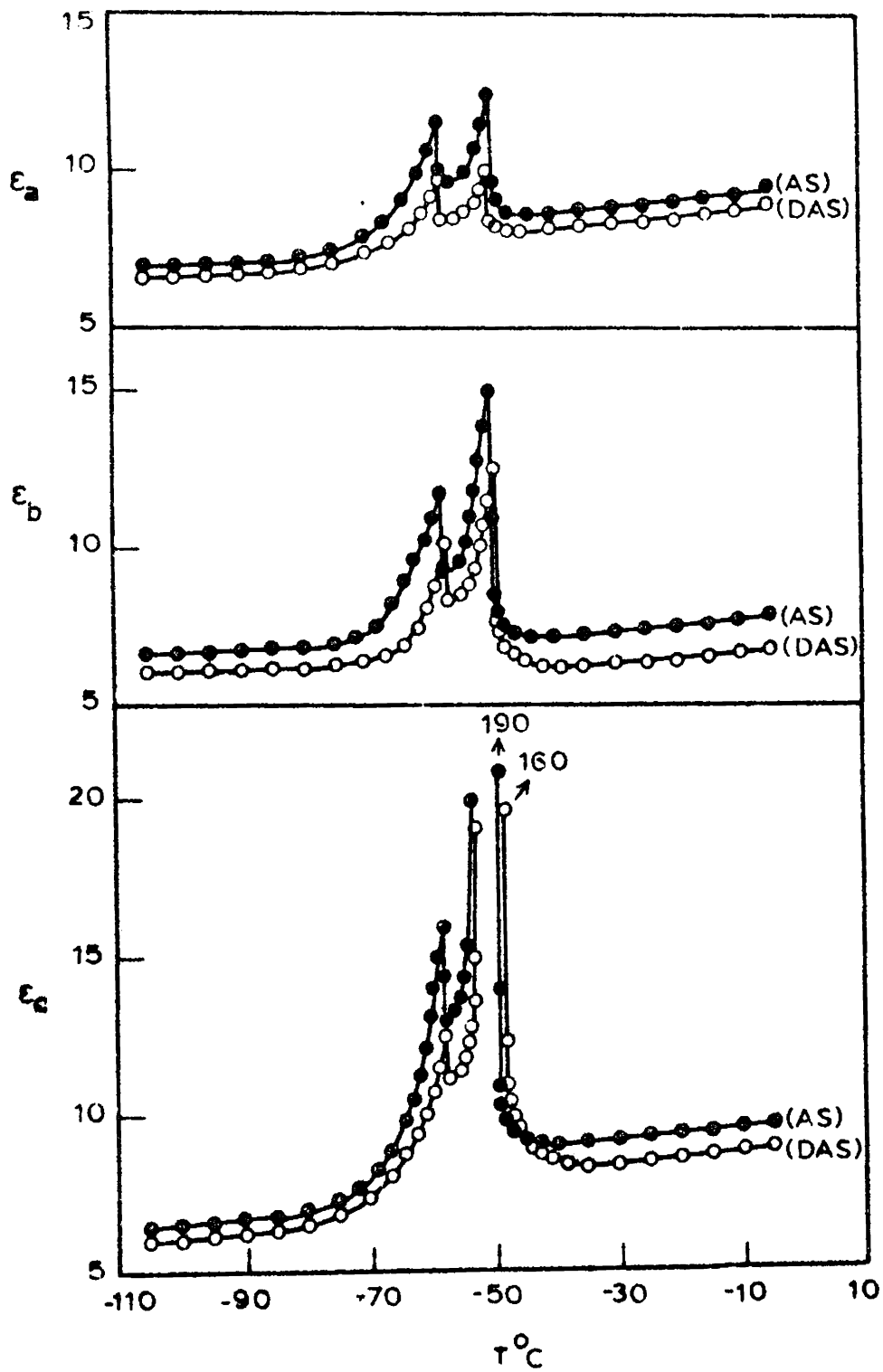
Fig.6.3 Axiswise dielectric plots for $(NH_4)_2SO_4$ (AS) and $(ND_4)_2SO_4$ (DAS) in the low-temperature region.

by using a reliable and improved experimental procedure as explained in chapter II are shown in Fig. 6.3 (Since no thermal hysteresis is noted for both transitions, the average values of the dielectric constants in the heating and cooling runs are plotted). These dielectric plots show two distinct peaks at -49.5 and -58°C. In the case of the plot corresponding to the ferroelectric (c-) axis of AS, the dielectric constant reaches maximum values of 190 and 16.1 (160 and 11.6 for DAS) at these two transition points respectively. Unlike the earlier results by Yoshihara et al. [17], the position of the peaks in this case is found to be independent of the axis of the crystal. Also the magnitude of the anomalies are found to be much higher in the present case where the measurements have been made with a direct reading instrument rather than a with bridge. As in the case of the conductivity results [8] (chapter IV), the deuteration of the sample does not change the transition points. The dielectric behaviour of the deuterated samples is found to be exactly the same as in the case of pure original samples.

6.4   Discussion

6.4.1   Phase transitions in $LiNH_4SO_4$ and $LiND_4SO_4$

The results of electrical conductivity measurements on DLAS conclusively show that, this crystal also undergoes two phase transitions at -1.5 and 191°C as suggested by conductivity studies [5,9] (chapter III). Hence it is

evident that in DLAS the high temperature transition point
is shifted upwards by 4.5°C and the low temperature transition
point is shifted downwards by 11.5°C, in comparison with the
transitions in LAS. As already mentioned in chapter III, the
upward shift of the high temperature transition point can
be explained as due to the difference in the activation
energies required for the onset of free rotation of the
$(NH_4)^+$ and $(ND_4)^+$ ions. The downward shift of the low
temperature transition point can also be explained in a
similar way as given in chapter III. The substitution of
deuteratons in the place of protons reduces the mean ampli-
tude of their vibrations and thereby alters the effective
lengths of the hydrogen bonds in the crystal [23]. This
effect can be considered as equivalent to an increase in
internal pressure. Knowing that the low temperature transi-
tion point of LAS shifts downwards with increase in pressure
[24], one can expect a downward shift of this transition
point on deuteration.

6.4.2   Phase transitions in $(NH_4)_2SO_4$ and $(ND_4)_2SO_4$

6.4.2.1.   The high temperature transition: From the experi-
mental results it is obvious that AS and DAS undergo new
phase transitions [7] at 151.5°C and at 162°C (these tempera-
tures are the average values of the transition temperatures
in the heating and cooling runs made at an extremely slow
rate of 1°C/hr). The decomposition of the crystal within

this temperature range studied here can certainly be ruled out since the results are very well reproducible for several heating and cooling cycles for the same sample; and after the measurements it was possible to recover the clear and transparent samples without any damage. This was true in the case of the earlier conductivity measurements [3-4,25] also, where the measurements were extended upto $200^{\circ}C$. The upward shift in the transition temperature in the deuterated samples brings out explicitly the role played by $(NH_4)^+$ ions in this transition unlike the low temperature transitions occurring in this crystal. The studies of electrical conductivity [3,4] (chapter IV) in AS suggest that around $150^{\circ}C$, the $(NH_4)^+$ ions in AS start free rotation from a state of torsional oscillation. Hence the transition observed here in AS with a very large variation in the dielectric constant can be assigned to the onset of free rotation of $(NH_4)^+$ ions in AS, and the upward shift in the transition temperature of DAS corresponds to the additional energy required for the unrestricted rotation of the $(ND_4)^+$ ions due to mass variation.

It is well known that in AS there are two type of ammonium ions viz. $(NH_4)_I^+$ and $(NH_4)_{II}^+$[26]. Evidences [27] show that the dipolemoment of $(SO_4)^{2-}$ ions are much smaller when compared to that of $(NH_4)_I^+$ and $(NH_4)_{II}^+$. Above the transition point $(NH_4)_I^+$ and $(NH_4)_{II}^+$ can have unhindered rotation so that these dipoles easily orient themselves in the field direction. This will make a major contribution

to the orientational part of the polarizability which explains the high value of the dielectric constant observed above the transition point. In the paraelectric phase $(NH_4)^+_{II}$ is surrounded by six $(SO_4)^{2-}$ ions and out of the various hydrogen bonds, the one with notation H(5) [26] having a bond length 1.85 $\overset{o}{A}$ is much stronger than the others. $(NH_4)^+_I$ has five $(SO_4)^{2-}$ ions surrounding it and the shortest O-H bond length is 1.97 $\overset{o}{A}$, thus giving a slightly weaker binding. Therefore the activation energies and hence the temperatures for the onset of free rotation of these two type of $(NH_4)^+$ ions need not be the same. This may cause the transition a gradual one which explains the finite slope in all the ε vs. T curves (Fig. 6.2) in the transition region.

6.4.2.2. The low temperature transition: The indication from the electrical conductivity measurements that, the well known ferroelectric phase transition occurring in AS at $-49.5^{o}C$ is actually a double transition (chapter IV) have been confirmed here by the observation of two distinct dielectric peaks at $-49.5^{o}C$ and $-58^{o}C$ in the ε vs. T plots for AS (Fig. 6.3). It has also been confirmed that the deuteration of the crystal does not affect these transition points. The mechanisms involved in these transitions can be understood by considering the successive distortions of the nonequivalent ammonium ions in the crystal. Since the distortion of the ammonium ions is the cause of these two transitions,

deuteration does not affect these two transition temperatures as mentioned earlier. A detailed analysis of the mechanism of this transition has been given in chapter IV [5].

6.5   Conclusions

Axiswise measurements of dielectric constants of $LiNH_4SO_4$, $LiND_4SO_4$, $(NH_4)_2SO_4$ and $(ND_4)_2SO_4$ from liquid nitrogen temperature to temperatures well below the melting points of each of these crystals confirm the following results already obtained from the electrical conductivity measurements.

1. The deuterated analogue of lithium ammonium sulphate, viz. $LiND_4SO_4$ exhibits two phase transitions at -1.5 and $191^\circ C$ corresponding to the two transitions at 10 and $186.5^\circ C$ respectively in $LiNH_4SO_4$.

2. The upward shift of the high temperature transition point in $LiND_4SO_4$ by $4.5^\circ C$ is attributed to the additional energy required for the onset of free rotation of the $(ND_4)^+$ ions.

3. The downward shift of the low temperature transition point by $11.5^\circ C$ has been explained as due to an internal pressure due to deuteration.

4. Abnormally large variations in the values of ϵ_a, ϵ_b and ϵ_c are observed in $(NH_4)_2SO_4$ at $151.5^\circ C$ with a thermal hysteresis of $9^\circ C$ and this confirms the phase transition already suggested from electrical conductivity studies (chapter IV).

5. The transition temperature is $162^{\circ}C$ for $(ND_4)_2SO_4$, showing an upward shift of $10.5^{\circ}C$ with respect to the corresponding transition temperature in $(NH_4)_2SO_4$ implying ammonium ions are involved in the process. The transition observed in $(NH_4)_2SO_4$ can be assigned to the onset of free rotation of the ammonium ions and the upward shift of this transition temperature in $(ND_4)_2SO_4$ corresponds to the additional energy required for the unrestricted rotation of $(ND_4)^+$ ions in $(ND_4)_2SO_4$.

6. Measurements of dielectric constant of $(NH_4)_2SO_4$ from 50 to $-196^{\circ}C$ establish two distinct phase transitions instead of one, at temperatures -49.5 and $-58^{\circ}C$.

7. The above transition temperatures remain unchanged in $(ND_4)_2SO_4$. Explanation based on successive distortions of nonequivalent ammonium ions is offered for these transitions.

A very important conclusion obtained after comparing the results of chapters III and IV and the results of this chapter is that, in detecting a new phase transition in crystals which come under the class of improper ferroelectrics, electrical conductivity measurement is much more sensitive than the dielectric method, since in these type of crystals, the variation of electrical conductivity at the transition point is much larger (1 to 3 orders of magnitude in several cases) than the corresponding changes in the dielectric constants (The high temperature phase change of AS is a notable exception).

REFERENCES

[1] U. Syamaprasad and C.P.G. Vallabhan, Solid State
    Commun. 34, 899 (1980)

[2] U. Syamaprasad and C.P.G. Vallabhan, National Acad.
    Sci. Lett. (India) 3, 364 (1980)

[3] U. Syamaprasad and C.P.G. Vallabhan, Solid State
    Commun. 38, 555 (1981)

[4] U. Syamaprasad and C.P.G. Vallabhan, Proc. Nuclear
    Phys. and Solid State Phys. Symp. (India) Paper
    No.SLA10 (1980)

[5] U. Syamaprasad and C.P.G. Vallabhan (Communicated)

[6] U. Syamaprasad and C.P.G. Vallabhan (Accepted for
    presentation in Nuclear Phys. and Solid State
    Phys. Symp. Bombay 1981)

[7] U. Syamaprasad and C.P.G. Vallabhan, J. Phys. C
    (to appear in Vol.14 1981)

[8] U. Syamaprasad and C.P.G. Vallabhan, Solid State
    Commun. (In Press)

[9] U. Syamaprasad and C.P.G. Vallabhan (Accepted for
    presentation in Nuclear Phys. and Solid State
    Phys. Symp. Bombay 1981)

[10] T. Mitsui, T. Oka, Y. Shiroishi, M. Takashige, K. Iio
     and S. Swada, J. Phys. Soc. Japan 39, 845
     (1975)

[11] S. Hoshino, K. Vedam, Y. Okaya and R. Pepinsky, Phys. Rev. 112, 405 (1958)

[12] R. Guillien, Compt. rend. 208, 980 (1939)

[13] L. Couture et al. Compt. rend. 243, 1804 (1956)

[14] B.T. Mathias and J.P. Remeika, Phys. Rev. 103, 262 (1956)

[15] H.G. Unruh, Solid State Commun. 8, 1951 (1970)

[16] A.T. Anistratov and U.G. Martynov, Soviet Phys. Cryst. 15, 256 (1970)

[17] A. Yoshihara, T. Fujimura and K.I. Kamiyoshi, Phys. Stat. Solidi(a) 34, 369 (1976)

[18] T. Ikeda, K. Fujibayashi, T. Nagai and J. Kobayashi, Phys. Stat. Solidi(a) 16, 279 (1973)

[19] K. Ohi, J. Osaka and H. Uno, J. Phys. Soc. Japan 44, 529 (1978)

[20] A. Onodera, Y. Sugatha and Y. Shiozaka, Solid State Commun. 27, 243 (1978)

[21] H.G. Unruh, E. Sailer, H. Hussinger and O. Ayere, Solid State Commun. 25, 871 (1978)

[22] D.E. O'Reilly and T. Tsang, J. Chem. Phys. 46, 1291 (1967)

[23] D. Hadzi, Hydrogen Bonding (Pergamon Press, New York)

[24] T.T. Checkmasova, I.S. Kabanov and V.I. Yuzvak, Phys. Stat. Solidi(a) 44, K155 (1977)

[25] V. Hugo Schmidt, J. Chem. Phys. 38, 2783 (1963)

[26] E.O. Schlemper and W.C. Hamilton, J. Chem. Phys.
      44, 4498 (1966)

[27] K.V. Ramanathan and R. Srinivasan, Chem. Phys. Lett.
      56, 359 (1978)

CHAPTER VII

IONIC THERMO-CURRENT (ITC) STUDIES IN
$LiNH_4SO_4$ AND $(NH_4)_2SO_4$

Abstract

An extensive study of ionic thermo-current (ITC) in pure and doped samples of $LiNH_4SO_4$ and $(NH_4)_2SO_4$ are presented in this chapter. Both crystals exhibit four distinct peaks in their ITC spectra for the pure and doped case. A detailed investigation of these ITC spectra as a function of impurity concentration, poling temperature, poling time and polarizing field have been carried out, and these studies reveal the origin and nature of each of these peaks. The numerical values of the following parameters have been calculated from the experimental results: (a) the activation energies in the various phases of the crystal; (b) the reorientation energy, (c) the association energy and (d) the frequency factor for the relaxation time of the I-V complexes.

7.1   Introduction

The dielectric relaxations in solid materials are in general studied by means of dielectric loss measurements in which alternating electric fields with frequencies ranging from 10^{-1} to 10^{12} Hz have been applied on different type of solids under a very wide range of temperature [1]. In the case of dipolar relaxation the maximum of the dielectric loss occurs at resonance frequency ω_0, which is inversely proportional to the relaxation time τ_0 of the dipoles at the temperature of the measurements [$\tau(T) = \tau_0 \exp(E/kT)$]. By measuring τ at different temperatures one obtains the characteristic parameters of the dipoles viz. τ_0 and E.

In some cases when the relaxation time of the dipoles is of the order of a few seconds, their relaxation can be studied by measuring the charging and discharging current through the dielectric using a constant electric field, at constant temperature [2].

The new method of ITC has been proposed by Bucci et al.[3] and this gives a complete picture of the temperature dependent relaxations and allows the parameters τ_0 and E to be obtained by means of a single measurement. In recent years the ITC technique has been accepted as a very effective and sensitive method for the investigation of various phenomena like impurity-vacancy (I-V) complexes

and space charge effects associated with ions, electrons
and holes in ionic, ceramic and polymeric solids [4-15].
The technique relies upon utilising the response to an
electric field of the dipole moment formed between a charge
compensating point defect and an aliovalent impurity ion.
A significant portion of the paired impurity-vacancy complexes
can be aligned away from random orientations within a
lattice by the application of a steady electric field. The
resulting non-random orientations can be immobilised by
freezing the crystal to a low temperature without disturbing
the electric field. Upon removing the electric field and
warming the specimen at a constant rate, the aligned defects
relax and reorient back to random positions. In doing so
they produce bursts of displacement current which can be
monitored as a peak in the plot of detected displacement
current against temperature. The shape of the peak with
respect to the dependence of the displacement current upon
temperature, its magnitude and temperature location can all
be related to the concentration of impurity-vacancy pairs
and to their energy of reorientation. The ITC technique
is very sensitive so that it is capable of detecting dipole
concentrations of about 10^{15} dipoles/cm^3 [16]. Furthermore
this technique is the most accurate one for the determina-
tion of the energy of migration of the charge carriers and
the reorientation energy of the impurity-vacancy complexes
[9,10].

If one increases the temperature of a poled
crystal so that the thermal energy of the lattice is suffi-
cient enough to bring about the dissociation of these dipoles,
the resulting nonuniform space charge formed by the released
mobile carriers can also cause an ITC. Some of the earlier
experiments suggested that a space charge is formed as a
result of a current flow through a crystal and it has been
previously proposed by Bucci and Riva [17] that a nonuniform
space charge can give rise to an ITC peak. When the tempera-
ture is lowered, the thermal energy of the lattice is insuffi-
cient to provide the activation energy of motion of the charge
carriers and they become effectively immobile thereby freezing
in a nonuniform space charge. If the sample is now heated at
a given rate with no external applied voltage in the circuit,
a current peak can now be observed. The reason for this
current flow is that the space charge is now thermally
released and it moves in the internal electric field due to
the nonuniform charge distribution.

Eventhough ITC studies in crystals provide valuable
information with very good accuracy, it has hitherto been
mostly confined to cubic crystals of alkaly halide type; a
notable exception being that due to Kessler [12] who applied
this method in NH_4Cl to observe some ITC peaks. Here we
have made detailed studies in the case of two noncubic
crystals viz.(1) lithium ammonium sulphate (LAS) and

ammonium sulphate (AS), the significance of which are already presented in chapters III, IV and VI [18-26]. We report in this chapter the observation of four distinct peaks in the ITC spectra of both LAS and AS measured from liquid nitrogen temperature to temperatures well below their melting/decomposition points [27]. Extensive analysis of these peaks are made by studying their characteristics as a function of impurity concentration (n), poling temperature (T_p), poling time (t_p) and poling voltage (E_p). One of the peaks observed in each case (for LAS and AS) is identified as due to protons released from $(NH_4)^+$ and hence it is the first observation of "ITC" peaks caused by protons which may be called thermally stimulated protonic current (TSPC) or protonic thermocurrent (PTC).

7.2   Theoretical Background

7.2.1 ITC arising from the reorientation of I-V dipoles

Let us consider an ideal dielectric containing only one type of noninteracting dipoles of moment p and relaxation time τ (Fig. 7.1): (1) In the absence of an electric field, the dipoles are oriented randomly.(2) If one applies an electric field E_p at the temperature T_p for an interval of time $t_p \gg \tau(T_p)$, the dipoles will be polarized to saturation and in the mean time an exponential current decay will be observed. (3) At this point the
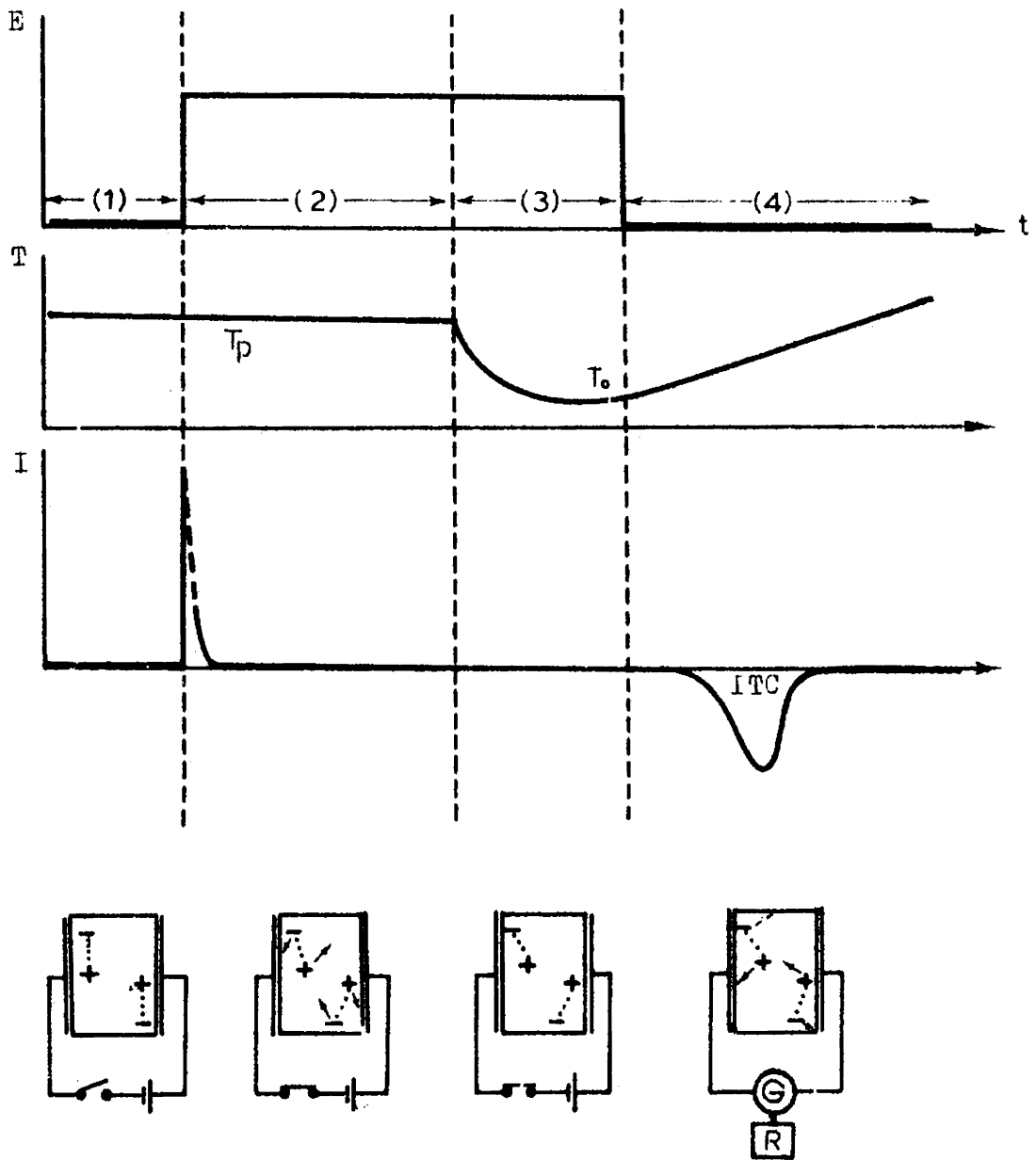
Fig.7.1 The process of ITC (see the explanation in pages 157 and 159).

158

dielectric is cooled down to such a low temperature (T_0) that the relaxation time $\tau(T_0)$ is of the order of several hours or longer. (4) At $T = T_0$, the electric field E_p is turned off and the condenser containing the dielectric is directly connected to the input of the current detector. While the electronic and atomic polarization relax, the dipoles remain oriented in the same configuration obtained at T_p. Then the dielectric is warmed up with a constant rate $b = dT/dt$: the relaxation time becomes shorter and shorter and a depolarization current $I(T)$ will be detected as the dipoles lose their preferred orientation. During the time this process occurs, the current first increases exponentially, reaches a maximum and then drops to zero. We call this current as ITC due to I-V dipoles.

The theoretical expression for the depolarization current due to the reorientation of I-V dipoles can be written as [16,28].

$$I(T) = (N_d p^2 \alpha E_p/kT_p)[\tau_0 \exp\{E/kT\}]^{-1} x$$

$$x \exp(-\int_{T_0}^{T} [b\tau_0 \exp\{E/kT'\}]^{-1} dT')$$

$$(7.1)$$

Where N_d is the number of I-V dipoles in the crystal, α is a geometrical factor depending on the orientation of the complexes, E is the activation energy for reorientation of

the complexes and τ_0 is the frequency factor for the relaxation time. The low temperature tail of the $I(T)$ peak obeys the relation

$$\ln I(T) = \text{Const.}(-E/kT) \qquad (7.2)$$

so that the activation energy E can be easily obtained using relation (7.2). When the relaxation process obeys the classical rate theory, the temperature dependence of the relaxation time is given by

$$\tau = \tau_0 \exp(E/kT) \qquad (7.3)$$

Again the activation energy E along with the frequency factor for the relaxation time can be obtained directly by plotting the temperature against the right hand side of the following equation

$$\tau_0 \exp(E/kT^*) = \int_{T^*}^{\infty} I(T)dT/I(T^*), \qquad (7.4)$$

in which the numerator is the area under the ITC peak from $T = T^*$ to $T = \infty$ and the denominator is the value of the current at $T = T^*$. Thus the activation energy can be computed by the integration of the entire ITC peak using equation (4) or by using equation (2) where, only the low temperature tail of the peak is used. Both must lead to the same value of activation energy when the reorientation of the I-V complexes is the cause for the ITC peak.

7.2.2 ITC arising from nonuniform space charge

The theory of space charge polarization has been developed by MacDonald [29,30]. The equation representing the build-up or release of space charge cannot be integrated exactly. When an ionic space charge builds up during the polarization of the dielectric, there will be a band in the ITC spectrum, rerepresenting its thermal release, which has the following properties: (1) The temperature of its maximum T_M is not well defined. As T_p increases T_M also increases, (2) the area delimited by the band is not a linear function of the applied electric field, particularly at low fields; (3) the shape of the band does not yield the activation energy.

The current density in a polarized crystal is described [29,31] in terms of the drift carriers resulting from the polarization field and the concentration gradient. For describing the current density in a crystal containing aliovalent impurities Kessler and Caffyn [13] modified it as follows:

$$j(x) = (Const.)exp(-E_m/kT)exp(-E_a/2kT)$$

$$x \ \partial n_c(x,0)/\partial x \qquad (7.5)$$

Where E_m represents the activation energy for migration of the carriers and E_a the association energy of the

complexes. $n_c(x,0)$ denotes the concentration of the frozen-in complexes. Hence if log $I(T)$ is plotted as a function of T^{-1} according to equation (7.5) a straight line will be obtained with slope proportional to $(E_m + \frac{1}{2}E_a)$. The energy of migration can be obtained separately from the equation

$$\ln I(T) = Const.(-E_m/kT), \qquad (7.6)$$

which corresponds to the space charge region for the pure crystal.

7.3   Experimental

The methods of preparation of single crystals of LAS and AS are given in chapters III and IV. The pure samples used were obtained after five recrystallisations of extra pure BDH Analar grade salt using triply distilled water. Doping of the crystals with Cu^{2+} and Zn^{2+} was done by adding specific amount of $CuSO_4$ and $ZnSO_4$ in the solution. The purity of the samples was tested by an atomic absorption spectrometer (Perkin-Elmer 306) and it was confirmed that the inherent impurity levels in the pure samples were below the detection limit of the instrument. The nominal concentrations of the divalent impurities (Cu^{2+} and Zn^{2+})in the doped samples ranged from 10 to 200 ppm. Polished samples for measurement were prepared by cutting slices of typical size 5 x 5 x 0.5 mm^3 from large single crystals. Quick drying silver conducting

paint was applied on the broader faces of the sample as the electrodes. The sample holder, vacuum chamber for temperature variation studies used in this experiment and measurement temperature have been described in chapter II.

The ITC measurements were made in the usual way by polarizing the sample at a temperature T_p (ranging from 30 to 290°C) for a certain time t_p (1-30 minutes) with a field E_p (0.1-10 KV/cm) and then quenching the sample to liquid nitrogen temperature. The sample thus prepared was heated there after at a constant rate of about 0.1°C/sec. and the discharge current (ITC) was measured using an electrometer (ECIL EA815) and recorded together with the thermo-couple voltage on an X-Y recorder (Digital Electronics Model 2000).

7.4   Experimental Results

7.4.1 Lithium Ammonium Sulphate

7.4.1.1.   ITC spectra of pure and doped LAS: Figure   7.2 shows the ITC spectra of pure and doped (with Cu^{2+} and Zn^{2+}) LAS single crystal along the ferroelectric (a-)axis. For the pure crystals, the spectrum consists of four distinct peaks of varying magnitude. The temperatures at which their maxima (T_m) occur are -25, 10, 186 and 235°C. Let us denote them as peaks A, B, C and D respectively in the order of increasing temperature as shown in Fig. 7.2. Peak B occurring at 10°C is quite sharp and narrow with a height
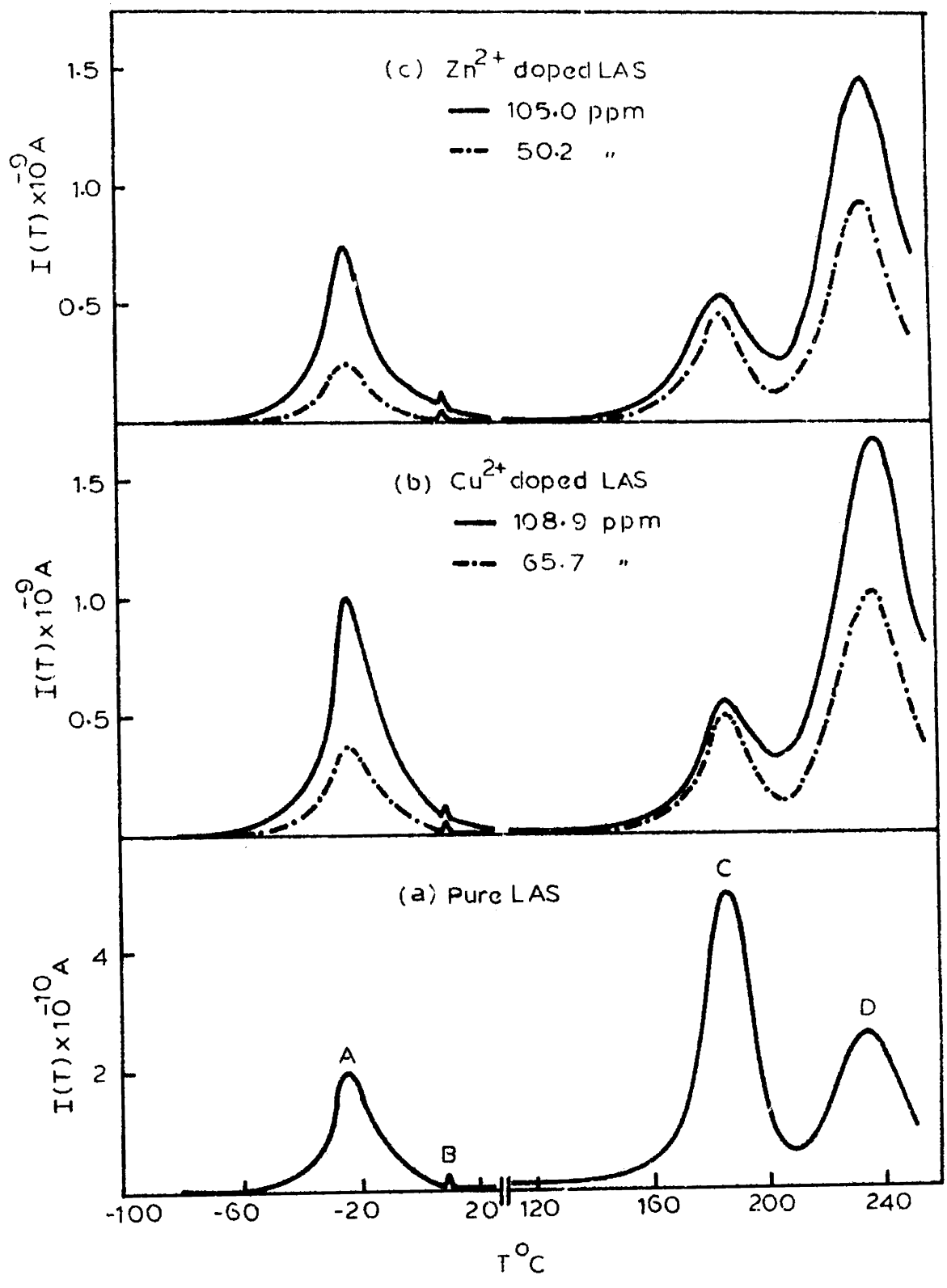
Fig.7.2 ITC spectra of pure and doped LAS: E_p = 5KV/cm, T_p = 250°C, t_p = 10 minutes, T_o = −196°C and b = 0.1°C/sec.

164

approximately one order of magnitude less than that for the remaining ones. In the case of doped samples also, the ITC spectrum consists of four peaks corresponding to the peaks A, B, C and D in pure LAS. But here T_m depends on the dopant material in the case of peaks A and D while it is independent of the impurity for peaks B and C. Also the heights of the peaks A and D viz. $I_A(T_m)$ and $I_D(T_m)$ increase rapidly with impurity concentration whereas no significant change is observed in the case of $I_B(T_m)$ and $I_C(T_m)$. The enhancement of $I(T_m)$ with impurity levels is stronger in the case of peak D which is having a height approximately twice that of peak A.

7.4.1.2. Effect of poling temperature (T_p) : To study the effect of poling temperature on the nature of the ITC peaks, the samples were polarized at different temperatures for a fixed time (10 minutes) and quenched to liquid nitrogen temperature, a method similar to the usual peak cleaning technique. The ITC spectra for samples polarized at 30, 170, 200 and 290°C are shown in Fig. 7.3. It is found that the sample polarized at 30°C shows a maximum peak height for peak A and a minimum for peaks C and D. The intensity and shape of peak B (not shown in Fig. 7.3) are found to be unaffected by this process. For sample polarized at 170°C (just below the high temperature transition point of LAS) $I_D(T_m)$ is found to be unaffected. In the case of a sample polarized at 200°C (just above the high temperature transition point of LAS)
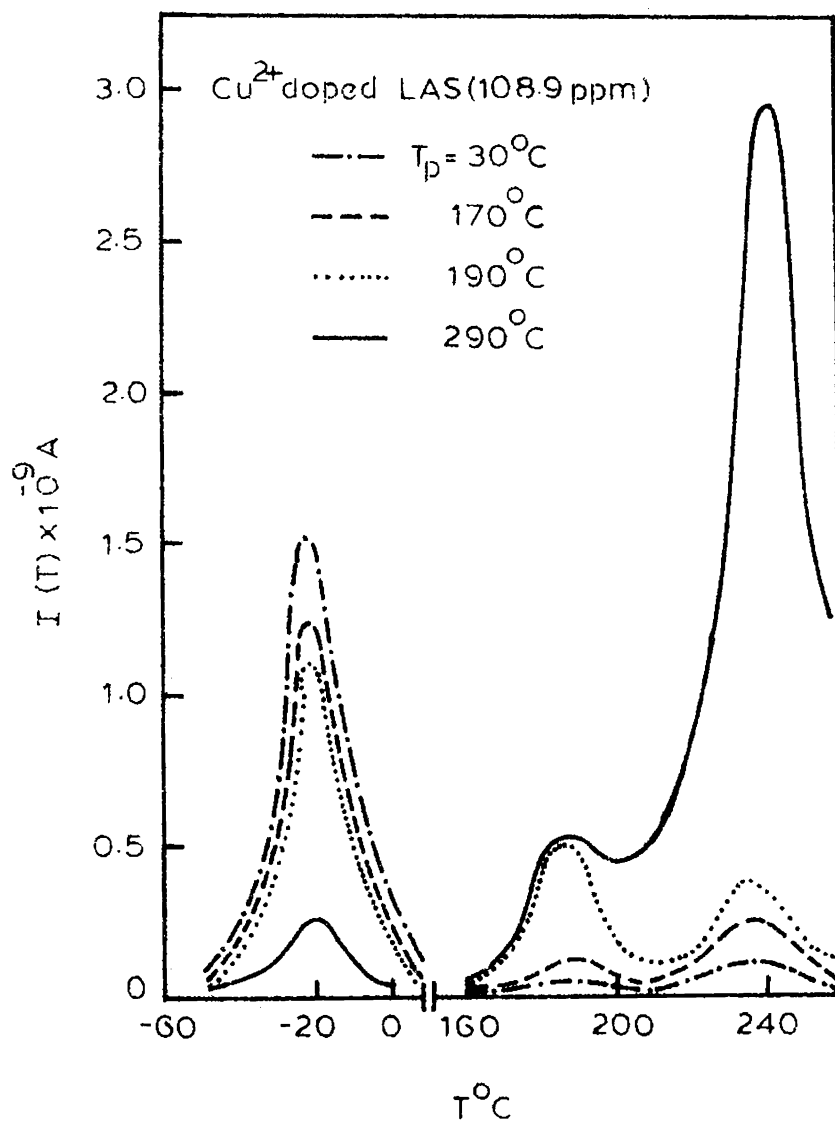
Fig. 7.3 Effect of T_p on the ITC spectrum of .... d pad
LAS : E_p 5KV/cm, t_p 10 minutes, ... −19
and b 0.1°C/sec.
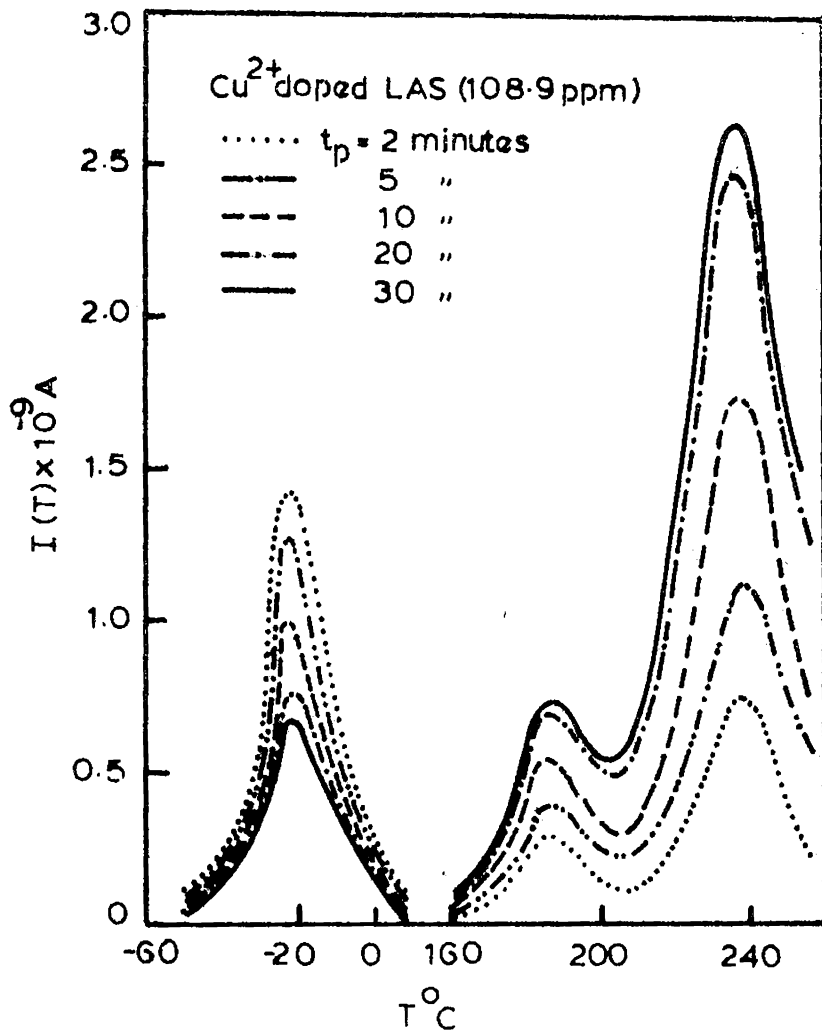
Fig.7.4 Effect of t_p on the ITC spectrum of Cu^{2+} doped LAS : $E_p = 5KV/cm$, $T_p = 250^\circ C$, $T_o = -196^\circ C$, and $b = 0.1^\circ C/sec$.
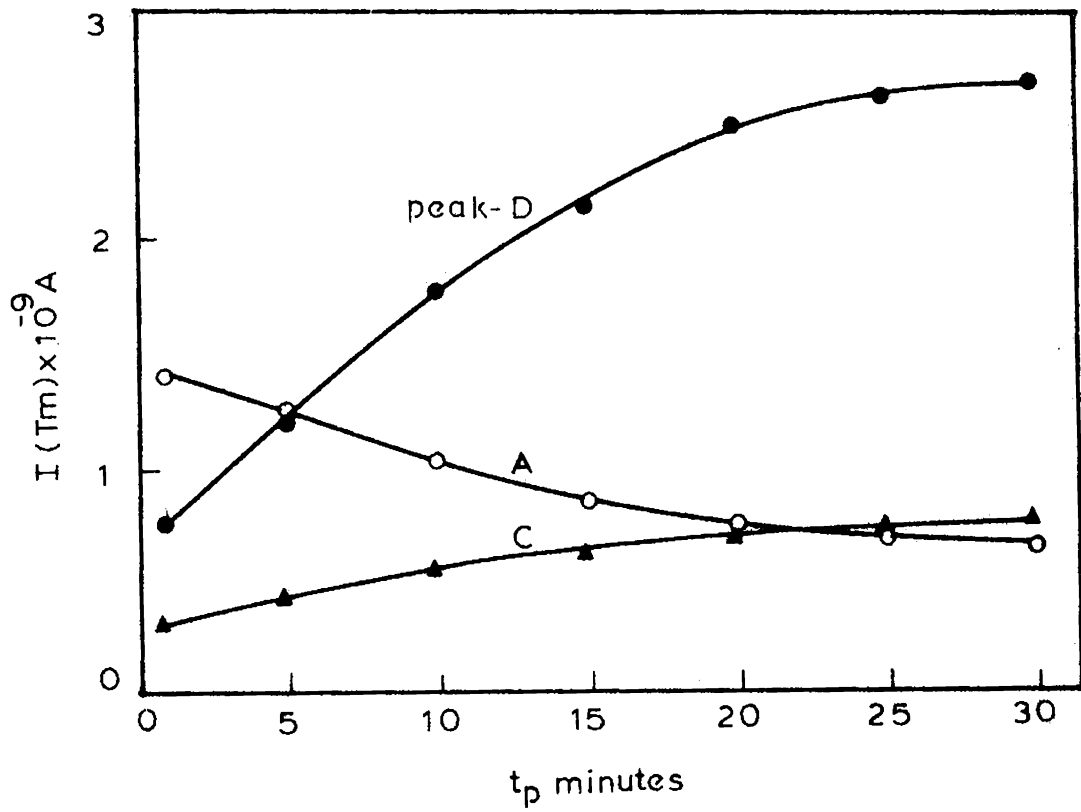
Fig.7.5 Variation of the current maxima $I(T_m)$ for peaks
A, C and D as a function of poling time (t_p) :
E_p = 5KV/cm, T_p = 250°C, T_0 = -196°C and
b = 0.1°C/sec.

168

$I_C(T_m)$ reaches almost its maximum value while $I_D(T_m)$ shows

only a slight increase which again is at the expense of

$I_A(T_m)$. The crystal polarized at $290^\circ C$ shows a maximum height

for peak D and a minimum height for peak A while $I_C(T_m)$

retains its previous maximum value. It is to be noted that

the position of the peak D is shifted to a higher temperature

by $7^\circ C$ in the case of a sample polarized at $290^C C$.

7.4.1.3. Effect of polarizing time (t_p): As ionic conducti-

vity and polarization are extremely sensitive to thermal

treatment we made ITC measurements on samples containing a

fixed amount of impurity ions by varying t_p, while keeping

E_p constant. Fig. 7.4 shows the effect of polarizing time

on the ITC spectrum of doped LAS containing 108 ppm of Cu^{2+}

polarized at $250^\circ C$ and Fig. 7.5 shows the current maxima

$I(T_m)$ for each of these peak plotted as a function of t_p.

For values of t_p ranging from 1 to 10 minutes $I_C(T_m)$ and

$I_D(T_m)$ are found to be increasing linearly with t_p along with

a corresponding linear decrease in $I_A(T_m)$, whereas for t_p

greater than 10 minutes this change is not linear and for

t_p greater than 20 minutes the height of these three peaks

remain unaffected. In all these cases peak B (not shown in

Figs. 7.4 and 7.5) remains unchanged.

7.4.1.4. Effect of polarizing field (E_p): The ITC spectra

of LAS doped with Cu^{2+} (108 ppm) for different polarizing

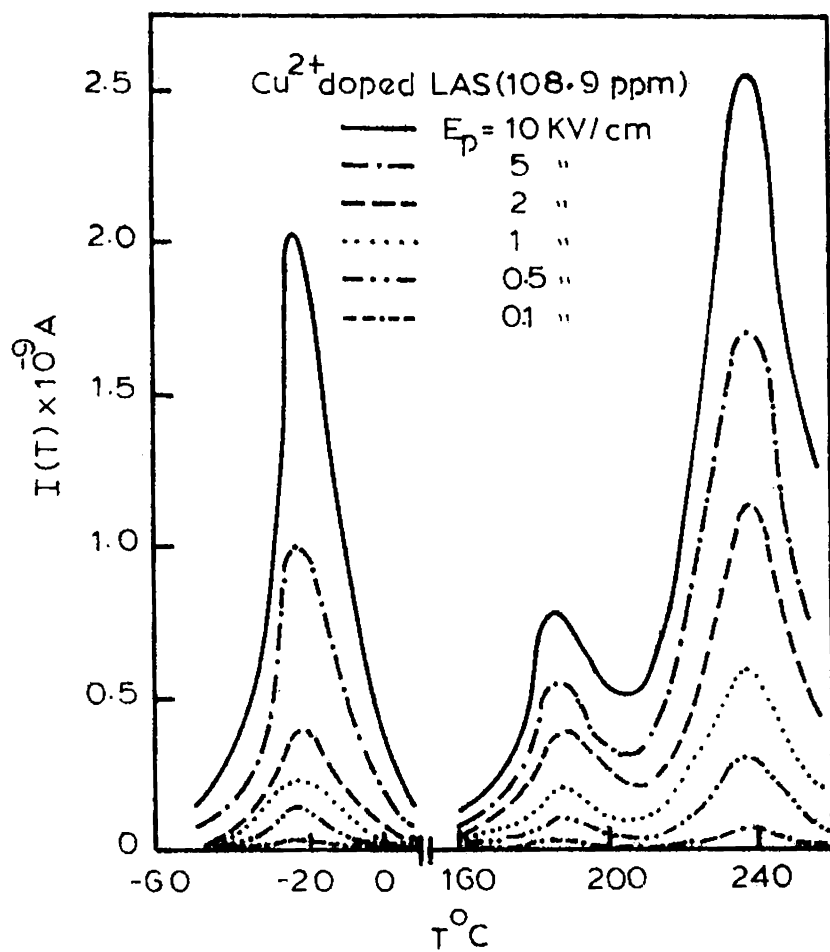fields are shown in Fig. 7.6. In Fig. 7.7 the current maxima

Fig.7.6 Effect of E_p on the ITC spectrum of Cu^{2+} doped LAS : $T_p = 250^\circ C$, $t_p = 10$ minutes, $T_o = -196^\circ C$ and b 0.1$^\circ C$/sec.
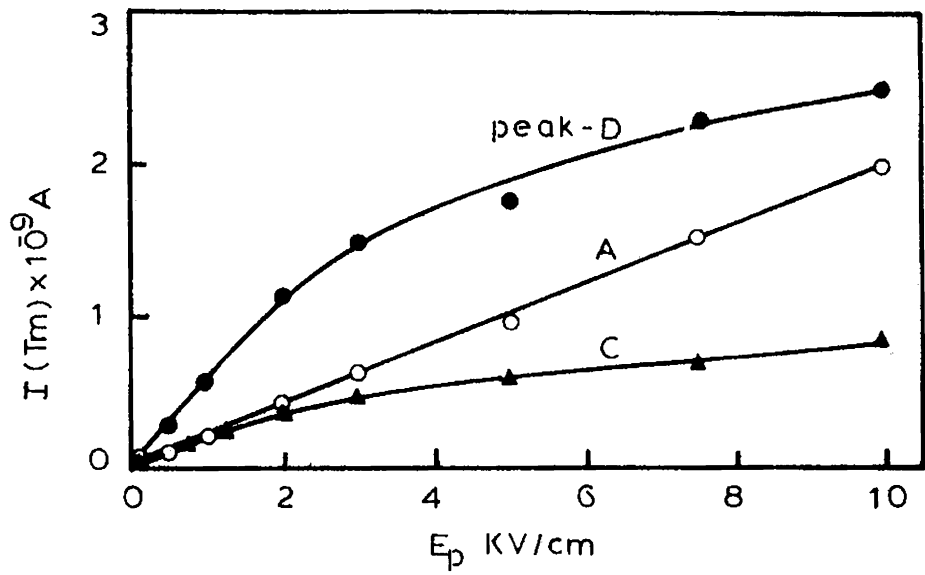
Fig.7.7 Variations of the current maxima $I(T_m)$ for
the peaks A, C and D with respect to poling
voltage (E_p) : $T_p = 250^{\circ}C$, t_p 10 minutes,
$T_o = -196^{\circ}C$ and $b = 0.1^{\circ}C/sec$.

171

for each of these peak are plotted as a function of E_p. In the case of peak A the plot is found to be linear throughout the range (0.1 to 10 KV/cm). The corresponding plots for peaks C and D are linear only upto about 2 KV/cm and saturation effects are found to occur beyond this value. In the case of peak B (not shown in Figs. 7.6 and 7.7) no variation is observed with respect to its shape or magnitude.

7.4.2. Ammonium Sulphate

7.4.2.1. ITC spectra of pure and doped AS: Fig. 7.8(a) shows the ITC spectra for pure and doped (with Cu^{2+} and Zn^{2+}) AS single crystals along the c-axis. The ITC spectrum for the pure crystal consists of four peaks occurring at -50, -10, 151 and 195°C. Let us denote these peaks as peak P, Q, R and S in the order of increasing temperature. In the case of doped samples also the spectra consist of four peaks corresponding to the peaks for the pure sample. Here T_m and $I(T_m)$ depend on the dopant material for the peaks Q and S while the position or intensity of peaks P and R are unaffected by impurities. In all the cases peaks P and Q; and R and S are very close and it is found that the usual peak cleaning methods cannot improve the resolution.

7.4.2.2. Effect of poling voltage (E_p): In Fig. 7.8(b), $I(T_m)$ for different peaks are plotted as a function of E_p for AS doped with Cu^{2+} (122 ppm). In the case of peak P (not shown in Fig.) no variation is observed with respect
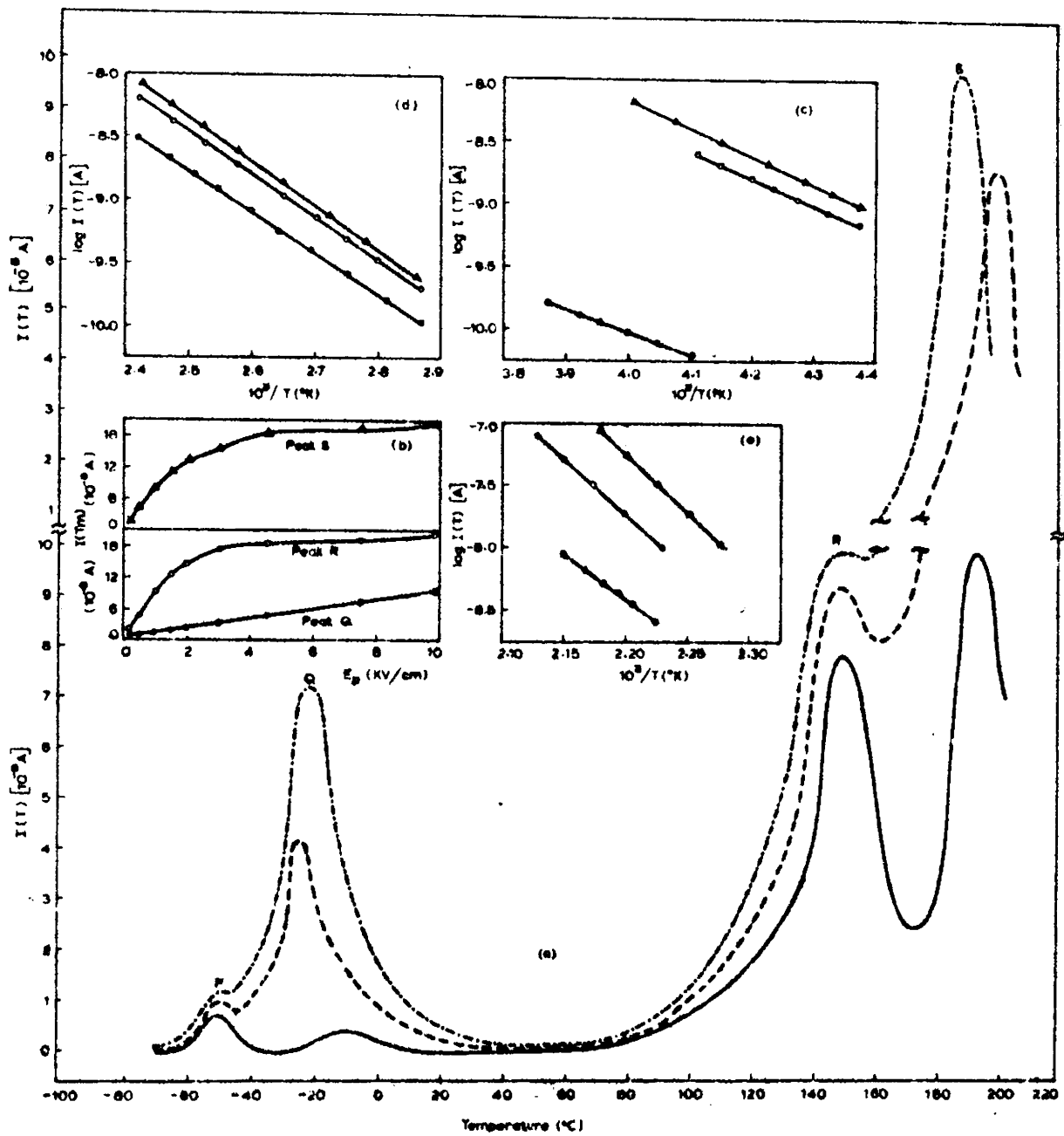
Fig. 8 (a) ITC spectra of pure and doped $(NH_4)_2SO_4$, (b) Effect of poling voltage on peak heights, (c)/(d) and (e) log I vs $10^3/T$ plots corresponding to peaks Q, R and S.

to its shape or magnitude. The plot for peak Q is found to be linear throughout the range (0.1 to 10 KV/cm). The plots for peaks $\dot{R}$ and S are found to be linear upto about 1.5 KV/cm and saturation effects are found beyond this value.

7.5   Analysis of the ITC Peaks

7.5.1 ITC peaks in $\overline{Li}NH_4SO_4$

Of the four peaks observed in the ITC spectrum of LAS, the one at $10^{\circ}C$ viz. peak B cannot be accepted as a typical ITC peak on the basis of its behaviour towards the various parameters n, T_p, t_p and E_p. Hence no consideration based on the above theories is given to this peak in the following analysis.

The plots of log I(T) vs T^{-1} for the low temperature tail of the peak A, C and D corresponding to the pure sample give three linear portions with different slopes as shown in figs. 7.9, 7.10 and 7.11 respectively. Using equation (7.2) the activation energy for the three regions are obtained as 0.48, 0.58 and 1.55 eV respectively. An independent analysis using integration of the entire peaks according to equation (7.4) shows that the activation energy value thus obtained corresponding to peak A (0.47 eV) agrees well with that obtained by using the tail of the peak. The values of activation energies obtained in a

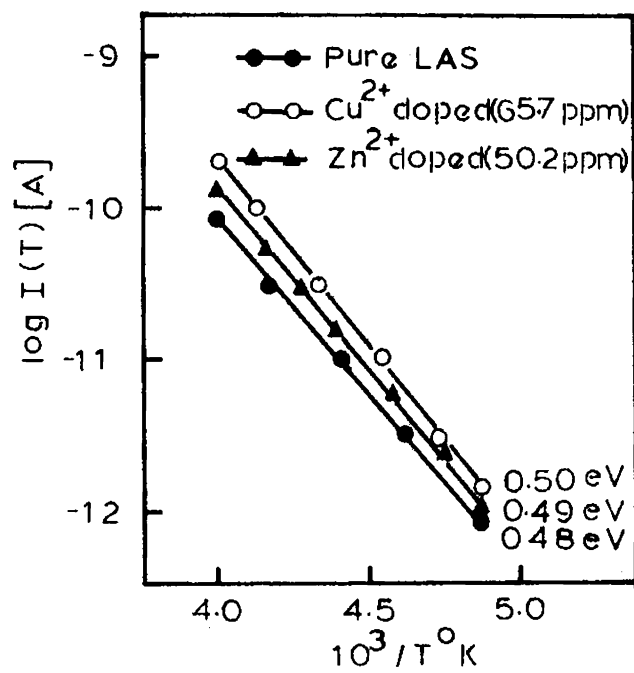Fig.7.9 log I(T) vs T^{-1} plots for the low-
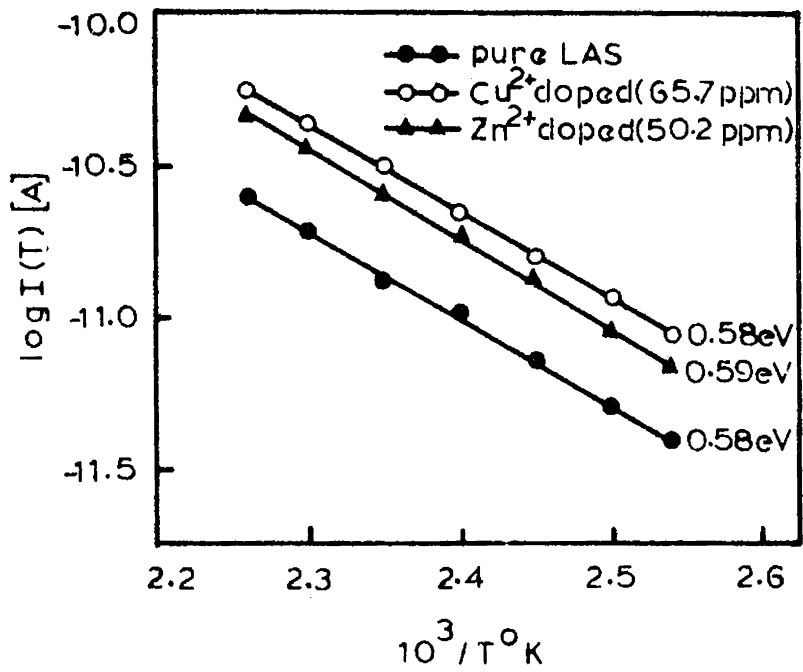temperature portion of peaks A.

Fig.7.10   log I(T) vs T^{-1} plots for the low-temperature portion of peaks C.
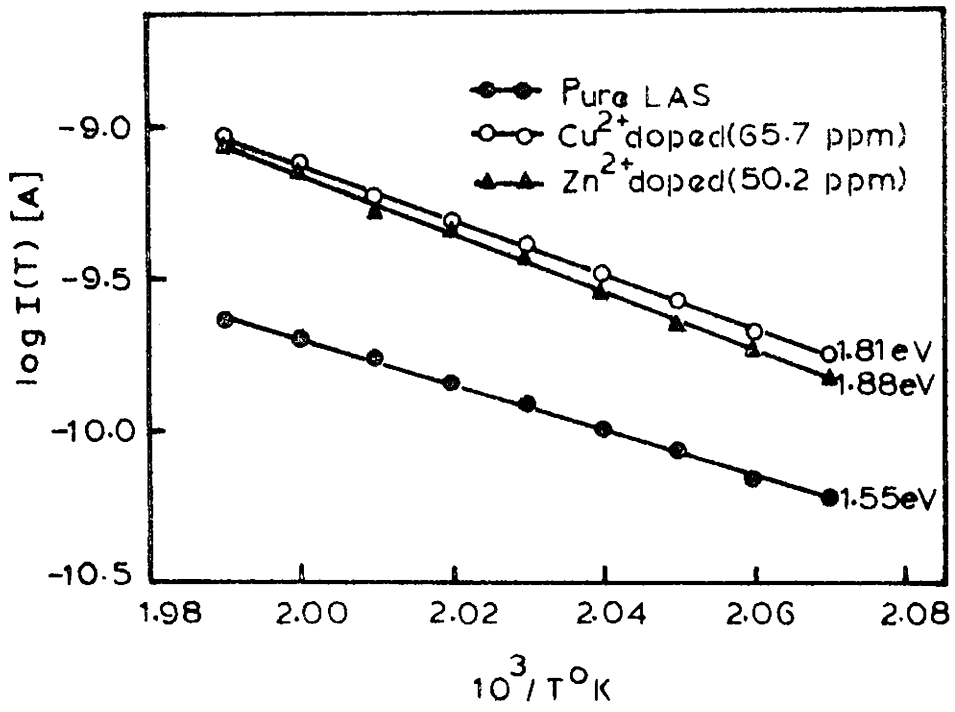
Fig.7.11 log I(T) vs T^{-1} plots for the low-temperature portion of peaks D.

177

similar way in the case of peaks C and D are greater than the corresponding values calculated using equation (7.2) approximately by a factor of 2. Hence it is evident that peak A is due to I-V complexes while peak C and D are not. Considering the changes in $I_C(T_m)$ and $I_D(T_m)$ with respect to n, T_p, t_p and E_p and keeping in mind that the reorientation of I-V complexes has been excluded as a cause of these peaks, we are led to conclude that these peaks arise from the nonuniform distribution of space charges within the crystal. The activation energies calculated for doped samples (Table 7.1) from the log I(T) vs T^{-1} plots, which are also found to be linear (Figs. 7.9, 7.10 and 7.11) show that there is significant increase in their values corresponding to peak D while only a slight increase is observed in the activation energy values corresponding to peak A when compared to these values for pure sample. But no such changes in activation energies are observed in the case of peak C.

The analysis of peak A for the doped samples using equation (7.4) gives the relaxation time of the I-V complexes present in these samples. Fig. 7.12 shows the log τ vs T^{-1} plot for the pure and doped samples using equation (7.4). The activation energies calculated from these plots are 0.47, 0.50 and 0.49 eV respectively for pure, Cu^{2+} doped (65.7 ppm) and Zn^{2+} doped (50.2 ppm) respectively, which
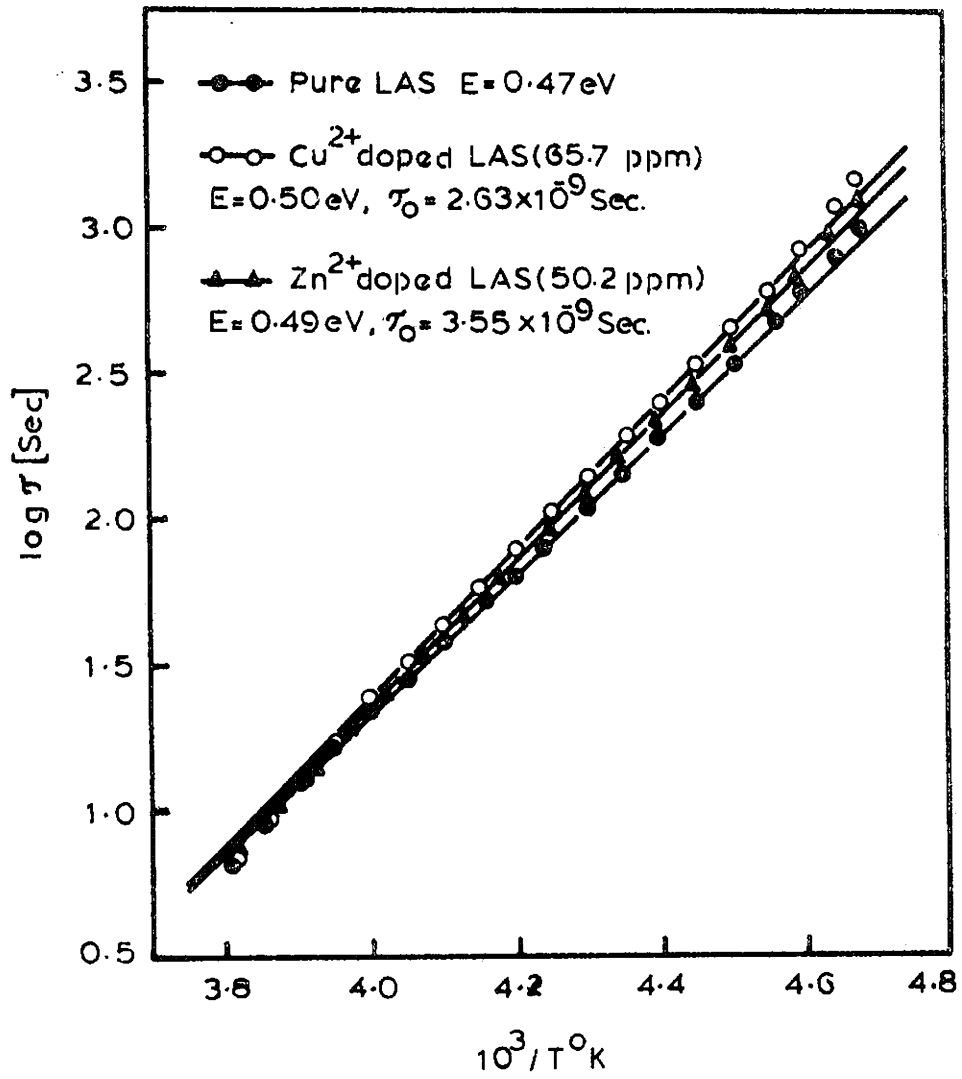
Fig.7.12 log τ vs T^{-1} plots corresponding to peaks A for different samples.

are in excellent agreement with those obtained by using equation (7.2) (Table 7.1). Using equation (7.3) the frequency factor for the relaxation time τ_o for the I-V complexes, in these samples are obtained as

$\tau_o(1) = 2.63 \times 10^{-9}$ sec. and $\tau_o(2) = 3.55 \times 10^{-9}$ sec. respectively.

7.5.2 ITC peaks in $(NH_4)_2SO_4$

As in the case of peak B in LAS, the peak P observed in the ITC spectrum of AS cannot be accepted as a typical ITC peak on the basis of its behaviour towards the different impurities and polarizing fields.

The log $I(T)$ vs T^{-1} plots for the low temperature tail of peaks Q, R and S corresponding to the pure sample give three linear regions with different slopes as shown in Figs. 7.8(c,d and e). Using equation (7.2) the activation energies for the three regions are obtained as 0.37, 0.66 and 1.42 eV respectively. The activation energies calculated for doped samples (Table 7.2) from the log $I(T)$ vs T^{-1} plots which are also found to be linear (Figs. 7.8c, d and e) show that there is appreciable increase in their values corresponding to peak S while only a slight increase is observed in the activation energy values corresponding to peaks Q and R compared to these values for pure samples. Taking into account the

variations of the position and shape of these peaks with respect to the different type of impurities and the changes in polarizing voltage we can see that peak P is not a typical ITC peak either due to I-V dipoles or due to the nonuniform space charge distribution (the peak corresponding to the latter will be observed only at higher temperature) peak Q is due to I-V dipoles; and R and S are due to nonuniform space charge carriers (detailed discussion is presented in Sec.7.6).

7.6 Discussion

7.6.1 The ITC spectrum of $LiNH_4SO_4$

When divalent metallic impurities (Z^{2+}) are substituted for monovalent ions in an ionic crystal like LAS, the condition for electrical neutrality [32] requires that the positive ion vacancies (V_p^-) or negative ion interstitials (X^-) should be created in the crystal. The impurities tend to become associated since this minimises the free energy. The degree of association therefore depends on the temperature [33]. In LAS containing divalent impurities the possible type of complexes present are ($Z^{2+}V_p^-$) and ($Z^{2-}X^+$)[18]; where Z^{2-} represents the inherent divalent anion impurities and X^+ the interstitial lithium ion. Since the concentration of Z^{2-} which remains the same as that in pure crystal, is only of the order of 10^{-6} molar fraction, the occurrence of ($Z^{2-}X^+$)

complexes can be neglected when compared to $(z^{2+}v_p^-)$. Hence in Cu^{2+} and Zn^{2+} doped LAS, the type of I-V complexes present are $(Cu^{2+}v_p^-)$ and $(Zn^{2+}v_p^-)$ respectively. A reorientation of these complexes which have permanent electric dipolemoments can give rise to the peak A in doped samples. Even pure sample contains inherent cationic impurities of the order of 10^{-6} molar fraction for the formation of such complexes and the ITC method is sensitive enough to detect complex concentrations as low as 10^{15} dipoles/cm^3. This explains the occurrence of peak A with appreciable height even in pure samples.

At $10^o C$ the crystal undergoes a structural phase transition [34,35]. The small sharp peak observed at this temperature can be due to the sudden large scale occurrence of the mobile carriers released during the rearrangement process of the crystal lattice or due to the loosening of the same when it undergoes a phase transition. As mentioned earlier this cannot be considered as a typical ITC peak.

The electrical conductivity studies in ammonium containing ionic crystals like NH_4Cl[36,37], $(NH_4)_2SO_4$ [20-23] (chapter III and VI), $LiNH_4SO_4$ [18,19,24-26] (chapter III and VI) and $(NH_4)_2H(SO_4)_2$ [38] (chapter V) reveal that the reorientation or free rotation of the ammonium groups in these crystals can lead to phase transitions and such motional effects of ammonium group generate a large number

of protonic defects which contribute significantly to the
conduction process. In LAS a transition of this type occurs
[18,19] at 186.5°C. Hence the ITC peak observed here at
186°C (peak C) in LAS is evidently due to a nonuniform distri-
bution of these protonic defects generated at this transition
point. Above 200°C the complexes $(Cu^{2+}V_p^-)$ and $(Zn^{2+}V_p^-)$ begin
to dissociate and when we quench the sample from 250°C to
liquid nitrogen temperature, the carriers thus generated
are immobilised giving rise to a nonuniform space charge.
The peak D observed at 235°C is certainly due to the thermal
release of these frozen-in carriers which drift in the
internal electric field caused by this nonuniform space
charge. An increase in concentration of impurities will
increase the total number of I-V complexes and this will
lead to a proportional increase in the number of carriers
giving rise to the space charge. Hence on increasing
the concentration of impurities, the height of the peaks A
and D will be enhanced correspondingly, which is confirmed
by the experimental results (Fig. 7.2). As the height of
peak C is independent of impurity concentration, it is
evident that the protons released at the transition point
form no stable complexes with any of the charge compensators
produced in the doping process within the temperature
range studied here.

At $30^{\circ}C$ nearly all the impurities and vacancies
are trapped in the complexes with practically no space charge
carriers. So the ITC spectrum for a sample polarized at
this temperature has a maximum height for peak A (due to
I-V complexes) and a minimum for peak C and D (Fig. 7.3).
At $170^{\circ}C$ a very small portion of these complexes are in
dissociated state forming space charges and this enhances
the height of peak D at the expense of peak A. For a sample
polarized at $200^{\circ}C$ (just above the phase transition tempera-
ture) a maximum value for $I_C(T_m)$ is observed with no further
increase in its value for higher poling temperatures. At
$290^{\circ}C$ most of the I-V complexes in the crystal are in disso-
ciated state providing a maximum number of space charge
carriers. Hence the ITC spectrum for the sample polarized
at this temperature shows a maximum for $I_D(T_m)$ and a minimum
for $I_A(T_m)$ with no significant change in $I_C(T_m)$. The changes
in $I_C(T_m)$ for samples polarized at 170, 200 and $290^{\circ}C$ once
again confirm that the sudden generation of the carriers
produced at the transition point ($186.5^{\circ}C$) is solely responsi-
ble for peak C. It has already been proved from electrical
conductivity studies on LAS and LDS that, the carriers
released at the high temperature transition point of LAS
is protons [24] (chapter III). So we can conclude that
peak C is due to a nonuniform distribution of protons and
hence peak C can be called a Thermally Stimulated Protonic
Current (TSPC) or Protonic Thermo Current (PTC) peak.

The variation (Fig. 7.4) of peak heights with poling time (T_p = 250°C) shows that the rate of dissociation of the I-V complexes in Cu^{2+} doped LAS at this temperature increases linearly with time upto 10 minutes, then levels off beyond this. We find that after 20 minutes the dissociation is practically complete. The linear variation of $I_A(T_m)$ and $I_D(T_m)$ with E_p (Fig. 7.7) undisputably confirms again that peak A is due to I-V complexes. Also a linear variation of $I_C(T_m)$ and $I_D(T_m)$ with E_p in the low field region and the occurrence of saturation effects for higher fields (Fig. 7.7) in the case of peaks C and D clearly show that the release of space charge carriers is responsible for their origin.

If we compare the activation energies obtained from the electrical conductivity measurements [18,19] with those from ITC experiments (Table 1) in the case of pure LAS the following conclusions can be made: The activation energies in the phases I(T ≥ 186.5°C) and II(10 ≤ T ≤ 186.5°C) obtained from conductivity measurements (1.51 and 0.58 eV respectively) agree very well with those obtained from ITC measurements which give activation energies (corresponding to peak D and C) as 1.55 and 0.58 eV respectively. In phase III (T ≤ 10°C) the activation energy for conduction is only 0.025 eV and this very low value is explained as due to the precipitation and complex formation of impurities

in this phase. The analysis of peak A (which exists in phase III) both by using the tail of the peak and by the integration of the entire ITC peak gives activation energy values 0.48 and 0.47 eV respectively. Both values show excellent mutual agreement; but the activation energy value obtained from conductivity measurements corresponding to phase III does not agree with this. This apparent discrepancy is not a real one, since the former corresponds to the reorientation of energy of the I-V complexes while the latter represents the migration energy of the carriers.

The activation energy values obtained from peak A for Cu^{2+} (65.7 ppm) and Zn^{2+} (50.2 ppm) doped samples (Table 1) represent the energies corresponding to the re-orientation of $(Cu^{2+}V_p^-)$ and $(Zn^{2+}V_p^-)$ complexes. In the region corresponding to peak C, in Fig. 7.10 we find that both $I_C(T_m)$ and T_m are unaltered by impurities indicating that impurity levels of this magnitude cannot affect the reorientation of the ammonium ions in the crystal. The increase in activation energy in the space charge region corresponding to peak D of the doped samples account for the energy of association of the complexes. The activation energy of the pure crystal in this region gives the energy of migration of the charge carriers. Hence using equation (7.5) and referring to table 1 the energies of association of the complexes $(Cu^{2+}V_p^-)$ and $(Zn^{2+}V_p^-)$ can be obtained as 0.52 and 0.66 eV respectively.

7.6.2   The ITC spectrum of $(NH_4)_2SO_4$

As observed in LAS at $10^{\circ}C$, the peak P in the ITC spectrum of AS can be attributed to the phase transition occurring in the crystal at this temperature. As mentioned earlier this peak cannot be considered as a typical ITC peak. Peak Q can be considered as a typical ITC peak due to I-V dipoles on considerations based on its behaviour towards different type of divalent cations and towards the polarizing field. Peak R can be considered as a protonic thermo-current (PTC) peak on the basis of the same reasons given in the case of peak C in LAS. The peak S observed around $195^{\circ}C$ may be attributed to the nonuniform space charge carriers released as a result of the dissociation of the I-V complexes.

From a comparison of the activation energies obtained from electrical conductivity measurements [20] (chapter IV) with those from ITC experiments (Table 2) in the case of pure AS it can be seen that the activation energy values except in the low temperature (ferroelectric) phase show mutual agreement. In the low temperature phase the activation energy value obtained from electrical conductivity measurements gives only the conduction activation energy of the carriers, whereas that obtained from ITC experiment gives the reorientation energy of the I-V complexes. Hence one does not expect any mutual agreement between the activation energy values obtained from the two experiments.

7.7   Conclusions

The study of the ITC spectra of pure and doped (with Cu^{2+} and Zn^{2+}) $LiNH_4SO_4$ single crystals in the temperature range -196 to $250^{\circ}C$ as a function of impurity concentration, poling temperature, poling time and polarizing field leads to the following conclusions:

1. Four distinct peaks denoted as A, B, C and D are observed in the case of pure as well as doped LAS.

2. Peak A can be assigned unambiguously to the reorientation of the I-V complexes. In samples doped with Cu^{2+} and Zn^{2+} these complexes are identified as $(Cu^{2+}V_p^-)$ and $(Zn^{2+}V_p^-)$ respectively.

3. Peak B observed at $10^{\circ}C$ is not a typical ITC peak. It can be explained as due to a sudden release of the carriers generated when the crystal undergoes a structural phase transition.

4. The third peak C observed at $186^{\circ}C$ arises from a non-uniform space charge distribution of protons released due to the motional effects of the ammonium ions when the crystal undergoes a reorientational type transition at this temperature. This is the first report that the protons released during the reorientational transition of a crystal can give rise to an ITC peak and this technique may be applied to a series of crystals of this type.

5. Peak D can be attributed to the nonuniform distribution of the space charge carriers released during the dissociation of the previously mentioned I-V complexes.

6. The values of the parameters obtained from the analysis of the above peaks include the energy of the carriers in the different phases of the crystal, the reorientation energy, frequency factor for the relaxation time and the association energy of the I-V complexes as shown in Table 1.

7. The comparison of the data with those available from the earlier conductivity studies are found to be in excellent agreement.

A similar ITC measurement has also been carried out on $(NH_4)_2SO_4$ which leads to the following conclusions.

8. Four peaks viz. peaks P, Q, R and S are observed in the ITC spectra of pure and doped (with Cu^{2+} and Zn^{2+}) AS.

9. Of the four peaks, the first one (P) occurring at $-50^\circ C$ does not show the properties of a typical ITC peak and it is considered as a peak corresponding to the ferroelectric transition point of the crystal occurring at this temperature.

10. Peak Q is a typical ITC peak arising from the reorientation of the I-V dipoles in the crystal.

11. Peak R observed at $151^\circ C$ can be considered as a protonic thermo-current peak which arises from the nonuniform distribution of protons released at the high temperature transition point of the crystal.

12. Peak D is accepted as a typical ITC peak and the origin of which is attributed to the nonuniform space charge distribution of the carriers released due to the dissociation of the I-V complexes present in the crystal.

13. The activation energy values corresponding to the different peaks are calculated for pure as well as doped samples and are given in Table 2.

14. Eventhough peak P in AS and peak B in LAS originate as a result of the low temperature phase transitions of the crystals, the former is not so sharp as the latter. This may be explained as due to the existence of a double transition in AS at the temperature corresponding to peak P.

An analysis of the ITC spectra of both LAS and AS gives a general conclusion as follows:

15. These ammonium containing crystals exhibit peaks in the ITC spectra corresponding to their low temperature as well as high temperature phase transitions. The peaks corresponding to the high temperature transitions arising from the non-uniform space charge distribution of protons show the properties of a typical ITC peak (which can be called protonic thermo-current peak) whereas the peaks observed at their low temperature transition points do not show such behaviour. Hence there exists excellent prospects for the study of the high temperature phase transitions of other ammonium containing crystals using the method of protonic thermo-current.

Table 1

Values of various parameters calculated from the ITC spectra of pure and doped LAS and their comparison with d.c. electrical conductivity data

Crystal	Procedure	Peak A			Peak C			Peak D				
		T_m (°C)	$I_A(T_m)$ (10^{-10} A)	E (eV)	T_m (°C)	$I_C(T_m)$ (10^{-10} A)	E (eV)	T_m (°C)	$I_D(T_m)$ (10^{-10} A)	E (eV)	τ_0 (10^{-9} sec.)	E_a (eV)
Pure LAS	ITC-using equation (2)	-25	2.0	0.48	186	5.0	0.58	235	2.5	1.55		
Pure LAS	ITC-using equation (4)			0.47								
Pure LAS	D.C.Electrical conductivity			0.025			0.58			1.51		
LAS + Cu²⁺ (65.7 ppm)	ITC-using equation (2)	-26	3.7	0.50	186	5.2	0.58	238	11	1.81		0.52
LAS + Cu²⁺ (65.7 ppm)	ITC-using equation (4)			0.50							2.63	
LAS + Zn²⁺ (50.2 ppm)	ITC-using equation (2)	-25.5	2.5	0.49	186	4.9	0.59	237	9.5	1.88		0.66
LAS + Zn²⁺ (50.2 ppm)	ITC-using equation (4)			0.49							3.55	

Values of various parameters calculated from the ITC spectra of pure and doped AS, and their comparison with d.c. electrocal conductivity data.

Crystal	Procedure	Peak Q T_m(°C)	E(eV)	Peak R T_m(°C)	E(eV)	Peak S T_m(°C)	E(eV)
Pure AS	ITC	-10	0.37	151	0.66	195	1.42
Pure AS	D.C. Electrical conductivity			150	0.67		1.50
AS + Cu^{2+} (122 ppm)	ITC	-35	0.42	151	0.69	199	1.69
AS + Zn^{2+} (256 ppm)	ITC	-38	0.43	151	0.70	187	1.79

REFERENCES

[1]   R.F. Meakins, Progress in Dielectrics ed. J.B. Birks
      (John Wiley and Sons, New York 1961) Vol.3

[2]   R.W. Drefus, Phys. Rev. 121, 1675 (1961)

[3]   C. Bucci and R. Fieschi, Phys. Rev. Lett. 12,
      16 (1964)

[4]   M. Puma, E. Laredo, M.E. Galavis and D.R. Figueroa,
      Phys. Rev. B22, 5791 (1980)

[5]   D. Kostopoulos, P. Varotsos and S. Mourikis, J. Phys.
      C 13, 3003 (1980)

[6]   E. Laredo, M. Puma and D. Figueroa, Phys. Rev. B19,
      2224 (1979)

[7]   D.L. Kirk and R.M. Innes, J. Phys. C 11, 1105 (1978)

[8]   G.E. Mathews and J.H. Crawford Jr., Phys. Rev. B15,
      55 (1977)

[9]   J. Prakash and F. Fischer, Phys. Stat. Solidi (a)
      39, 499 (1977)

[10] A.M. Hor, P.W.M. Jacobs and K.S. Moodie, Phys. Stat.
      Solidi (a) 38, 293 (1976)

[11] B.P.M. Lenting, J.A. Numan, E.J. Bijvank and
      H.W. den Hartog, Phys. Rev. B14, 1811 (1976)

[12] A. Kessler, Solid State Commun. 12, 697 (1973)

[13] A. Kessler and J.E. Caffyn, J. Phys. C5, 1134 (1972)

[14] L.W. Barr and A.B. Lidiard, Physical Chemistry An
      Advanced Treatise (New York Academic Press)
      Vol.X (1970)

[15] Capelletti and R. Fieschi, Electrons, Charge Storage
      and Transport in Dielectrics ee MM Perlman
      (Princeton : Electrochem. Soc.) 1973

[16] C. Bucci, R. Fieschi and Guidi, Phys. Rev. 148,
      816 (1966)

[17] C. Bucci and R. Siva, J. Phys. Chem. Solids 26,
      363 (1965)

[18] U. Syamaprasad and C.P.G. Vallabhan, 34, 899 (1980)

[19] U. Syamaprasad and C.P.G. Vallabhan, National Acad.
      Sci. Lett. (India) 3, 364 (1980)

[20] U. Syamaprasad and C.P.G. Vallabhan, Solid State
      Commun. 38, 555 (1981)

[21] U. Syamaprasad and C.P.G. Vallabhan, Proc. Nuclear
      Phys. and Solid State Phys. Symp. (India)
      Paper No.SLA10 (1980)

[22] U. Syamaprasad and C.P.G. Vallabhan, J. Phys. C
      (to appear in Vol.14 1981)

[23] U. Syamaprasad and C.P.G. Vallabhan, Solid State
      Commun. (In Press)

[24] U. Syamaprasad and C.P.G. Vallabhan (communicated)

[25] U. Syamaprasad and C.P.G. Vallabhan (Accepted for publication in Nuclear Phys. and Solid State Physics Symp. Bombay 1981)

[26] U. Syamaprasad and C.P.G. Vallabhan (Accepted for publication in Nuclear Phys. and Solid State Physics Symp. Bombay 1981)

[27] U. Syamaprasad and C.P.G. Vallabhan (communicated)

[28] C. Bucci, Phys. Rev. 164, 1200 (1967)

[29] J.R. McDonald, J. Chem. Phys. 30, 806 (1959)

[30] J.R. McDonald, J. Chem. Phys. 29, 1346 (1958)

[31] R.J. Friauf, J. Chem. Phys. 22, 1329 (1954)

[32] A.B. Lidiard, Handbuch der Physik 20, 246 (1957)

[33] Y. Haven, J. Chem. Phys. 21, 171 (1953)

[34] R. Pepinsky, K. Vedam, Y. Okaya and S. Hoshino, Phys. Rev. 111, 1457 (1958)

[35] W.A. Dollase, Acta Crystallogr. B25, 2298 (1969)

[36] Y.V.G.S. Murti and P.S. Prasad, Physica 79B, 243 (1975)

[37] Y.V.G.S. Murti and P.S. Prasad, Proc. Nuclear Phys. and Solid State Phys. Symp. (India) 17C, 67 (1974)

[38] U. Syamaprasad and C.P.G. Vallabhan, J. Phys. C 14, L571 (1981)